JAERI-Conf
2003-011

SELECTED MATERIALS OF THE INTERNATIONAL WORKSHOP ON RADIATION RISK AND ITS ORIGIN AT MOLECULAR AND CELLULAR LEVEL FEBRUARY 6-7, 2003

November 2003

(Ed.) Miroslav PINAK

日本原子力研究所
Japan Atomic Energy Research Institute

本レポートは、日本原子力研究所が不定期に公刊している研究報告書です。
入手の問合わせは、日本原子力研究所研究情報部研究情報課（〒319-1195　茨城県那珂郡東海村）あて、お申し越しください。なお、このほかに財団法人原子力弘済会資料センター（〒319-1195　茨城県那珂郡東海村日本原子力研究所内）で複写による実費頒布をおこなっております。

This report is issued irregularly.
Inquiries about availability of the reports should be addressed to Research Information Division, Department of Intellectual Resources, Japan Atomic Energy Research Institute, Tokai-mura, Naka-gun, Ibaraki-ken 319-1195, Japan.

編集兼発行　日本原子力研究所

JAERI-Conf 2003-011

Selected Materials of the International Workshop on Radiation Risk and its Origin at Molecular and Cellular Level

February 6-7, 2003

(Ed.) Miroslav PINAK

Department of Health Physics
Tokai Research Establishment
Japan Atomic Energy Research Institute
Tokai-mura, Naka-gun, Ibaraki-ken

(Received July 8, 2003)

The workshop "International Workshop on Radiation Risk and its Origin at Molecular and Cellular Level" was held at The Tokai Research Establishment, Japan Atomic Energy Research Institute, on the 6th and 7th of February 2003. The Laboratory of Radiation Risk Analysis of JAERI organized it. This international workshop attracted scientists from several different scientific areas, including radiation physics, radiation biology, molecular biology, crystallography of biomolecules, modeling and bio-informatics. Several foreign and domestic keynote speakers addresses the very fundamental areas of radiation risk and tried to establish a link between the fundamental studies at the molecular and cellular level and radiation damages at the organism. The symposium consisted of 13 oral lectures, 10 poster presentations and panel discussion. The 108 participants attended the workshop. This publication comprises of proceedings of oral and poster presentations where available. For the rest of contributions the abstracts or/and selections of presentation materials are shown instead.

Keywords: Radiation Risk, DNA & Cellular Damage, Enzymatic Recognition & Repair, Simulation & Experimental Approaches

JAERI-Conf 2003-011

放射線リスクと分子・細胞レベルの影響メカニズムに関する国際ワークショップ資料集

2003年2月6日～7日，東海研究所　東海村

日本原子力研究所東海研究所保健物理部
（編）Miroslav PINAK

（2003年7月8日受理）

本国際ワークショップは、放射線リスクとその分子・細胞レベルにおける影響のメカニズムに関する最新の研究成果について検討するために、2003年2月6日と7日の両日、日本原子力研究所東海研究所において保健物理部・放射線リスク研究室が主催して開催された．ワークショップには、放射線物理学、放射線生物学、分子生物学、生体分子の結晶学、分子モデリング、バイオインフォマティクスなどさまざまな研究分野に携わる研究者が参加し、放射線リスクに関連のある基礎研究分野についての基調講演が国内外の研究者により行われた．この基調講演に基づき、分子・細胞レベルの基礎研究と生体レベルの放射線障害とをどのように結び付けていけばよいか議論がなされた．シンポジウムは、口頭発表13件、ポスター発表10件、およびパネルディスカッションから構成され、108人が参加した．

本報文集は、これらの口頭およびポスター発表のうち、プロシーディング原稿をいただいた場合にはプロシーディングを、またそれ以外の発表に関しては、発表要旨に一部発表に用いられた図版を加えまとめたものである．

東海研究所：〒319-1195　茨城県那珂郡東海村白方白根2-4

Contents

目次

This is a blank page.

1. Opening Address

Welcome to International Workshop on Radiation Risk and its Origin at Molecular and Cellular Level

K. Saito

Radiation Risk Analysis Laboratory, Dept. of Health Physics, JAERI

Radiation risk for low-dose radiation is essential concern for peaceful uses of nuclear energy and radiation technology. Much precious knowledge on biological radiation effects has been accumulated by the epidemiological study at Hiroshima and Nagasaki. However, it is not expected that this kind of epidemiological approach thoroughly elucidate the radiation effect due to low-dose radiation that workers are exposed to in nuclear facilities under normal operation, or that general public are exposed to in the environment. This ambiguity concerning low-dose radiation effect has cased many arguments especially from a viewpoint of radiation protection. Though it has been emphasized that mechanism study would play an important role in elucidating the low-dose effect, there has existed a large gap between mechanisms at molecular or cellular level and radiation risk, which is an indicator of health effect on human. Nevertheless, recent remarkable advances in biology researches give us a good opportunity to consider a relation between radiation effects at molecular and cellular levels and the radiation risk.

This workshop comprises of thirteen oral lectures and several poster presentations introduced by specialists in diverse research fields related to radiation effect as are radiation biology, molecular biology, bioinformatics, structural biology, computer simulation, risk modeling, etc.

It is also intended to serve as a platform for discussion on how the mechanism study could contribute to the risk estimates in future. Furthermore, we strongly hope the workshop will give a chance to enhance friendship and collaboration among participants.

We sincerely hope all participants will enjoy the workshop and winter at Tokai.

2. Program of the Workshop

February 6 (Thursday)

Opening			13:00-13:30
	Opening talk	Hideo Matsuzuru, JAERI	13:00-13:10
	Introduction talks:	Miroslav Pinak (JAERI)	13:10-13:20
		Ohtsura Niwa (Kyoto University)	13:20-13:30
S1	**Radiation risk and link to molecular studies**		13:30-15:00
	Session chairs: Kimiyaki Saito, Ohtsura Niwa		
L1	How does ionizing radiation cause genomic instability? Possible role of Slow Release Radicals.	Charles A. Waldren, RERF	13:30-14:00
L2	Aspects of Mechanism for Radiation-Related Cancer Suggested by the Age-Time Patterns of Excess Risk.	Donald A. Pierce, RERF	14:00-14:30
L3	Dose Rate Effects on the Process of Carcinogenesis.	Kazuo Sakai, CRIEPI	14:30-15:00
Break			15:00-15:15
S2-1	**Experimental & simulation approaches to radiation effects on DNA – complementary effort; 1st part** 1		5:15-16:45
	Session chairs: Hisashi Ishida, Marc Dobler		
L4	Molecular Dynamics simulation toward Radiation induced DNA damages.	Hiroshi Yamaguchi, NIRS	15:15-15:45
L5	Can't Walk and Chew: A Non-stationary View of DNA Repair.	Roman Osman, Mount Sinai School of Medicine, New York	5:45-16:15
L6	Molecular *in silico* biology of DNA repair enzymes: A trial of genome function prediction through gene positional information.	Kei Yura, ITBL	16:15-16:45
Break			16:45-17:00

Graphical representation of modeling results 17:00-17:20

DNA damage & Enzymatic Repair: Impact of DNA damage and its repair determined by computational simulation (movie)Miroslav Pinak, JAERI

Poster session 17:20-18:30

Exhibition (FUJITSU, Ltd, HITACHI, Ltd.)

Reception, Akogi club 19:00-21:00

February 7, (Friday)

S2-2 Experimental & simulation approaches to radiation effects on DNA – complementary effort; 2nd part 9:30-11:30

Session chairs: Nobuo Niimura, Akira Ito

L7 Physical and chemical track structure of charged particles.
Shuzo Uehara, Kyushu University 9:30-10:00

L8 Modeling of Dose Rate Effects on Cellular Responses to Low Dose Gamma-Irradiation.
Junji Magae[1] and Hiromitsu Ogata[2], ([1]IRI, [2]NIPH)
10:00-10:30

L9 Recent Development of Radiation Chemistry in Aqueous Solutions.
Yosuke Katsumura, Tokyo University10:30-11:00

L10 Three-dimensional structural view of branch migration in DNA homologous recombination. Kosuke Morikawa, BERI 11:00-11:30

Lunch 11:30-13:00

Closed meeting (panelists) 12:25-12-55

S3 Novel biochemical approaches in radiation molecular biology
13:00-14:30

Session chairs: Akinari Yokoya, Shin Saigusa

L11 Functional Analysis of Repair Enzymes for Oxidative DNA Damage in mammalian cells. Akira Yasui, Tohoku University 13:00-13:30

L12 Misincorporation of oxidized dNTPs by archaeal Y-family DNA polymerases.
Takehiko Nohmi, NIHS 13:30-14:00

L13 Role of RecA protein in radiation resistance of Deinococcus radiodurans.
Issay Narumi, JAERI 14:00-14:30

Panel discussion 14:35-15:15

Chair: O. Niwa

Panelists: H. Ishida, Y. Katsumura, K. Morikawa, I. Narumi, N. Niimura, T. Nohmi, R. Osman, D. A. Pierce, S. Saigusa, Ch. A. Waldren, H. Yamaguchi

Summary 15:20-15:30

Miroslav Pinak, (JAERI)

Workshop adjourn 15:30

3. List of Presentations

3.1. Oral presentations

L1 A.M. Ueno, DB Vannais, M Lenarczyk and C.A. Waldren
How does ionizing radiation cause genomic instability? Possible role of Slow Release Radicals.

L2 Donald A. Pierce
Aspects of Mechanism for Radiation-Related Cancer Suggested by the Age-Time Patterns of Excess Risk.

L3 Kazuo Sakai
Dose Rate Effects on the Process of Carcinogenesis.

L4 H. Yamaguchi , T. Suzuki , J.G. Siebers, A. Furukawa, R.Osman
Molecular Dynamics simulation toward Radiation induced DNA damages.

L5 Roman Osman
Can't Walk and Chew: A Non-stationary View of DNA Repair.

L6 Kei Yura, Hidetoshi Kono, Nobuhiro Go
Molecular *in silico* biology of DNA repair enzymes: A trial of genome function prediction through gene positional information.

L7 Shuzo Uehara and Hooshang Nikjoo
Physical and chemical track structure of charged particles.

L8 Junji Magae and Hiromitsu Ogata
Modeling of Dose Rate Effects on Cellular Responses to Low Dose Gamma-Irradiation

L9 Yosuke Katsumura
Recent Development of Radiation Chemistry in Aqueous Solutions.

L10 Kosuke Morikawa
Three-dimensional structural view of branch migration in DNA homologous recombination.

L11 Akira Yasui
Functional Analysis of Repair Enzymes for Oxidative DNA Damage in mammalian cells.

L12 Masatomi Shimizu, Petr Gruz, Hiroyuki Kamiya, Su-Ryang Kim, Francesca M. Pisani, Yusuke Kanke, Hideyoshi Harashima and Takehiko Nohmi
Misincorporation of oxidized dNTPs by archaeal Y-family DNA polymerases.

L13 Issay Narumi, Katsuya Satoh, Hirofumi Ohba, Masahiro Kikuchi
Role of RecA protein in radiation resistance of Deinococcus radiodurans.

3.2 Poster Presentations

(alphabetical order by first author)

P1 Ken Akamatsu, Kentaro Fujii and Akinari Yokoya
A basic approach for radiation chemical dose-response estimation for thymine decomposition products.

P2 Jonas Danielsson and Aatto Laaksonen
Photochemistry of Urocanic acid: a human skin UV receptor.

P3 H. Date, H. Tomozawa, T. Takamasa, K. Okamoto, M. Shimozuma
Development of RISA (Radiation Induced Surface Activation) Detectors for Onsite Sensing and Microdosimetry.

P4 K. Fujii, K. Akamatsu and A. Yokoya
Photon Stimulated Desorption of Ions from DNA Components induced by Core Excitation.

P5 Yasuhiko Kobayashi, Tomoo Funayama, Seiichi Wada, Mitsumasa Taguchi
Irradiation of single mammalian cells with a precise number of energetic heavy ions.

P6 Hisashi Ishida and Nobuhiro Go
Molecular Dynamics of Damaged DNA and Oxoguanine DNA Glycosylase Complex.

P7 S. Ohno, M. Taguchi, Y. Kobayashi and H. Watanabe
An ion-track structure model applied to estimate cross sections for SV40 DNA strand breaks in aqueous solution.

P8 Noriyuki Ouchi
On the biologically based modeling and simulation of carcinogenesis.

P9 Katsuya Satoh[1], Seiichi Wada[1,2], Issay Narumi[1], Masahiro Kikuchi[1], Tomoo Funayama[1], and Yasuhiko Kobayashi[1]
Detection of DNA strand breaks in mammalian cells using the radioresistant bacterium PprA protein.

P10 Naoya Shikazono, Satoshi Kitamura, Chihiro Suzuki, Hiroshi Watanabe, Shigetmitsu Tano and Atsushi Tanaka
Chracterization of carbon ion-induced mutations in *Arabidopsis thaliana.*

P11 J.-G. Siebers, H. Yamaguchi and R. Osman
Essential Dynamics of T4 Endonuclease V.

P12 Shigeru Sugaya, Katsuo Sugita, Kazuko Kita and Nobuo Suzuki
X-ray induced DNA synthesis and its regulation by SMT3A gene in Nevoid basal cell carcinoma syndrome (NBCCS) cells.

P13 Shigenori Tanaka
Ab Initio Approach to Nanoscale Dynamics of DNA.

4. Oral Presentations

This is a blank page.

JP0450228

4.1

Vitamin C, Added after Irradiation, Reduces the Mutant Yield and Alters the Spectrum of CD59$^-$ Mutations in A_L Cells Irradiated with High LET Carbon Ions

A.M Ueno[1,3], D.B Vannais[1], M. Lenarczyk[1], and C.A. Waldren[1,2]

[1]Department of Radiological and Environmental Health Sciences, Colorado State University, Fort Collins, CO 80523,USA. [2]Current address: Radiation Effects Research Foundation (RERF), 5-2 Hijiyama Park, Minami-ku, Hiroshima 732-0815, Japan. [3]National Institute of Radiological Sciences, 4-9-1 Anagawa, Inage-ku, Chiba, 263-8555, Japan.

Abstract

Miazaki, Watanabe, Kumagai and their colleagues reported that induction of HPRT$^-$ mutants by X-rays in cultured human cells was prevented by vitamin C (ascorbate) added 30 minutes after irradiation. They provided data that that mutation extinction was due to neutralization by vitamin C of radiation-induced long-lived mutagenic radicals (LLR) with half-lives of several hours. We find that post-irradiation treatment with vitamin C reduces, but does not eliminate, the induction of CD59$^-$ mutants in human-hamster hybrid A_L cells exposed to high-LET carbon ions (LET of 100 KeV/μm). The lethality of the carbon ions was not altered by vitamin C. Preliminary experiments indicate that post-radiation addition of vitamin C also changes the quality of CD59$^-$ mutations induced by the carbon beam. The change in spectrum is seen as a reduction in prevalence of small mutations (not detectable by PCR) and of mutants displaying transmissible genomic instability (TGI) measured by chromosome translocation frequencies. Our results confirm the essential effect of vitamin C on X-ray induced mutation and suggest a role for LLR in genomic instability.

Key Words: Long lived radicals (LLR), A_LCD59 mutation, High LET radiation, mutant spectra, vitamin C

INTRODUCTION

A dogma of radiation biology holds that radiation-induced genetic effects result only from direct interaction of radiation with DNA or via production of highly reactive, oxygen radical species (ROS) like H• and OH• which damage DNA within fractions of a second after radiation[1,2]. Miyazaki, Watanabe, Kumagai and their colleagues employed sophisticated spectroscopic analysis to reveal long lived radiation induced radicals (LLR) with half-lives of minutes to hours. LLR are endogenous to plant and animal cells and are increased in a dose dependent manner by ionizing radiation mainly in (>99.8%) in the interior of protein polymers from which they escape by atomic tunneling[3-11]. Thus for LLR, which can be thought of as being 'slow-release' radicals, 'unreactive' does not mean biologically irrelevant. They also found that vitamin C scavenged LLR and completely eliminated HPRT$^-$ mutant induction in human cells exposed to X-rays, even when it was added several minutes after radiation, long after classical ROS had dissipated. On the other hand, DMSO, which effectively scavenges classical radicals but not LLR, affected mutation only if present during radiation. Exactly how LLR cause genetic effects is not yet known.

We here show that vitamin C added after irradiation reduces, but does not eliminate, induced CD59$^-$ mutants in A_L cells exposed to high LET radiation and provide preliminary evidence that vitamin C alters the quality of mutations induced. The major change in mutant spectrum is a reduction in the prevalence of CD59$^-$ mutants containing small mutations and in the fraction of mutants displaying transmissible genomic instability (TGI) measured as chromosomal translocations. Our data essential verify the finding of Miyazaki, Watanabe, Kumagai et al. regarding effects of vitamin C on radiation mutation provide evidence for a role of LLR role in radiation-induced genomic instability.

MATERIALS AND METHODS

Radiations: Carbon beam irradiations were carried out at the HIMAC (Heavy Ion Medical Accelerator) facility of the National Institutes of Radiological Sciences (NIRS), Chiba, Japan as described [12]. The beam energy was 290MeV/nucleon, LET was 100 KeV/μm, the dose rate was 0.5 Gy/min. Vitamin C, 5 mM, was added 30 minutes after radiation. Because access to the HIMAC beam is necessarily limited, other protocols have not been evaluated

A_L mutation assay: quantifying yields of CD59$^-$ mutants Quantification of CD59$^-$ mutant induction by radiation was carried out as described[13-18].

The A_L/CD59 assay uses a human - CHO hybrid cell line (A_L) in which the scored genetic markers are located on a human chromosome, number 11. Cell surface antigens such as CD59 encoded by genes like the *CD59* gene on the human chromosome provide convenient, quantitative, selectable markers. Only a small portion of the human chromosome 11 is necessary for cell survival so that marker mutations and survival are disassociated. The increased sensitivity so obtained allows mutation to be measured at low-relevant doses of mutagen. Thus antimutagens can also be studied at low doses.

In the present experiments, populations of A_L cells were exposed to high LET carbon ions. Vitamin C (5 mM) was added 30 min after irradiation and removed 20 hrs later. Aliquots of cells were plated for survival, the rest were incubated and subcultured for a 10 day period of mutation expression. Antibody against CD59 and rabbit serum complement were then added to populations of A_L cells under conditions which kill all wild-type cells leaving $CD59^-$ mutants which form scorable colonies. The mutant fraction, M_F, was calculated as: M_F = (the number of mutant colonies/number of cells inoculated) x 1/plating efficiency in medium containing complement but without antisera where M_F was expressed as mutants per 10^5 clonable cells. M_F were determined at least three times for each treatment, each complete experiment was repeated at least twice.

Determining mutational spectrum in populations of $CD59^-$ mutants

Procedures used to define spectra of *$CD59^-$* mutants have been described[15,16,18,19]. Briefly, individual colonies of $CD59^-$ mutants were picked, expanded, their DNA extracted, and the presence or absence of genetic loci on human chromosome 11 was determined by PCR analysis. Mutations ranged from small, intragenic lesions to deletions of more than 133 mbp of the human chromosome 11. Primers and conditions used for the 1860 individual PCR reactions used to define spectra have been reported [18,19]. PCR conditions were adjusted to give a robust signal for human genes and no signal from the corresponding CHO genes which allows detection Gy PCR of translocations between human chromosome 11 and CHO chromosomes. The PCR analysis was verified by FISH analysis. Patterns of marker loss defined mutations of 37 kinds of which 36 were 'simple' in that contiguous markers were lost extending on either side from *CD59* gene. Simple mutants remain clonal over long periods of culture. The 37th category, called 'complicated', consists of mutants in which translocations and deletions involving human chromosome 11 arise during culture at abnormally high

rates[19]. Complicated mutants display typical characteristics of transmissible genomic instability (TGI)[20].

RESULTS

Survival curves for irradiated A_L cells without and with delayed vitamin C

As shown in Fig. 1a, addition of vitamin C after radiation did not affect survival of A_L cells. A similar lack of effect of vitamin C on killing was reported for human cells exposed to X-rays[7].

CD59$^-$ mutant induction in irradiated A_L cells without and with delayed vitamin C

Although survival was not altered, the fraction of CD59$^-$ mutants recovered from irradiation populations of A_L was reduced by vitamin C added after radiation to about 1/3 the level found without vitamin C (Fig. 1b). We also found that RibCys [2(R,S)-D-ribo-(1',2',3',4'-Tetrahydroxybutyl)-thiazolidine-4(R)-carboxylic acid [21], added after radiation, reduced the mutagenicity of carbon beam irradiation but less than vitamin C. RibCys reduced the mutant yield by about half (data not shown). Neither vitamin C nor RibCys was mutgenic of themselves (data not shown). Like vitamin C RibCys, did not alter the lethality of high LET radiation.

This result for vitamin C with high LET radiation and CD59 mutants is similar to that reported by M. Watanabe, T. Miyazaki, J. Kumagai and colleagues[7,9,10,11] for X-irradiation and HPRT mutation in human cells, except for the important difference that they found that mutation was completely suppressed whereas we found reduction using the same protocol but not elimination of mutation.

Spectra of mutations in CD59$^-$ mutants

We thought that this difference in of mutant suppression might be explained because large-scale mutations that are not detected by the HPRT assay [22] are scored by the A_L CD59 assay[13-19]. We have begun, therefore, to define mutant spectra produced by carbon ions (2.5 Gy) without and with post irradiation addition of vitamin C. The markers on human chromosome 11 used to define spectra are shown in Fig. 2. Loss of any or all of the 4 exons of the CD59 gene and of 11 other genes on human chromosome 11 was determined by PCR analysis of DNA from 87 CD59$^-$ clones: 27 from control populations, 31 from clones given carbon ions alone, and 29 from populations exposed to radiation then vitamin C. Based on this analysis, each mutant was placed into one of four classes: **[A]** intragenic, defined

as a mutation not detected by PCR analysis of the *CD59* gene; **[B]** Intragenic deletions, mutants missing one to four of the *CD59* exons but with all other markers on chromosome 11 retained. These range in size from loss of a few bases to deletions of about 3 mbp; **[C]** 'large' deletions, ranging from 3 to 133 mbp, defined as missing all four *CD59* exons and at least one marker outside of the *CD59* gene, and; **[D]** mutants displaying (TGI) seen as abnormally high levels over time of translocations that involve human chromosome 11 and CHO chromosomes as measured cytogenetically or by PCR analysis. The distribution of mutations is shown in Fig. 3.

DISCUSSION

Our results confirm that mutagenic effects of radiation, here high LET radiation, can be significantly reduced by vitamin C added after radiation, and indicate, for the first time, a role for LLR in triggering genomic instability. Although the number of mutants analyzed is too small to provide statistical significance, our results suggest that smaller mutations [Class 1 and Class 2] are due to LLR, while large deletions are caused by immediate effects of radiation.

We further found that (i): DMSO reduced both killing and mutation but only when present during radiation; (ii) lycopene which has been reported significantly to reduce rates of spontaneous mutation[23] had no effect on the lethality or mutagenicity of the carbon beam (results not shown).

Our finding that vitamin C reduces but does not eliminate mutation measured at the CD59 is not inconsistent with the results of Watanabe, Miyazaki, Kumagai and colleagues who found that vitamin C eliminated mutation measured at the HPRT locus, since the larger kinds of CD59 mutations that were not affected by vitamin C are not detectable in the HPRT assay, e.g.[22,24]. The difference is found in levels of mutant suppression we found compared with experiments with X-rays may also reflect qualitative differences in the kinds of DNA damage produced by high vs. low LET radiation and the repair-ability of these damages[25]. The finding that post-addition of vitamin C does not affect survival of either X-rays or carbon beam implies that large deletions are more lethal than mutagenic, whereas mutations of other kinds are more mutagenic than lethal.

Mutation reduction by post-radiation addition of chemicals is not limited to vitamin C. It has, for example, been reported that certain other water soluble chemicals such as (-)-epigallocatechin-3-*O*-gallate (EGCG)[9], and WR-1065 [N-(2-mercaptoethyl)-1,3-propanediamine], can also

reduce mutation when added after irradiation with high LET carbon, gamma-rays or fission spectrum neutrons[26,27].

Our results suggest that TGI can be initiated by LLR. However, long-term TGI which can persist for years is obviously not caused by continued, direct activity of LLR which exist for few hours. It seems likely that classical radicals and LLR can trigger TGI by mechamisms which remain to be elucidated. Whatever the mechanisms, we suggest that chemicals like vitamin C that scavenge LLR induced by high LET radiations may help reduce cancer risk in astronauts, and that relationships of LLR to TGI deserve further study.

ACKNOWLEDGEMENTS

Supported by The Japanese Science Technology Agency, WALAD Fund, NIH-NCI 36447, NASA-NSCORT W19133. We thank Drs. M. Watanabe, T. Miyazaki, J. Kumagai for valuable discussions, the staff at NIRS for expert assistance with radiations.

FIGURE LEGENDS

Fig. 1. Dose response curves for CD59$^-$ mutant induction in populations of A_L cells treated with vitamin C (5 mM) after irradiation with carbon ions. Vitamin C reduced the slope (M_Y) of the dose response curve from about 100 to 30. (M_Y = mutants/10^5 mutants/clonable cells/Gy). The average background mutant fraction (M_F) was 80±25 mutants/10^5 clonable cells. The curve was fit using a simple linear model: (○) Carbon beam alone (■) Carbon beam + vitamin C.

Fig. 2. Cartoon of human chromosome 11 showing the markers used to define mutant spectra for CD59$^-$ mutants. Inter-marker distances are in mbp as determined from the current NCBI Uni STS website map for human chromosome 11.

Fig. 3. Distribution of CD59$^-$ mutants in four mutation classes. White bars, unirradiated populations; hatched bars, carbon ions, 2.5 Gy; black bars, carbon ions plus vitamin C. **'A'** class are 'point' or intragenic mutations; **'B'**, intragenic deletions with loss of one to four of the *CD59* exons; **'C'**, deletions ranging from 3 to 133 mbp.; **'D'** TGI mutants, display elevated levels of chromosomal translocations between human chromosome 11 and CHO chromosomes. **'C'** mutants, which are relatively unaffected by vitamin C are poorly detected in the HPRT assay and would not be seen. Of 87 mutants analyzed, 27 were from controls, 31 from the carbon beam exposures and 29 from the carbon beam + vitamin C. $^*M_F$ = the total mutant fraction (M_F) for each treatment (from Fig. 1) multiplied by the percent of those mutants of a class. $^*M_F$ provides a measure of the relative proportion of mutants of each class, including background mutants, in populations of cells after various treatments. The changes in $^*M_F$ for different treatments are not statistically significant.

REFERENCES

1. Biaglow,J.E. *et al.* Role of glutathione and other thiols in cellular response to radiation and drugs. *Drug Metab. Revs.* **20**, 1-12 (1989).

2. Livesey,J.C., Reed,D.J. & Adamson,L.F. Radiation-Protective Drugs and Their Reaction Mechanisms. Noyes Publications, Park Ridge, NJ (1985).

3. Miyazaki,T., Hayakawa,Y., Suzuki,K., Suzuki,M. & Watanabe,M. Radioprotective effects of dimethylsulfoxide in golden hamster embryo cells exposed to g-rays at 77 K: Part I. Radical formation as studied by ESR. *Radiat. Res.* **124**, 66-72 (1990).

4. Yoshimura,T., Miyazaki,T., Mochizuki,K., Suzuki,M. & Watanabe,M. Do OH radicals react with organic substances in gamma-irradiated frozen cells of golden hamster embryo? *Radiat. Phys. Chem.* **40**, 45-48 (1992).

5. Yoshimura,T., Matsuno,K., Miyazaki,T., Suzuki,K. & Watanabe,M. Electron spin resonsance studies of free radicals in gamma-irradiated golden hamster embryo cells: Radical formation at 77 and 295 K, and radioprotective effects of vitamin C at 295 K. *Radiat. Res.* **136**, 361-365 (1993).

6. Matsumoto,T. *et al.* Reaction of long-lived radicals and vitamin C in g-irradiated mammalian cells and their model systems at 295 K. Tunneling reaction in biological systems. *Radiation Physics and Chemistry* **49**, 547-551 (1997).

7. Koyama,S., Kodama,S., Matsumoto,T., Miyazaki,T. & Watanabe,M. Radiation-induced long-lived radicals which cause mutation and transformation. *Mutation Res.* **421**, 45-54 (1998).

8. Kumagai,J., Kumada,T., Watanabe,M. & Miyazaki,T. Electron spin echo study of long-lived radicals which cause mutation in g-ray irradiated mammalian cells. *Spectrochimica Acta Part A* **56**, 2509-2516 (2000).

9. Kumagai,J. *et al.* Scavenging of long-lived radicals by (-)-epigallocatechin-3-*O*-gallate and simultaneous suppression of mutation in irradiated mammalian cells. *Radiation Physics and Chemistry* **64**, 293-297 (2002).

10. Kumagai,J. ESR and ESSM analysis of long-lived protein radicals which induce gene mutation and transformation. *Radiation Biology Research Communications* **37**, 85-103 (2002).

11. Kumagai,J. *et al.* Long-lived mutagenic radicals induced in mammalian cells by ionizing radiation are mainly localized to proteins. *Radiat. Res.* **In Press**, (2003).

12. Fukumura,A. *et al.* Carbon beam dosimetry intercomparison at HIMAC. *Phys Med Biol* **43**, 3459-3463 (1998).

13. Waldren,C., Correll,L., Sognier,M.A. & Puck,T.T. Measurement of low levels of x-ray mutagenesis in relation to human disease. *Proc. Natl. Acad. Sci. USA* **83**, 4839-4843 (1986).

14. Hei,T.K. *et al.* Mutagenic effects of a single and an exact number of alpha particles in mammalian cells. *Proc. Natl. Acad. Sci. USA* **94**, 3765-3769 (1997).

15. Kraemer,S.M., Ueno,A., Kronenberg,A. & Waldren,C.A. Measuring the spectrum of mutations induced by nitrogen ions and protons in the human-hamster hybrid cell line, A_LC. *Radiat. Res.* **154**, 743-751 (2000).

16. Wu,L.-J. *et al.* Targeted cytoplasmic irradiation with alpha particles induces mutations in mammalian cells. *Proc. Natl. Acad. Sci. USA* **96**, 4959-4964 (1999).

17. Waldren,C.A. *et al.* Mutant yields and mutational spectra of the heterocyclic amines MeIQ and PhIP at the S1 locus of human-hamster A_L cells with activation by chick embryo liver (CELC) co-cultures. *Mutation Res.* **425**, 29-46 (1999).

18. Ueno,A., Vannais,D., Lenarczyk,M. & Waldren,C.A. Ascorbate added after irradiation reduces the mutant yield and alters the spectra of CD59$^-$ mutants in A_L cells irradiated with high LET carbon beam. *Journal of Radiation Research* **In press, 2003**, (2003).

19. Kraemer,S.M., Vannais,D.B., Kronenberg,A., Ueno,A.M. & Waldren,C.A. Gamma-ray mutagenesis studies in a new human-hamster hybrid, A_L CD59$^{+/-}$, which has two human chromosomes 11 but is hemizygous for the *CD59* gene. *Radiat. Res.* **156**, 10-19 (2001).

20. Morgan,W.F., Day,J.P., Kaplan,M.I., McGhee,E.M. & Limoli,C.L. Genomic instability induced by ionizing radiation. *Radiat. Res.* **146**, 247-258 (1996).

21. Roberts,J.C., Francetic,D.J. & Zera,R.T. L-cysteine prodrug protects against cyclophosphamide urotoxicity without compromising therapeutic activity. *Cancer Chemotherapy Pharmacology* **28**, 166-170 (1991).

22. Thacker,J. Nygaard,O.F., Sinclair,W.K. & Lett,J.T. (eds.), pp. 77-124 (Academic Press, Inc, New York,1992).

23. Mure,K. & Rossman,T.G. Reduction of spontaneous mutagenesis in mismatch repair-deficient and proficient cells by dietary antioxidants. *Mutation Res.* **480-481**, 85-95 (2001).

24. Evans,H.H. The prevalence of multilocus lesions in radiation-induced mutants. *Radiat. Res.* **137**, 131-144 (1994).

25. Ward,J.F. Radiation mutagenesis:The initial DNA lesions responsible. *Radiat. Res.* **142**, 362-368 (1995).

26. Grdina,D.J., Nagy,B. & Meechan,P.J. Effect of an aminothiol (WR-1065) on radiation-induced mutagenesis and cytotoxicity in two repair-deficient mammalian cell lines. *Anticarcinogenesis and Radiation Protection* **2**, 287-295 (1991).

27. Evans,H.H., Evans,T.E. & Horng,M.F. Antimutagenicity of WR-1065 in L5178Y cells exposed to accelerated ^{56}Fe ions. *Radiat. Res.* **158**, 110-114 (2002).

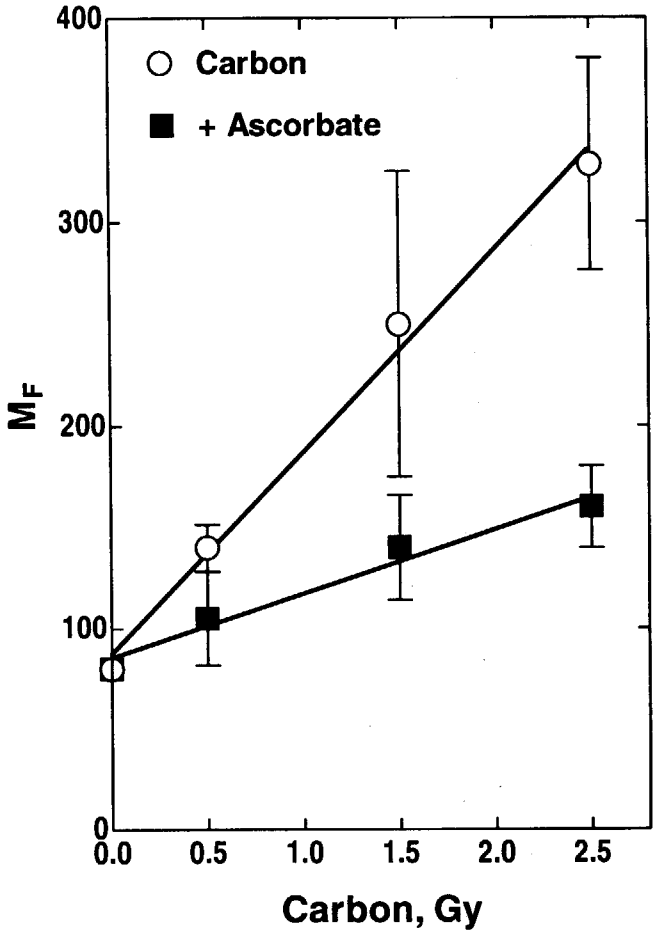
400
300
200
100
0
M_F
Carbon
+ Ascorbate
0.0
0.5
1.0
1.5
2.0
2.5
Carbon, Gy

Fig. 1

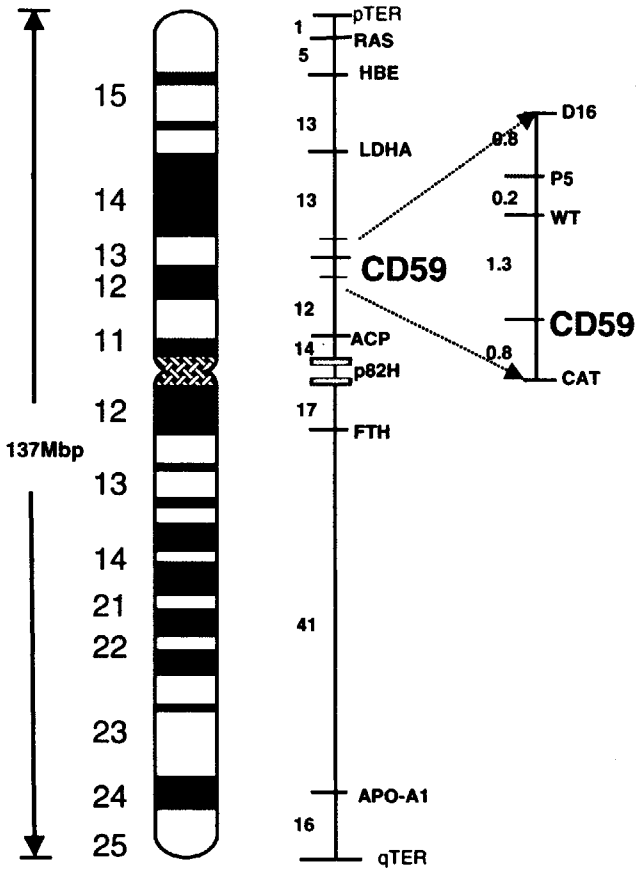
15
14
13
12
11
12
137Mbp
13
14
21
22
23
24
25
pTER
1
RAS
5
HBE
13
LDHA
13
CD59
12
14
ACP
p82H
17
FTH
41
APO-A1
16
qTER
D16
0.8
P5
0.2
WT
1.3
CD59
0.8
CAT

Fig. 2

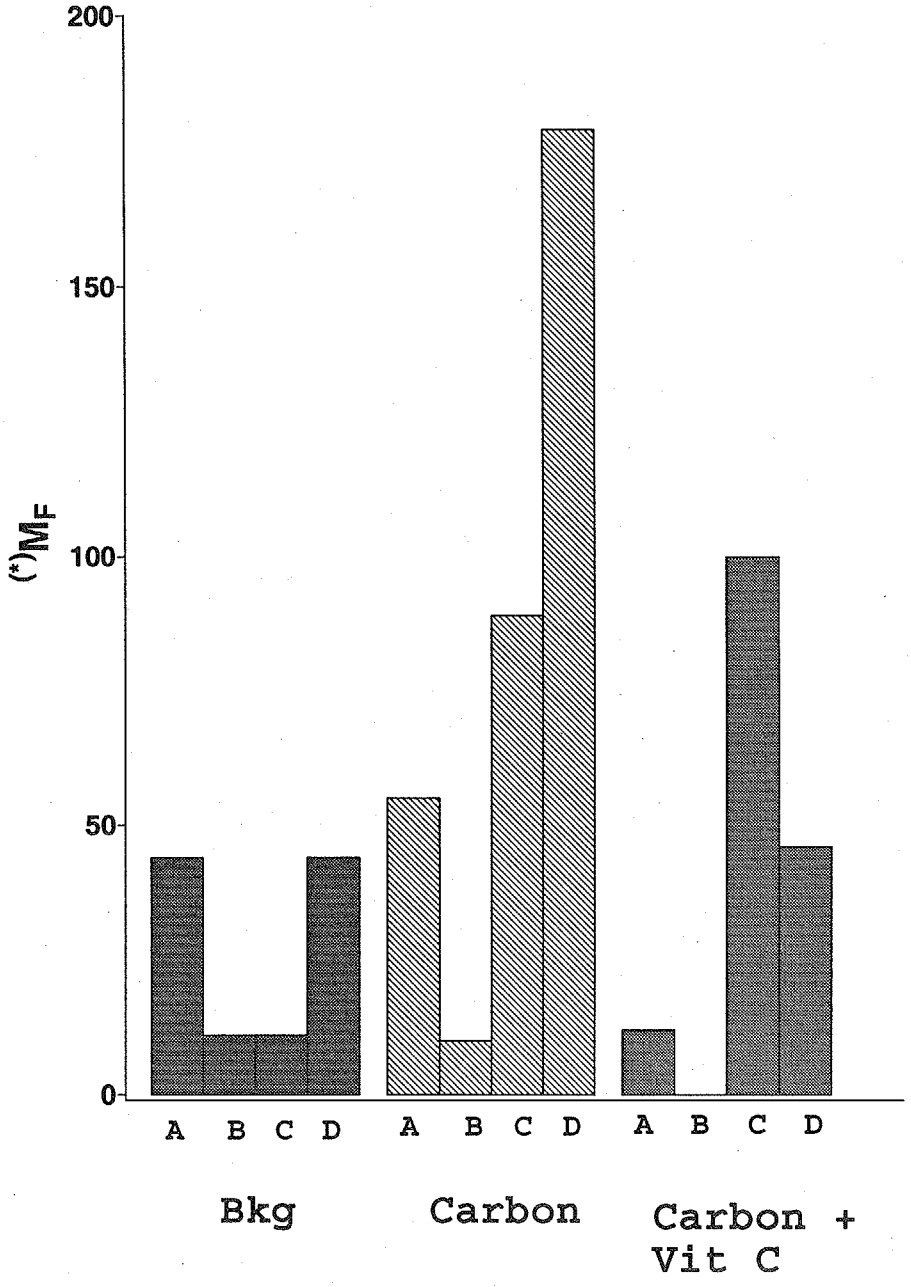

Fig. 3

4.2

Aspects of Mechanism for Radiation-Related Cancer Suggested by the Age-Time Patterns of Excess Risk

Donald A. Pierce

Radiation Effects Research Foundation, Hiroshima and Nagasaki

It was surprising to find about 15 years ago that A-bomb survivor cancer rates are elevated for all of lifetime, and insufficient attention was given to the implications of this. It natural to think that a brief radiation exposure can with some chance cause one of the mutations required for malignancy, thereby putting a cell one step ahead in the process for all remaining lifetime. Our analysis of this suggests that the radiation-induced mutation is not usually the first or the last of those required, but the next one in the sequence to occur after the exposure age. From this view the usual terminology "radiation-induced" cancer, and associated "latent period", can be seriously misleading. For example, the time from exposure to radiation-related cancer would be that required for the remaining mutations to accumulate.

When the lifetime cancer rate elevation was revealed, it was first thought to be by an age-constant factor, but recently it has been found that this factor decreases moderately with attained age. Stochastic analysis of the process described above shows that this is to be expected. These considerations further suggest, as is strongly confirmed by the data, that the effect of an increment of radiation exposure is equivalent to an abrupt increase in one's "cancer age", corresponding to the time interval that would be required for the radiation-induced mutations to otherwise occur spontaneously or to other causes. The time interval is about 0.5 years per 100mSv for men, and twice that for women reflecting their 50% lower natural cancer rates. Such a characterization of the excess cancer risk provides a very accurate and comprehensive description of radiation effects, and could be useful in radiation protection considerations and communication.

There are also implications for carcinogenesis in general, since the analysis and data indicate that the required spontaneous mutations for even a late-life malignancy begin their accumulation in the involved malignant cell at very young ages. Indeed, simulations suggest that most of the variation in ages at which cancer occurs is due to the period between the penultimate and ultimate of required mutations.

Age-Time Patterns of Radiation-Related Cancer: Basic Ideas

- Initially, most thought an single exposure would cause a "wave" of excess cancer, vanishing after 25 years or so
- But by about 1985, we found that age-specific cancer rates were elevated by a factor constant for most or all of lifetime
- How could this be? Insufficient attention was given to the implications, for both radiation-related cancer and carcinogenesis in general

1980's and Still-Common View of the Relative Risk

(ERR is the % increase in age-specific cancer rate)

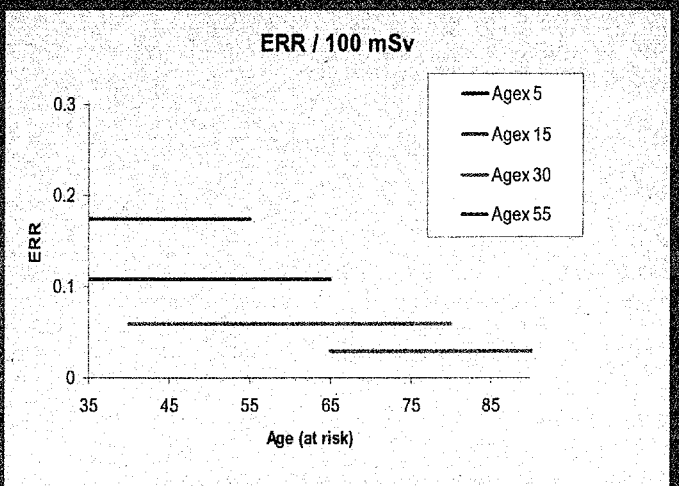

But the Current Understanding is as Shown Here

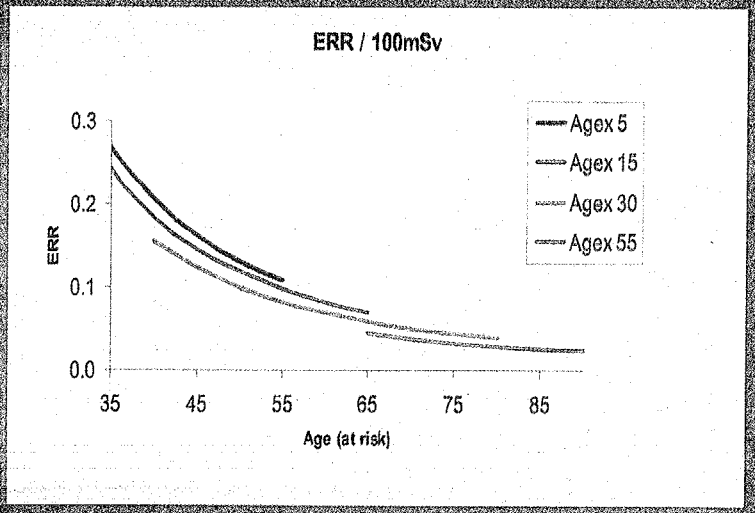

JAERI 2003 Pierce

* Solid CA less thyroid, uterus

3

Reasons Why ERR Should Look Like This

Considering malignancy of a cell as due to accumulated mutations, suppose as a substantial idealization that:

A. The spontaneous rate of the next mutation in a cell depends arbitrarily on its mutational status, but not otherwise on age

B. A brief radiation exposure momentarily increases all relevant mutation rates by a factor $(1+\beta d)$ where d is the dose

JAERI 2003 Pierce

4

Implication of This

- If cancer rate for unexposed is $\lambda_0(a)$, that under exposure to dose d is $\lambda_d(a) = \lambda_0(a + \beta d)$
- The remarkable thing is that, aside from the idealized assumptions, this almost perfectly describes the actual radiation cancer risks for A-bomb survivors
- The age increase is about 2-3 days per mSv

JAERI 2003 Pierce 5

Simplest Evaluation of the Age-Increment Description

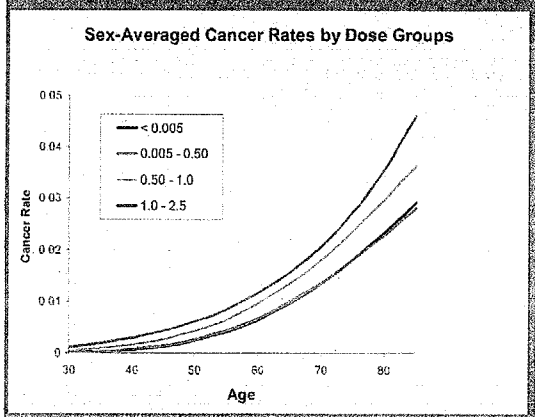

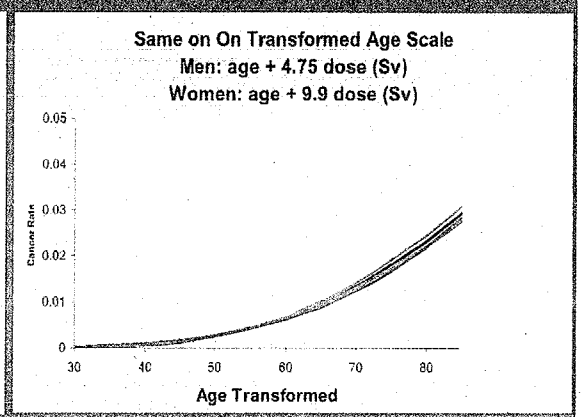

The age increment removes the most basic evidence of a radiation effect on cancer rates

JAERI 2003 Pierce 6

Same Results by Exposure Age

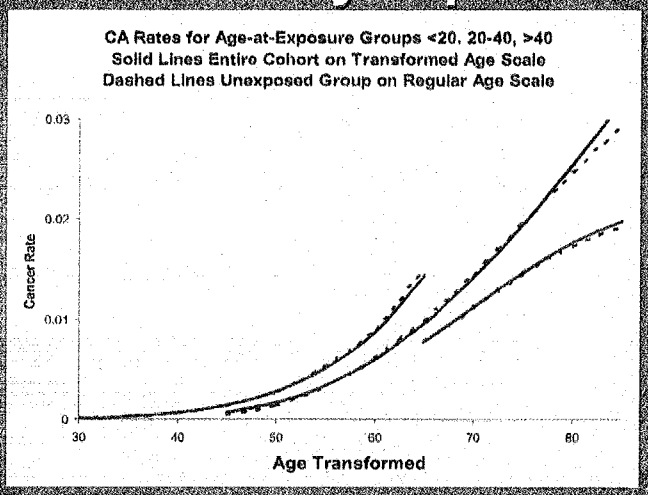

Effect seen here is birth cohort variation in background cancer rates

Implications for Relative Risk

- Recall the relation $\lambda_d(a) = \lambda_0(a + \beta d)$
- It is well known that for most of life natural cancer rates take form $\lambda_0(a) \propto a^p$
- Thus the RR could be expected to take form

$$RR = \frac{(a+\beta d)^p}{a^p} = (1+\beta d/a)^p = 1 + p\beta d/a + \cdots$$

$\nearrow$ ERR

Age-Change Result vs Description

Here we plot more precisely $ERR = \frac{\lambda_0(a+\beta d)}{\lambda_0(a)} - 1$

Decreases with age, but with no exposure age effect

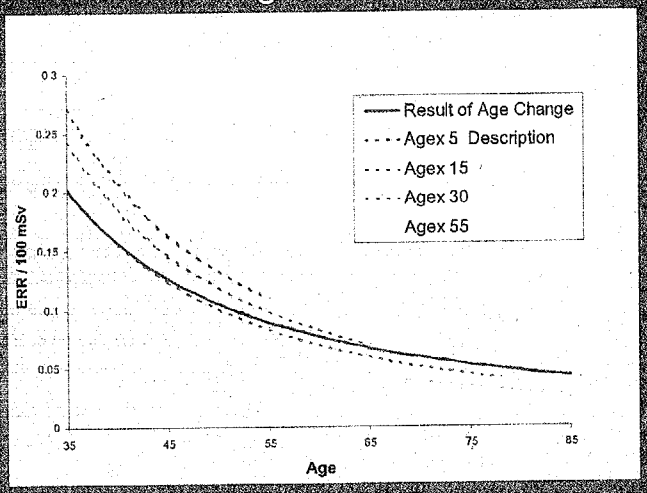

Several Refinements Will Explain the Modest Age-at-Exposure Effect

- Slight improvement in characterizing birth cohort variations in background rates
- Allowing that part of the birth cohort effect acts additively with radiation
- Modest increase at young ages of mutation rates per unit time

Implications for Radiation & Cancer

- Radiation does not "cause" cancers, but can contribute to the required accumulation of mutations
  - This is why excess risk lasts for all of lifetime
  - Also is why relative risk declines with age
- An increment of exposure has the same effect as some advance in "cancer age"
  - Approximately 2-3 days per mSv
  - Also applies to prolonged exposures (radon for miners)
  - Also applies to other mutagens (cigarette smoking)
- There is strong interchangeability, or equivalence, between cancer-relevant spontaneous mutations and those caused by radiation

JAERI 2003 Pierce 11

Implications for Carcinogenesis in General

- For any given cancer case, accumulation of required mutations begins at a very early age
- By middle age, all persons have roughly the same number of cells that are nearly transformed
- Most of the variation of both cancer age and whether one gets cancer is due to the waiting time for the ultimate required mutation

JAERI 2003 Pierce 12

4.3

Dose Rate Effects on the Process of Carcinogenesis

Kazuo Sakai
Low Dose Radiation Research Center
Central Research Institute of Electric Power Industry

The biological effects of ionizing radiation depend not only on the dose, but also on the dose rate at which the dose is delivered. Generally, in the case of low LET radiation, the biological effects are reduced, as the dose rate is lowered. The dose rate effect is one of the most significant factors for estimating the risk of cancer from ionizing radiation.

There are a number of steps from DNA to cancer: DNA damage induction, accumulation of certain types of mutations, cellular malignant transformation, and, finally, proliferation of the malignant cells. Biological organisms possess protective mechanisms which suppress these steps: DNA repair and apoptosis. For risk estimation based on the molecular mechanism, the influence of the dose rate on these protective mechanisms as well as on the steps in carcinogenesis should be clarified. Recently reported animal experiments clearly demonstrated the importance of these protective mechanisms in the reduction of harmful effects of ionizing radiation when irradiated at a low dose rate.

The current risk estimation is mainly based on the data on A-bomb survivors exposed at a high dose rate. Some of the epidemiological studies on residents in high natural background areas and those exposed to occupational radiation over prolonged periods showed little increase, or, in some cases, a decrease in cancer mortality, indicating the significance of the dose rate effects.

For high LET radiations, the dose rate effect is less significant, as has been demonstrated by studies in cultured cells and experimental animals. Interestingly, however, an apparent threshold is observed in some epidemiological studies among those internally exposed to alpha particles. Many interesting and important issues remain, and the experimental and epidemiological data, both current as well as some classical, will be reviewed and the importance of the dose rate effects in the assessment of cancer risk will be discussed.

4.4

Molecular Dynamics simulation toward Radiation induced DNA damages.

H. Yamaguchi[1] , T. Suzuki[2] , J.G. Siebers[3], A. Furukawa[1], R.Osman[4]

1 National Institute of Radiological Sciences, Chiba, Japan

2 Graduate School of Science and Technology, Chiba University, Chiba, Japan

3. RIKEN, Gene Bank, Bioimfo Bank, Tsukuba, Japan

4. Dept. Physiology and Biophysics, Mount Sinai School of Medicine, New York, US.

The various biological effects of ionizing radiation are generally thought to be a consequence of lesions to DNA. Of all the lesions, nonreparable DNA double strand breaks (dsb) have been attributed to cellular inactivation by ionizing radiation. Still less in known about processes to lead a dsb by the interaction of water radicals (indirect effect) with DNA as well as the direct deposition of energy in DNA (direct effect). And it has been mentioned that radiation damages including the dsb are nonspecific in chemical form produced and site in a sequence of bases. Recently experimental findings have been reported as to the latter that (1)193 nm light produces single strand breaks (ssb) in single-stranded DNA as well as double-stranded DNA preferentially at guanine, (2) subsequent hole migration is inferred with localization mainly at guanine to explain these high efficiency of each guanine to cause ssb, (3)yield of the ssb at guanine depends on local sequence around the guanine for the double-stranded DNA, whereas that of the single-stranded DNA does not. Little is known yet the reason why the ssb does occur preferentially at guanine.

Here molecular dynamics simulations were performed for a dodecamer DNA containing a ssb, which has been represented by a 3'-OH deoxyribose and 5'-OH phosphate in the middle of the strand. Molecular force field parameters of the 5'-OH phosphate region were determined from *ab initio* calculation at the HF/6-31G level using the program package *GAMESS*. The DNA was placed in a periodic boundary box with water molecules and Na^+ counter ions to produce a neutralized system. After minimization, the system was heated to 300 K, equilibrated and a production run at constant NTP was executed for 1 ns using *AMBER 4.1*.

After the MD run snapshots of the ssb-containing DNA show surprisingly small conformational changes compared to normal DNA. Comparisons between ssb-containing DNA and the normal in terms of interaction energy between adjacent base steps suggest that the ssb at guanine may create more stable situation around the guanine than that of normal.

4.5

Abstract

Can't Walk and Chew: A Non-stationary View of DNA Repair

Roman Osman
Department of Physiology and Biophysics
Mount Sinai School of Medicine
New York, NY 10029, USA

Structures of damaged DNA in complex with repair enzymes show that they distort the DNA and induce a base flip into an extra helical conformation. These two dynamic elements control the efficiency of base excision repair. Through combined experimental and theoretical approaches we investigate the effect of sequence on the efficiency of uracil DNA glycosylase (UDG). We show that local DNA structure and dynamics play a role in UDG efficiency. Specifically, sequences requiring less distortion energy are better UDG substrates. Fluorescence spectroscopy using the adenine analogue, 2-aminopurine, and molecular dynamics (MD) simulations suggest a sequence-dependent bending flexibility. A full kinetic analysis of UDG activity allows the formulation of a relationship between local DNA bending flexibility and UDG activity. In an effort to extend the study to G•U mismatches, the fluorescent guanine analogue 6-methylisoxanthopterin (6MI) was characterized by spectroscopy and quantum chemistry. MD simulations of DNA with G•U and 6MI•U mismatch show sequence-dependent bending and opening properties, which depend on hydrogen bonding and base stacking. Based on the results of the simulations and experiments we present a model of specific recognition of damage by repair enzymes.

4.6

Molecular *in silico* biology of DNA repair enzymes: A trial of genome function prediction through gene positional information

Kei Yura, Hidetoshi Kono, Nobuhiro Go
Quantum Bioinformatics Group, Japan Atomic Energy Research Institute

One of the greatest challenges in post genome-sequencing era is to retrieve information out of genome sequences. We have obtained genome sequences of more than 100 species, but we have not fully been able to obtain biological information out of them. The amino acid sequences of the proteins encoded in those genomes are basically well predicted, yet biological functions of half of those proteins are remained to be discovered. A challenge for the field of bioinformatics is to establish methods to predict biological functions of those proteins. Conventional methods of function prediction are based on amino acid sequence similarity between ones predicted from genome sequences and ones of sequences in databases. Those methods do not utilize all the information in genome sequences, but only coding regions of them. We are, therefore, in a trial to utilize information other than coding regions for gene function predictions.

Proteins that functions in a concerted manner are expected to be transcribed and translated at the same time and transported to the same cellular compartments. The seemingly most effective system for co-transcription is an operon system found in prokaryotic genomes. In the operon system, a single promoter controls consecutive genes on the genome and hence the genes are transcribed at the same time. We, therefore, analyzed the functional correlations of proteins encoded in the same operons and found out that there were cases that functionally related proteins are encoded by genes within the same operon, though strength of the relationships varies on species. Based on this observation, we developed a method to predict biological functions of proteins encoded in the same operons. The method is applied to the prediction of new proteins related to DNA repair systems as a trial. In the workshop, we will discuss the result of our predictions.

JP0450229

4.7

Physical and chemical track structure of charged particles

Shuzo Uehara and Hooshang Nikjoo*

School of Health Sciences, Kyushu University, Fukuoka 812-8582, Japan

*MRC Radiation & Genome Stability Unit, Harwell, Oxfordshire, OX11 0RD, UK

Abstract

Recent progress in Monte Carlo track structure codes in radiation biology is summarised. First is a new generation of codes which simulate the full slowing down tracks of low energy ions; LEPHIST (1 keV- 1 MeV) for protons and LEAHIST (1 keV- 8 MeV) for alpha-particles. Second is a chemistry code, CHEMKURBUC, for simulation of prechemical and chemical stages of electron tracks. The reliability of the codes are verified by various quantities such as stopping powers, *W*-values, lineal energy distributions, and time-dependent *G*-values for water radicals. These codes are useful for dosimetric calculations and understanding the basic mechanism of radiation action on living cell.

Key words:

Monte Carlo track structure, Charge exchange, Microdosimetry, Chemistry code, *G*-values

1. Introduction

Monte Carlo track structure (MCTS) codes are useful tools in radiation dosimetry and biophysical modelling and have contributed significantly to the understanding of the mechanism of radiation effects [1,2]. The authors have developed a suite of codes generating physical track for electrons (KURBUC - 10 eV to 10 MeV) [3], protons (LEPHIST - 1 keV to 1 MeV) [4] and alpha-particles (LEAHIST - 1 keV to 8 MeV) [5] in water. Recently we completed the development of a chemistry code CHEMKURBUC for electron track in liquid water. This paper provides a summary of recent progress in Monte Carlo track structure codes in radiation biology.

2. Low energy ion codes

For ion energies lower than 0.3 $MeVu^{-1}$, interactions involving electron capture and loss by the moving ions become an increasingly important component of the energy loss processes. We have developed, for the first time, a new generation of MCTS codes which simulate the full slowing down tracks of low energy ions. The codes take into account all primary interactions including charge transfer processes in addition to elastic scattering, ionization and excitation. Cross-sections for bare & dressed ions and neutral atom impact were obtained from experimental data for water vapour targets. Where data were lacking the existing experimental data were fitted and extrapolated. A comprehensive

derivation of all cross sections can be found in references [4-6]. To examine the accuracy of cross sections and mean energy loss per collision data, analytical calculations of nuclear and electronic stopping powers were performed. The calculated stopping powers agreed with the ICRU data [7] within a few percentage uncertainties. The tracks of secondary electrons were generated using the electron code KURBUC. Tracks were analysed to provide confirmation on the reliability of the codes and information on physical quantities such as range, W-values, restricted stopping power, radial dose profiles and microdosimetric parameters. A detailed description can be found elsewhere [4,5].

In this paper we demonstrate an example of model calculation in microdosimetry. Tissue equivalent proportional counter (TEPC) is the principal instrument for measuring the distribution of energy deposited in a specific volume [8]. The instrument is commonly designed as a spherical or a cylindrical volume with varying sensitive volume. Figure 1 shows the dose distribution $yd(y)$ in the lineal energy y, in which the area between any two values of y indicates the dose delivered in that range. This is the standard representation of a microdosimetric spectrum. Distributions of lineal energy were simulated for 1 MeV electrons, protons and alpha-particles through a wall-less counter, 1 μm diameter, using electron, proton and alpha-particle tracks generated by the codes KURBUC, LEPHIST and LEAHIST, respectively. Values obtained for the frequency average y_F and the dose average y_D for protons and alpha-particles are in agreement with the published data.

3. Chemistry code

The KURBUC code provides the initial yields of the formation of the species H_2O^+, H_2O^* and sub-excitation electron e^-_{sub} (E<7.4 eV) at ~ 10^{-15}s. Table 1 shows the products after completion of the physical stage for various electron energies in which excited water molecule, H_2O^*, are divided into three groups: A^1B_1, B^1A_1 and Rydberg states; diffuse bands and dissociative excitations. The variation of relative yields is small over a broad range of electron energies. The code CHEMKURBUC extends the code KURBUC to the prechemical and chemical stages of electron tracks in liquid water. In the prechemical stage, during the period between 10^{-15} - 10^{-12}s, the products after completion of the physical stage, H_2O^+, H_2O^* and e^-_{sub} are converted into molecular products. Table 2 shows dissociation schemes and branching ratios taken from Ballarini et al. [9]. The spatial distribution of the chemical products at the prechemical stage was taken from Hill and Smith [10] and Cobut et al. [11]. The distribution of the distances traveled by sub-excitation electrons undergoing thermalisation processes is an important critical point in the simulation of water radiolysis. We used the average electron thermalisation distance with electron energy given by Terrissol and Beaudre [12].

A step-by-step approach was adopted for the chemical stage starting at 10^{-12}s until 10^{-6}s. During each time step of length τ, water radicals and their products were allowed to diffuse randomly with a diffusion coefficient D. Table 3 shows the values of diffusion coefficients for 11 species given by Beaudre [13]. The root mean square distance traveled, λ, was calculated according to $\lambda = (6D\tau)^{1/2}$,

and the actual distance was extracted from a Gaussian distribution. The parameter λ distributes around 0.1 nm at $\tau = 10^{-12}$s as shown in Table 3. At the end of each time step, the pair of species closer than their reaction radius were removed and replaced by the reaction products. Otherwise, the species diffuse with a random direction. A reaction radius a for each pair of interacting species A and B is derived through the relationship $a = k/4\pi(D_A+D_B)$, where k is the reaction rate constant. If the distance between A and B is shorter than $2a$, the reaction occurs. In this work we considered 11 species and 26 chemical reactions. Table 4 shows chemical reactions and values of reaction rate constants k as given by Beaudre [13].

The time-dependent yields of water radicals and molecular products generated subsequent to irradiation of water with electrons of various energies were calculated in the time range between 10^{-12}s and 10^{-6}s. Figure 2 shows calculated time-dependent yields of radical species OH and e^-_{aq} produced by 10 keV electrons in liquid water. Figure 3 shows the calculated time-dependent yields of OH and e^-_{aq} produced by 1 MeV electron tracks (only the first 10 keV of the tracks were used for the calculations) in comparison with various experimental data for OH [14] and for e^-_{aq} [14-20]. Asymptotic limit at 1 μs for e^-_{aq} is in agreement with the experimental data.

4. Summary

We have given a summary of recent progress of our data base for Monte Carlo track structure (MCTS) codes in radiation biology. We have developed a new generation of MCTS codes which simulate the full slowing down tracks of low energy ions by taking into account all primary interactions. Both the proton code, LEPHIST, and the alpha-particle code, LEAHIST, are effective below the Bragg peak region as low as 1 keV. We have developed a new chemistry code, CHEMKURBUC, which simulates the prechemical and chemical stages of electron tracks in liquid water. The new developments enable us to work on the biophysical aspects of ionising radiation of environmental interests such as radon and mechanistic interpretation of experiments with neutrons. The developments described in this paper provide the necessary tools to investigate the chemistry of low-energy ions in the chemical and biological environments.

References

[1] Nikjoo,H. and Uehara,S., Chapter 17 in: Charged particle and photon interactions with matter: chemical, physicochemical, and biological consequences with applications, edited by A.Mozumder and Y.Hatano, Marcel Dekker, New York. (in press)

[2] Nikjoo,H., Goorley,T., Fulford,J., Takakura,K. and Ito,T., Radiat.Prot.Dosim. **99** (2002) 91.

[3] Uehara,S., Nikjoo,H. and Goodhead,D.T., Phys.Med.Biol. **38** (1993) 1841.

[4] Uehara,S., Toburen,L.H. and Nikjoo,H., Int.J.Radiat.Biol. **77** (2001) 139.

[5] Uehara,S. and Nikjoo,H., J.Phys.Chem.B **106** (2002) 11051.

[6] Uehara,S., Toburen,L.H., Wilson,W.E., Goodhead,D.T. and Nikjoo,H., Radiat.Phys.Chem. **59** (2000) 1.

[7] ICRU, Report 49 (1993).

[8] Nikjoo,H., Khvostunov,I.K. and Cucinotta,F.A., Radiat.Res. **157** (2002) 435.

[9] Ballarini,F., Biaggi,M., Merzagora,M., Ottolenghi,A., Dingfelder,M., Friedland,W., Jacob,P. and Paretzke,H.G., Radiat.Environ.Biophys. **39** (2000) 179.

[10] Hill,M.A. and Smith,F.A., Radiat.Phys.Chem. **43** (1994) 265.

[11] Cobut,V., Frongillo,Y., Patau,J.P., Goulet,T., Fraser,M.J. and Jay-Gerin,J.P., Radiat.Phys.Chem. **51** (1998) 229.

[12] Terrissol,M. and Beaudre,A., Radiat.Prot.Dosim. **31** (1990) 175.

[13] Beaudre,A., These de l'Universite Paul Sabatier, Toulouse, France, no.371 (1988).

[14] Jonah,C.D. and Miller,J.R., J.Phys.Chem. **81** (1977) 1974.

[15] Jonah,C.D., Hart,E.J. and Matheson,M.S., J.Phys.Chem. **77** (1973) 1838.

[16] Jonah,C.D., Matheson,M.S., Miller,J.R. and Hart,E.J., J.Phys.Chem. **80** (1976) 1267.

[17] Buxton,G.V., Proc.R.Soc.Lond.A **328** (1972) 9.

[18] Shiraishi,H., Katsumura,Y., Hiroishi,D., Ishigure,K. and Washio,M., J.Phys.Chem. **92** (1988) 3011.

[19] Sumiyoshi,T. and Katayama,M., Chem.Lett. **12** (1982) 1887.

[20] Wolff,R.K., Bronskill,M.J., Aldrich,J.E. and Hunt,J.W., J.Phys.Chem. **77** (1973) 1350.

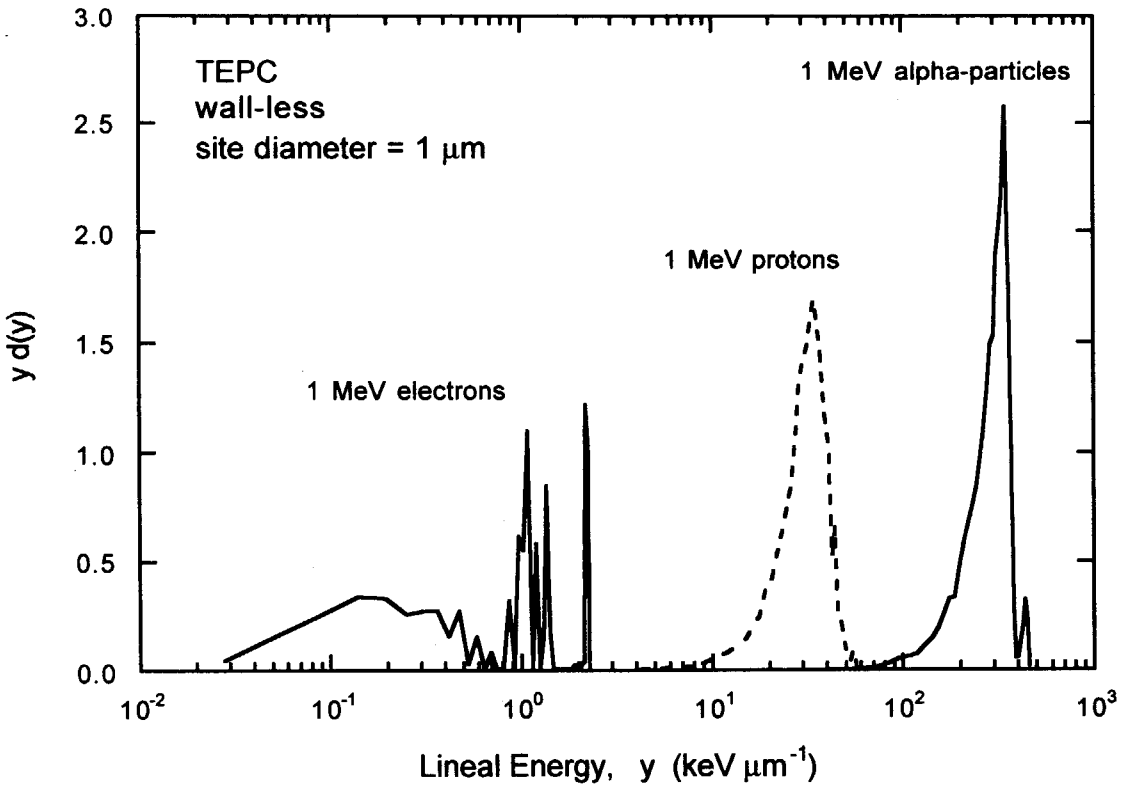

Fig. 1

Calculated lineal energy distributions $yd(y)$ of 1 MeV electrons, protons and alpha-particles in simulated wall-less tissue-equivalent proportional counter (TEPC) for a site diameter 1 μm. The values of y_F were 0.13, 26.4 and 244 keVμm^{-1}, and those of y_D were 0.52, 30.4 and 281 keVμm^{-1} for electrons, protons and alpha-particles, respectively.

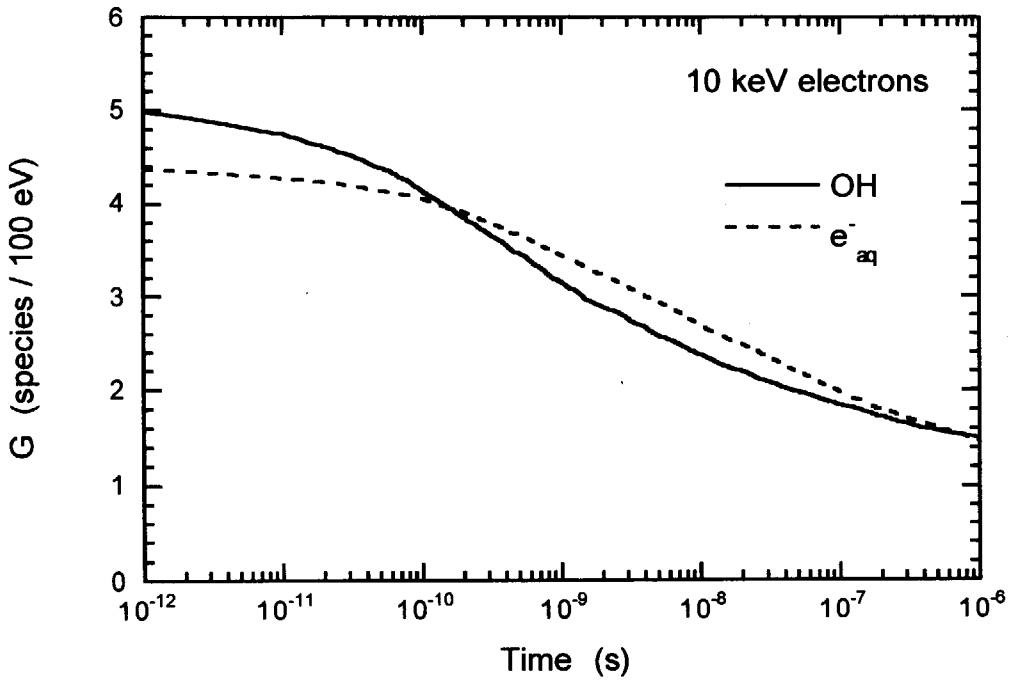

Fig. 2

Calculated time-dependent yields of radical species OH and e^-_{aq} produced by 10 keV electrons (full tracks) in liquid water.

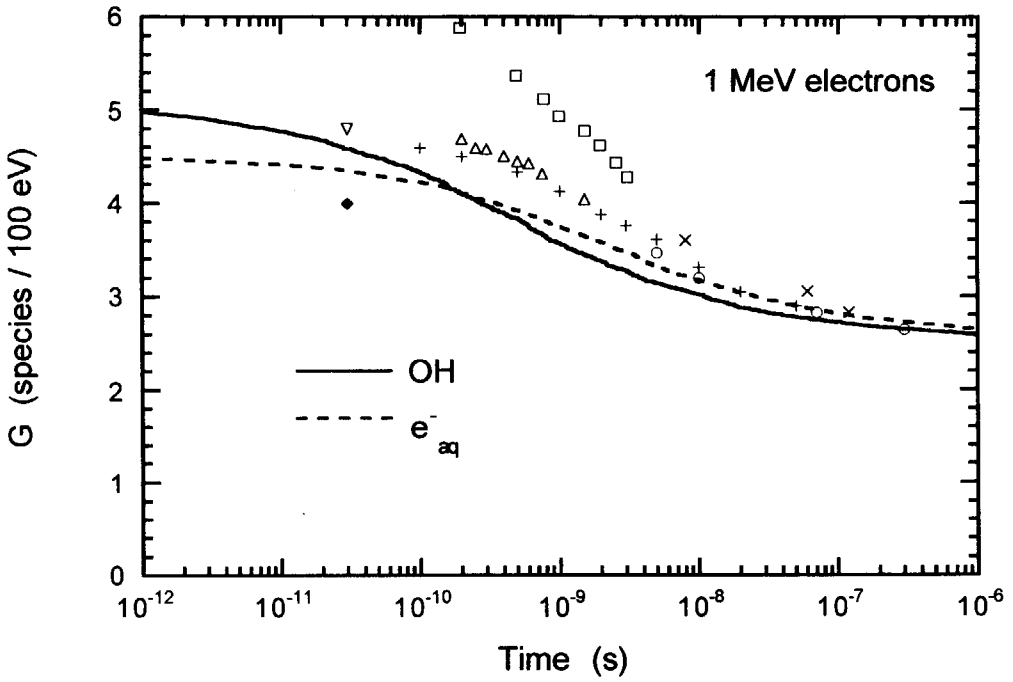

Fig. 3

Calculated time-dependent yields of OH and e^-_{aq} produced by 1 MeV electron tracks (the first 10 keV of the tracks only) in comparison with experimental data for OH (□ [14]) and for e^-_{aq} (+ [15,16], Δ [14], × [17], O [18], ∇ [19], ◆ [20]).

Table 1

Products after completion of the physical stage (sub-excitation electrons, ionised water molecules and excitations: A^1B_1, B^1A_1, Rydberg states (Ry); diffuse bands (db) and dissociative excitations (de)).

Electron Energy	e^-_{sub}	H_2O^+	H_2O^*		
			A^1B_1	B^1A_1	(Ry,db,de)
	%	%	%	%	%
200 eV	34.6	29.9	12.1	4.2	19.2
1 keV	33.5	32.5	11.7	3.7	18.6
10 keV	32.8	32.7	11.7	3.6	19.2
1 MeV	33.2	33.1	10.7	3.9	19.1

Table 2

Dissociation schemes and branching ratios [9].

Physical Product		Decay Channel	Probability (%)
e^-_{sub}		e^-_{aq}	100
H_2O^+		$H_3O^+ + OH$	100
H_2O^*			
	A^1B_1	H_2O	35
		$H + OH$	65
	B^1A_1	H_2O	23
		$H_3O^+ + OH + e^-_{aq}$	50
		$H + OH$	20
		$2H$	3.9
		$H_2 + H_2O_2$	3.1
	(Ry,db,de)	H_2O	50
		$H_3O^+ + OH + e^-_{aq}$	50

Table 3

Radical species and values of diffusion coefficients D ($10^{-9}m^2s^{-1}$) [13]. The root mean square distance traveled λ (nm) was calculated according to $\lambda = (6D\tau)^{1/2}$.

Species	D	λ ($\tau = 10^{-12}s$)
OH	2.8	0.130
e^-_{aq}	4.5	0.164
H	7.0	0.205
H_3O^+	9.0	0.232
H_2	5.0	0.173
H_2O_2	2.2	0.115
HO_2	2.0	0.110
O_2	2.1	0.112
OH^-	5.0	0.173
O_2^-	2.1	0.112
HO_2^-	2.0	0.110

Table 4

Chemical reactions and values of reaction rate constants k ($10^{10}dm^3mol^{-1}s^{-1}$) [13]. The reaction radius a (nm) is obtained by $a = k/4\pi(D_A+D_B)$.

Reaction	Products	k	a
$OH + OH$	$---> H_2O_2$	0.6	0.1416
$OH + e^-_{aq}$	$---> OH^-$	2.5	0.4525
$OH + H$	$---> H_2O$	2.0	0.2697
$OH + H_2$	$---> H$	0.0045	0.00076
$OH + H_2O_2$	$---> HO_2$	0.0023	0.00061
$OH + HO_2$	$---> O_2$	1.0	0.2753
$OH + O_2^-$	$---> O_2 + OH^-$	0.9	0.2427
$OH + HO_2^-$	$---> HO_2 + OH^-$	0.5	0.1376
$e^-_{aq} + e^-_{aq}$	$---> H_2 + 2OH^-$	0.55	0.0807
$e^-_{aq} + H$	$---> H_2 + OH^-$	2.5	0.2873
$e^-_{aq} + H_3O^+$	$---> H$	1.7	0.1664
$e^-_{aq} + H_2O_2$	$---> OH + OH^-$	1.3	0.2564
$e^-_{aq} + HO_2$	$---> HO_2^-$	2.0	0.4066
$e^-_{aq} + O_2$	$---> O_2^-$	1.9	0.3804
$e^-_{aq} + O_2^-$	$---> OH^- + HO_2^-$	1.3	0.2603
$H + H$	$---> H_2$	1.0	0.0944
$H + H_2O_2$	$---> OH$	0.01	0.00144
$H + HO_2$	$---> H_2O_2$	2.0	0.2936
$H + O_2$	$---> HO_2$	2.0	0.2904
$H + OH^-$	$---> e^-_{aq}$	0.002	0.00022
$H + O_2^-$	$---> HO_2^-$	2.0	0.2904
$H_3O^+ + OH^-$	$---> H_2O$	10.0	0.9439
$H_3O^+ + O_2^-$	$---> HO_2$	3.0	0.3571
$H_3O^+ + HO_2^-$	$---> H_2O_2$	2.0	0.2403
$HO_2 + HO_2$	$---> H_2O_2 + O_2$	0.000076	0.000025
$HO_2 + O_2^-$	$---> O_2 + HO_2^-$	0.0085	0.00274

4.8

Modeling of Dose Rate Effects on Cellular Responses to Low Dose Gamma-Irradiation

Junji Magae[1] and Hiromitsu Ogata[2]

[1]*Institute of Research and Innovation, 1201 Takada, Kashiwa 277-0861, Japan*
[2]*National Institute of Public Health, 2-3-6, Minami, Wako, Saitama 351-0197 Japan*

Linear non-threshold (LNT) theory which demonstrates that stochastic biological effects of radiation is linearly correlated to irradiation dose without threshold, is a basic theory for radioprotection. While LNT dose not consider irradiation time or dose-rate, biological responses to radiation are complex processes which are dependent on irradiation time as well as total dose, suggesting it necessary to include dose and dose-rate simultaneously to predict the risk of long term irradiation with low dose-rate. LNT is based on studies at high dose/high dose-rate, and experimental and epidemiological studies that can evaluate LNT at low dose/low dose-rate are not sufficiently accumulated. Because the quantitative relationship between biological responses and radiation exposure at low dose/low dose-rate remains to be elucidated, arguments for LNT at low dose/low dose-rate are confusing. In this study, we mathematically and statistically analyzed quantitative relationship among dose, dose rate and irradiation time using chromosomal breakage and proliferation inhibition of human cells as indicators of biological responses.

While we found no dose-rate effect in the exposure time less than 100 min, it turned evident in the exposure time more than 5 h, and these biological responses were dependent on dose-rate rather than dose when cells were irradiated for 5 to 30 days. We applied some mathematical models to analyze dose-response relationship, and found that observed data were fitted well by a generalized logistic regression model. By including "dose-rate", "irradiation time" and "total dose" to the model as explanatory variables, it was shown that dose-rate effect was remarkable when irradiation time was long. When dose-rate was very low (less than 0.01 Gy/h), the biological responses were reduced close to the control level. Furthermore, we used a numerical model of relationships between effective doses (ED_{50} or ED_{30}) and dose-rates to investigate dose-rate effect on dose-response curve. As a result of this analysis, it was clear that the dose-rate effect was remarkable at low dose-rate and that it was relatively trivial at high dose-rate. This relationship was well described by an exponential function when logarithm of effective doses and logarithm of dose-rates were plotted. By this model, it was suggested that biological risk was very low at low dose-rate and that it depends on total dose at high dose-rate. As the effective dose approaches infinity, the risk approaches to 0 at infinitely low dose rate. Our study demonstrates that biological responses at low dose-rate are remarkably affected by exposure time, and that they are dependent on dose-rate rather than total dose in the case of long-term irradiation.

4.9

Recent Development of Radiation Chemistry in Aqueous Solutions

Yosuke Katsumura
Nuclear Engineering Res. Lab., School of Engineering, The University of Tokyo
2-22 Shirakata Shirane, Tokai-Mura, Ibakagi, 319-1188, Japan
katsu@q.t.u-tokyo.ac.jp

Radiation chemistry of water is an important subject closely related not only to physical chemistry but also to nuclear technology and radiation biology and, thus, much work has been done up to now. It can be said that the basic understanding of radiation-induced reactions taking place in aqueous solutions has been well established from a practical viewpoint.

Recently, much experimental work on radiolysis of aqueous solutions at elevated temperatures has been conducted and primary yields of water decomposition products as a function temperature up to 300°C have been determined by different research groups in UK, Canada, USA and Japan. At nuclear power plants quality control of the coolant water plays a key role to reduce the radiation exposure to the workers in the plant and to keep the integrity of the plant. Radiolysis data is inevitably important to evaluate the chemical condition such as concentrations of radiation induced oxygen and hydrogen peroxide in the coolant water and corrosion potential of the material in nuclear power plants. It is known that these concentrations strongly control the condition of the stress corrosion cracking, so called SCC in the primary circuit of the reactor.

The values of $g(e^-_{aq})$, g(OH), $g(H_2)$ and g(H) are all increasing almost linearly with increasing temperature up to 300°C. Here, g(X) stands for the primary yield of the product X. About 40% increase was found for $g(e^-_{aq})$ and more than 80% for g(OH) at 300°C as compared with the data at ambient temperature. On the contrary, $g(H_2O_2)$ is decreasing. The theoretical calculations based on spur diffusion model and Monte Carlo method have been applied and the temperature dependence has been explained satisfactorily.

In addition, in these few years, several reports doing the experiment at much higher temperature in supercritical water (>374°C and >22.1 Mpa) have been published.

In the present paper, both recent radiation chemical experiments of aqueous solution at elevated temperatures and theoretical approaches will be reviewed.

Recent Development of Radiation Chemistry in Aqueous Solutions

Yosuke Katsumura

Nuclear Engineering Research Laboratory,
The University of Tokyo
2-22 Shirakata Shirane, Tokai, Ibaraki, 319-1188 Japan
katsu@q.t.u-tokyo.ac.jp

Introduction

Water, H_2O; most popular molecule

1902 Gas consisting H_2 and O_2 is constantly liberated from aqueous solution of radium bromide.

↓ *radiation chemistry of water*
100 years history

enough knowledge → practical applications

1. Physical chemistry, chemical kinetics
2. Radiation effects in nuclear technologies
3. Radiation biology & radiation therapy

Today's topics

(a) picosecond yield of e^-_{aq}
(b) radiolysis of water up to 300°C
(c) radiolysis of supercritical water

(a) picosecond yield of e^-_{aq}

Radiolysis of liquid water

H_2O -∧∧∧→ e^-_{aq}, H^+, OH, H_2, H_2O_2, ...

Temporal behavior of the species *ps -> μs, ms ...*

G-value of e^-_{aq}; hydrated electron

Univ of Tront; stroboscopic
4.0±0.2 (1973), 4.6 (1975) at 30 ps
ANL; stroboscopic & laser correlation (2000)
4.1 (1973), 4.6 (1976), 4.8 (1996), 4.0 (2000) at 100 ps
Hokkaido Univ.; stroboscopic
4.8 (1985) at 30 ps

"a big contradiction from 4.0 to 4.8 at ps time scale"
problem: dose evaluation

Reconciliation of the ps yield of e^-_{aq}

Experimental approach

$G(e^-_{aq})$ in ps scale and ns & μs under the same condition

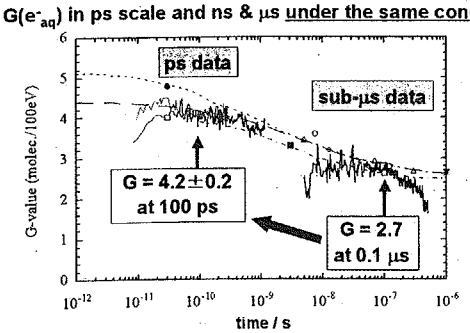

(a) picosecond yield of e^-_{aq}

- $G(e^-_{aq})$ in ps time region has been reevaluated by a fs laser driven pulse radiolysis system.
- A value of $G(e^-_{aq})$ = 4.2±0.2 was obtained.
- Monte Carlo calculation can explain the experimental results.

(b) radiolysis of water up to 300°C

Radiolysis of water at elevated temp.

- Importance of the (coolant) water chemistry in reactors
  - To reduce of exposure dose to personnel
  - To avoid the stress corrosion cracking (SCC)
  - ⇨ Water control
    - ◊ H_2 injection (HWC)
    - ◊ Noble Metal Chemical Addition (NMCA)

High temperature
High pressure
Intense radiation
⇒ Coolant chemistry
- Chemical condition
  $[H_2O_2]$, $[O_2]$
- Corrosion condition

Modeling of water radiolysis
- G-values, rate constants

⇒ Computer simulation

A reaction set for water radiolysis ≈ 40 reactions

	Forward reaction	Reverse reaction	Forward reaction rate const. at 285°C	Reverse reaction rate const. at 285°C
1	e^- + H2O	H + OH-	1.69E+02	-
2	e^- + H_3O^+	H	2.54E+11	1.00E+05
3	e^- + OH	OH-	3.17E+11	-
4	e^- + H2O2	OH + OH-	1.38E+11	-
5	H + H	H2	1.06E+11	-
6	e^- + HO2	HO2-	2.12E+11	-
7	e^- + O2	O2-	2.01E+11	-
8	e^- + e^- + H2O + H2O	OH- + H2 + OH-	1.74E+07	-
9	OH + OH	H2O2	4.76E+10	-
10	OH- + H	e^- + H2O	6.88E+08	-
11	e^- + H + H2O	OH- + H2	4.76E+09	-
12	e^- + HO2- + H2O	OH + OH- + OH-	6.67E+08	-
13	H + OH	H2O	2.12E+11	-
14	OH + H2	H + H2O	1.27E+09	1.10E+03
15	H + O2	HO2	2.01E+11	-
16	H + HO2	H2O2	2.11E+11	-
17	H + O2-	HO2-	2.11E+11	-
18	e^- + O2- + H2O	HO2- + OH-	1.13E+08	-
19	H + H2O2	OH + H2O	3.07E+09	-
20	OH + H2O2	H2O + HO2	3.91E+08	-
21	OH + HO2	H2O + O2	1.27E+11	-
22	OH- + H2O2	HO2- + H2O	1.72E+10	1.18E+05
23	HO2 + HO2	H2O2 + O2	9.29E+07	-
24	HO2	O2- + H^+	8.46E+06	5.29E+11
25	HO2 + O2-	O2 + HO2-	5.16E+08	-
26	H^+ + OH-	H2O	1.48E+12	1.81E-01
27	O2- + OH	OH- + O2	1.27E+11	-
28	2O2- +2H2O	O2 + H2O2 +2OH-	1.93E+05	-
29	2H2O2	2H2O + O2	-	-

G-values of water decomposition products at elevated temp.

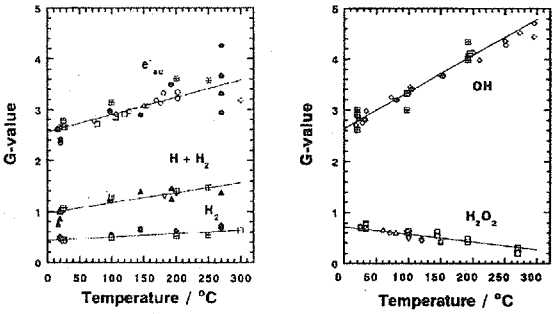

Modeling of BWR primary circuit

Block; (n, γ), flow velocity, pressure, temp., shape

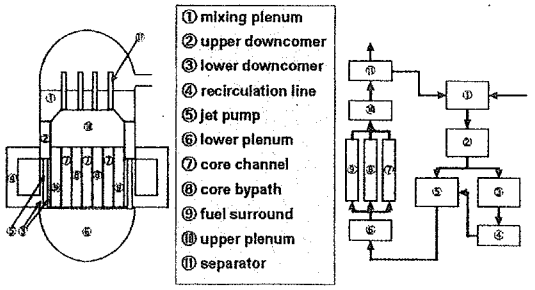

Analysis of $[H_2O_2]$

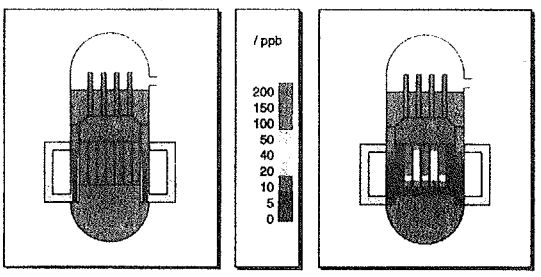

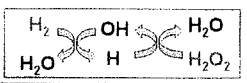

(b) radiolysis of water up to 300°C

Up to 300°C, data set of G-values and rate constants for the water decomposition products has been accumulated and widely used for practical application.

(c) radiolysis of supercritical water

What is supercritical water?

T_c > 374 °C, P_c > 22.1 MPa

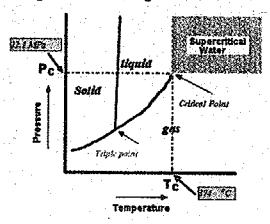

Density; pressure dependent
at 400°C 25 MPa 0.166 g/cc
35 MPa 0.475 g/cc
Low dielectric constant, ε
Hydrogen bond breakage
pK_w; pressure dependent
Large heat capacity

application
SCWO
(Supercritical Water Oxidation)
SCR
(Supercritical water-cooled reactor)

Radiolysis Study of SCW

- **Basic data for *SCR***
  - **G-value of water decomposition**
  - **Rate constants of the reactions**
- **Interests from *radiation chemistry***
  - **Observation of transient species in SCW**
  - **Effect of low dielectric constant**
- **Practical application to *SCWO***
- **Fundamental data for theoretical calculation**

→ *pulse radiolysis of SCW*
→ *steady state irradiation of SCW*

Schematic Diagram of SCW Experiment

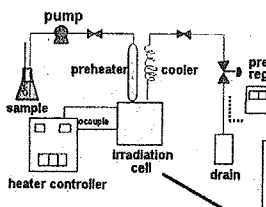

Cell structure

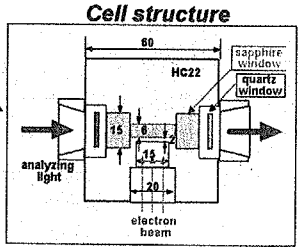

Optical path; 15 mm
Pulse; 10-100 ns
≈ 10-50 Gy/pulse

Estimate Yields of primary Species using Methyl Viologen as Scavenger

Important reactions of MV^{2+} aqueous solutions

in presence of NaCOOH → $G(e_{aq}^- + OH + H)$

$OH + HCOO^- \rightarrow COO^{\bullet-} + H_2O$	$3.2 \times 10^9\ M^{-1}s^{-1}$
$H + HCOO^- \rightarrow COO^{\bullet-} + H_2$	$2.1 \times 10^9\ M^{-1}s^{-1}$
$COO^{\bullet-} + MV^{2+} \rightarrow MV^{\bullet+} + CO_2$	$1 \times 10^{10}\ M^{-1}s^{-1}$
$e_{aq}^- + MV^{2+} \rightarrow MV^{\bullet+}$	$5 \times 10^{10}\ M^{-1}s^{-1}$

can be applied up to 200 °C !!

in presence of tert-butanol → $G(e_{aq}^-)$

$e_{aq}^- + MV^{2+} \rightarrow MV^{\bullet+}$	$5 \times 10^{10}\ M^{-1}s^{-1}$

Spectra of $MV^{+\bullet}$ at different temperatures

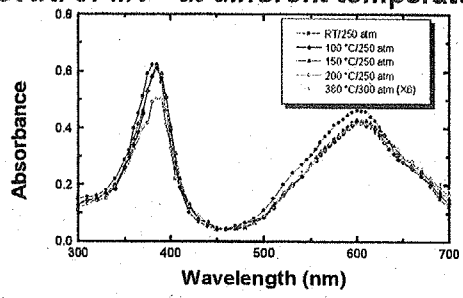

Absorption spectra of $MV^{+\bullet}$ recorded at 2 μs after electron pulse
For 380°C/ 300 atm: 0.5 mM MV^{2+} & 50 mM *tert*-butanol.
For other temperatures: 0.5 mM MV^{2+} &10 mM NaCOOH.

How to eveluate G-values of e^-_{aq}, H, OH

Reactions: at room temperature

$OH + HCOO^- \rightarrow COO^{-\bullet} + H_2O$	$3.2 \times 10^9\ M^{-1}s^{-1}$
$H + HCOO^- \rightarrow COO^{-\bullet} + H_2$	$2.1 \times 10^8\ M^{-1}s^{-1}$
$COO^{-\bullet} + MV^{2+} \rightarrow MV^{+\bullet} + CO_2$	$1 \times 10^{10}\ M^{-1}s^{-1}$

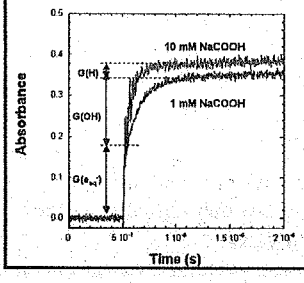

0.5 mM MV^{2+} solutions containing
1 and 10 mM NaCOOH.
Temperature: 100 °C,
Ar bubbling, dose: 30.6 Gy.

G-values of e_{aq}^-, OH, H *vs* temperature

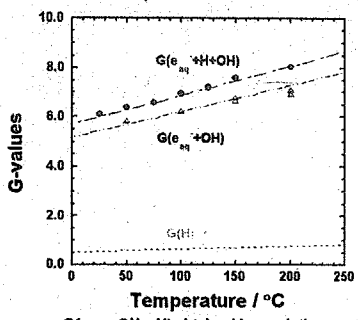

G(e_{aq}^- + OH + H) obtained in a solution containing
0.5 mM MV^{2+} & 10 mM NaCOOH at a dose of 23.1 Gy.
Dash line: from Elliot's report (AECL-11073, COG-94-167, 1994).

Temperature dependence of e^-_{aq}

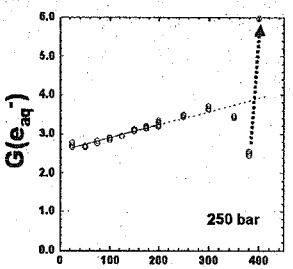

sample:
0.5 mM MV^{2+}
0.1 M tert-BuOH

ε values are from Shiraishi *et al. Radiat. Phys. Chem.* 33, 519 (1989) and extrapolated from 200 °C to 400 °C

First observation of $G(e^-_{aq})$ in SCW

Pressure dependence of $G(e^-_{aq})$

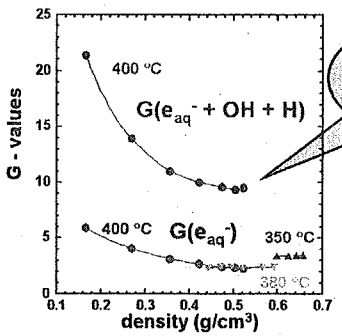

Pressure dependence !!!

Solution:
0.5 mM MV^{2+}
0.1 M tert-BuOH
or
0.1 M EtOH

(c) radiolysis of supercritical water

- Radiation chemistry of supercritical water has started.
- A significant pressure effect has been found.
- These new phenomena are good subjects for theoretical considerations.

Conclusion

- **$G(e^-_{aq})$ in picosecond has been reconciled. New data at ANL & UTNL are smaller than old ones. A Monte Carlo calculation is able to reproduce the new data**
- **Data of the G-values of water decomposition and rate constants up to 300°C have been measured and widely used for practical evaluation in power plants.**
- **The $G(e_{aq}^-)$ has been estimated for the first time in SCW. The values are strongly dependent on pressure (density) in SCW.**

4.10

Three-dimensional structural view of branch migration in DNA homologous recombination

Kosuke Morikawa

Department of Structural Biology
Biomolecular Engineering Research Institute (BERI),
6-2-3 Furuedai, Suita,
Osaka 565-0874, Japan
morikawa@beri.or.jp

At the late stage of recombinational repair in prokaryotes, RuvA, RuvB, and RuvC proteins process the Holliday junction through formation of two types of complexes, which catalyze branch migration (RuvAB) and resolution (RuvABC resolvasome), respectively. We determined the three-dimensional structures of all three protein components by X-ray crystallography. The crystal structure of the RuvA-Holliday junction complex revealed that two base pairs near the crossover point are disrupted, suggesting the positive mechanistic role of RuvA in the branch migration. The crystal structure of the *E.coli* RuvC dimer indicated the catalytic centre of this resolvase, and allowed us to build a Holliday junction model bound to RuvC. The crystal structure of the *Thermus thermophilus* RuvB protomer revealed the RuvB architecture, classified into the AAA+ family, and the environments of the ATP or ADP binding site. The X-ray structure of the RuvA-RuvB complex, determined more recently, has revealed that two RuvA tetramers form the symmetric and closed octameric shell, where four RuvA domain IIIs spring out in the two opposite directions to be individually caught by a single RuvB. The binding of domain III deforms the protruding β-hairpin in the N-terminal domain of RuvB, and thereby appears to induce a functional and less symmetric RuvB hexameric ring structure. The fitting of this complex structure into the averaged electron microscopic images of the RuvA-RuvB-junction DNA ternary complex allows the model building, which implies that the functional scheme with a fixed RuvA-RuvB interaction may be preferable to that with their rotational interaction.

4.11

Functional analysis of repair enzymes for oxidative DNA damage in mammalian cells

Akira Yasui (Department of Molecular Genetics, Institute of Development, Aging and Cancer, Tohoku University)

Most living organisms utilize oxygen as their major energy source, but they also suffer from the toxic effects of oxygen on their cells. Oxidative damage to DNA is thought to constitute a major factor in mutagenesis and genome instability. Furthermore, age-dependent accumulation of oxidative DNA damage in nuclear and mitochondrial DNA suggests that oxidative DNA damage is a causative factor for human aging as well. Living cells have, however, several defense systems against oxidative stress. One of the protection mechanisms is DNA repair, which removes oxidative DNA damage and restores genetic information. Thymine glycol, a potentially lethal DNA lesion produced by reactive oxygen species, can be removed by DNA glycosylase, *Escherichia coli* Nth (endonuclease III) or its mammalian homologue NTH1. We have previously found that mice deleted in the *Nth* homologue still retain at least two residual glycosylase activities for thymine glycol. We report herein that in cell extracts from the *mNth1*-knockout mouse there is a third thymine glycol glycosylase activity, that is encoded by one of three mammalian proteins with sequence similarity to *Escherichia coli* Fpg (MutM) and Nei (endonuclease VIII). Tissue expression of this mouse Nei-like (designated as *Neil1*) gene is ubiquitous and suggests that NEIL1 is a back-up glycosylase for NTH1 with unique substrate specificity and tissue specific expression.

DNA single-strand breaks (SSB) are another most frequent DNA lesions produced by reactive oxygen species and during DNA metabolism, but the cellular responses to and DNA repair of SSB remain elusive. Using human cells expressing UV damage endonuclease, which introduces SSB at various UV lesions, poly(ADP-ribose) synthesis occurs immediately in the UV-irradiated area. Simultaneously, but dependent on poly(ADP-ribosyl)ation, XRCC1 is translocated from nucleoli as well as nucleoplasmic foci to the SSB. The BRCT1 domain of XRCC1 protein is indispensable for its poly(ADP-ribose)-dependent recruitment to the SSB. Proliferating cell nuclear antigen and the p150 subunit of chromatin assembly factor 1 also accumulate at the SSB in a detergent-resistant form, that is significantly reduced by inhibition of poly(ADP-ribose) synthesis. Our results show the importance of poly(ADP-ribosyl)ation in sequential cellular responses to SSB.

REFERENCES

(1) Takao M, Kanno S, Kobayashi K, Zhang Q-M, Yonei S, van der Horst G, and Yasui A. A back-up glycosylase in *Nth1*-knockout mice is a functional Nei (endonuclease VIII) homologue. *J. Biol. Chem.* 277, 42205-42213, 2002.

(2) Chigancas V, Batista LF, Brumatti G, Amarante-Mendes GP, Yasui A, Menck CF. Photorepair of RNA polymerase arrest and apoptosis after ultraviolet irradiation in normal and XPB deficient rodent cells. *Cell Death Differ.* 9, 1099-1107, 2002.

(3) Schul W, Jans J, Rijksen YMA, Klemann HM, Eker APM, de Wit J, Nikaido O, Nakajima S, Yasui A, Hoeijmakers JHJ, and van der Horst GTJ. Enhanced repair of cyclobutane pyrimidine dimers and improved UV resistance in photolyase transgenic mice. *EMBO J.* 21, 4719-4729, 2002.

(4) Miiyabe I., Zhang QM., Kino K., Sugiyama H., Takao M., Yasui A., and Yonei S. Identification of 5-formyluracil DNA glycosylase activity of human hNTH1 protein. *Nucleic Acids Res.* 30, 3454-3463, 2002.

(5) Takao M, Kanno S, Shiromoto T, Hasegawa R, Ide H, Ikeda S, Sarker AH, Seki S, Xing JZ, Le XC, Weinfeld M Kobayashi K, Miyazaki J, Muijtjens M, Hoeijmakers JHJ, van der Horst G, and Yasui. A Novel nuclear and mitochondrial glycosylases revealed by disruption of the mouse *Nth1* gene encoding an endonuclease III homologue for repair of thymine glycol. *EMBO J.* 21. 3486-3493, 2002

4.12

Misincorporation of oxidized dNTPs by archaeal Y-family DNA polymerases

Masatomi Shimizu[1,4], Petr Gruz[1], Hiroyuki Kamiya[2], Su-Ryang Kim[1], Francesca M. Pisani[3], Yusuke Kanke[4], Hideyoshi Harashima[2] and Takehiko Nohmi[1]
([1]National Institute of Health Sciences, [2]Otsuma Women's Univ., [3]Hokkaido Univ., [4]Istituto di Biochimica delle Proteine, CNR, Italy)

The recently identified Y-family DNA polymerases comprise proteins from different species including bacteria, eukarya and archaea. The most distinct feature of the polymerases is their ability to replicate DNA past damaged sites (translesion DNA synthesis). Some reactions they catalyze are error free (correct bases are inserted opposite template lesions), while others are error prone. Thus, the polymerases appear to play important roles in DNA damage tolerance and mutagenesis. Currently, two Y-family DNA polymerases are purified from the archaeon *Sulfolobus solfataricus* strains P1 (*Sso* P1 DNA pol Y1 or DBH) and P2 (*Sso* P2 DNA pol Y1 or Dpo4) and their structural features are determined in very detail. Since the optimal growth temperature of *S solfataricus* is more than 80°C, and the DNA is continuously exposed to heat-induced deamination, depurination and oxidation, the Y-family DNA polymerases seem to be involved in the translesion bypass of damaged DNA in the organisms. In fact, these archaeal DNA polymerases are shown to bypass a variety of DNA lesions in the template DNA (1). Here, we report an additional feature of *Sso* P1 and P2 DNA pol Y1: incorrect incorporation of oxidized dNTPs (8-hydroxy-dGTP and 2-hydroxy-dATP) into nascent DNA. Oxidation of the dNTP pool as well as DNA is a main source of genome instability, and the incorporation of oxidized dNTPs into DNA leads to spontaneous mutagenesis and carcinogenesis. The archaeal Y-family DNA polymerases exclusively incorporated 8-hydroxy-dGTP opposite template A, and incorporated 2-hydroxy-dATP opposite template G more efficiently than opposite template T (Fig. 1). The estimated percentages of incorporation of 2-hydroxy-dATP opposite template G versus template T were 63% and 57% by P1 and P2 Y family DNA polymerases, respectively. The incorporated oxidized dNMPs did not block further extension of the nascent strand. In contrast, Klenow fragment exo$^-$ and *Sso* P2 DNA pol B1, which is responsible for the chromosomal replication of *S. solfataricus* P2, incorporated 8-hydroxy-dGTP opposite template A and C at almost equal efficiency, and exclusively incorporated 2-hydroxy-dATP opposite template T. The results suggest the possibility that the Y-family DNA polymerases promote mutagenesis through the erroneous incorporation of the oxidized dNTPs during DNA synthesis in addition to facilitating translesion DNA synthesis (2).

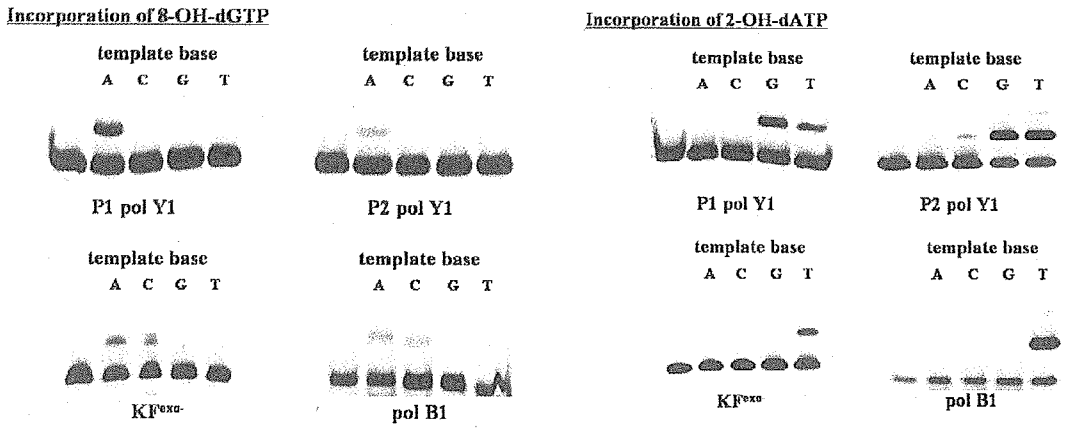

Fig. 1 Misincorporation of 8-hydroxy-dGTP and 2-hydroxy-dATP by Sso P1 and P2 DNA pol Y1.

References

1. Gruz, P., Pisani, F. M., Shimizu, M., Yamada, M., Hayashi, I., Morikawa, K., and Nohmi, T. Synthetic activity of Sso DNA polymerase Y1, an archaeal DinB-like DNA polymerase, is stimulated by processivity factors proliferating cell nuclear antigen and replication factor C, *J.Biol.Chem.* **276,** 47394-47401, 2001.

2. Shimizu, M., Gruz, P., Kamiya, H., Kim, S.-R., Pisani, F.M., Masutani, C., Kanke, Y., Harashima, H., Hanaoka, F. and Nohmi, T. Erroneous incorporation of oxidized DNA precursors by Y-family DNA polymerases, EMBO reports, in press.

4.13

Role of RecA Protein in Radiation Resistance of *Deinococcus radiodurans*

Issay NARUMI[1], Katsuya SATOH[1], Hirofumi OHBA[1,2], Masahiro KIKUCHI[1]
([1]JAERI Takasaki, [2]Grad. Sch. Arg., Utsunomiya Univ.)

Deinococcus radiodurans is well known as a representative of bacteria that exhibit resistance to ionizing radiation. They can survive exposure to γ radiation in excess of 5,000 Gy without any loss of viability or evidence of induced mutation. The dose causes fragmentation of its genome by introducing hundreds of DNA double strand breaks. Indeed, *D. radiodurans* reconstructs a functional genome from the fragments within a few hours. Since *D. radiodurans* genome is polyploid in nature, the repair process of the irradiation-induced DNA double strand breaks is thought to occur mainly through homologous intergenomic recombination.

Among proteins required for recombinational DNA repair, RecA is the most important protein. The RecA protein is found in virtually all bacteria, and structural and functional homologs of RecA is found in archaea and eukaryotes. Hence, recombinational DNA repair appears to be a ubiquitous process. The RecA protein of *Escherichia coli* is a multifunctional protein with roles in homologous genetic recombination, recombinational DNA repair, the regulation of DNA damage response, and SOS mutagenesis. *D. radiodurans* has a single RecA-encoding gene. The RecA proteins of *D. radiodurans* and *E. coli* exhibit 56% sequence identify. We have shown that the recombinational DNA repair activity of the *D. radiodurans* RecA protein is very similar to that of the *E. coli* counterpart.

As expression of the deinococcal *recA* gene was enhanced after γ irradiation, the *D. radiodurans recA* gene seemed to be a member of a DNA damage response regulon. However, the induction ratio was not so high. Instead, a remarkable increase in *recA* promoter activity was found in a middle stage of exponential growth under normal cultivation conditions. This elevated activity may reflect the basic functions of RecA, such as recombination during natural transformation and the repair of double strand breaks that can frequently arise during the cause of normal DNA replication.

As is the case with the *E. coli* RecA, the *D. radiodurans* RecA possesses co-protease activity by which LexA protein, a repressor of DNA damage response, is inactivated. We discovered a RecA mutant protein that is defective in the recombination activity but retains the co-protease activity. *D. radiodurans* carrying this RecA mutation was only slightly sensitive to ionizing radiation whereas *D. radiodurans* carrying a RecA null mutation was extremely radiation sensitive. This indicates that the regulatory function rather than the recombination function of RecA contributes to the extraordinary radiation resistance of *D. radiodurans*.

1. Narumi et al. (1999) Mutation Research DNA Repair 435: 233-243.
2. Kikuchi et al. (1999) FEMS Microbiology Letters 174: 151-157.
3. Narumi et al. (2001) Journal of Bacteriology 183: 6951-6956.
4. Satoh et al. (2002) Journal of Biochemistry 131: 121-129.

Recovery of DNA double stand breaks following γ-irradiation

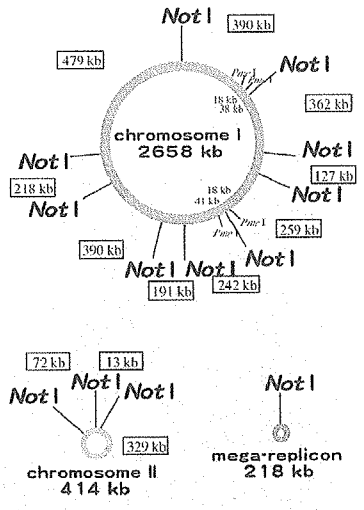

Physical Map of *D. radiodurans* genome

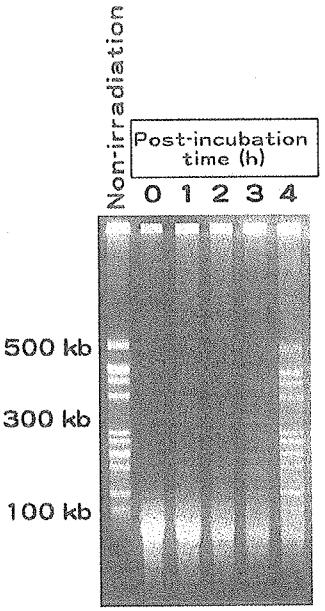

Pulsed-field gel electrophoresis analysis

Deinococcus radiodurans genome is polyploid in nature

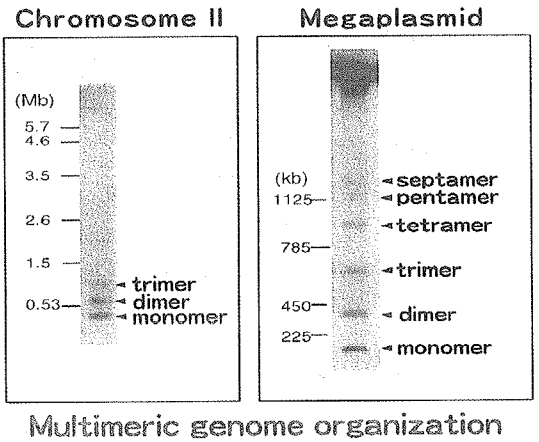

Multimeric genome organization

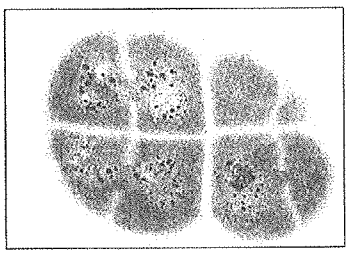

Nucleoid structure of stationary phase cells

Templates for homologous recombination are always available !

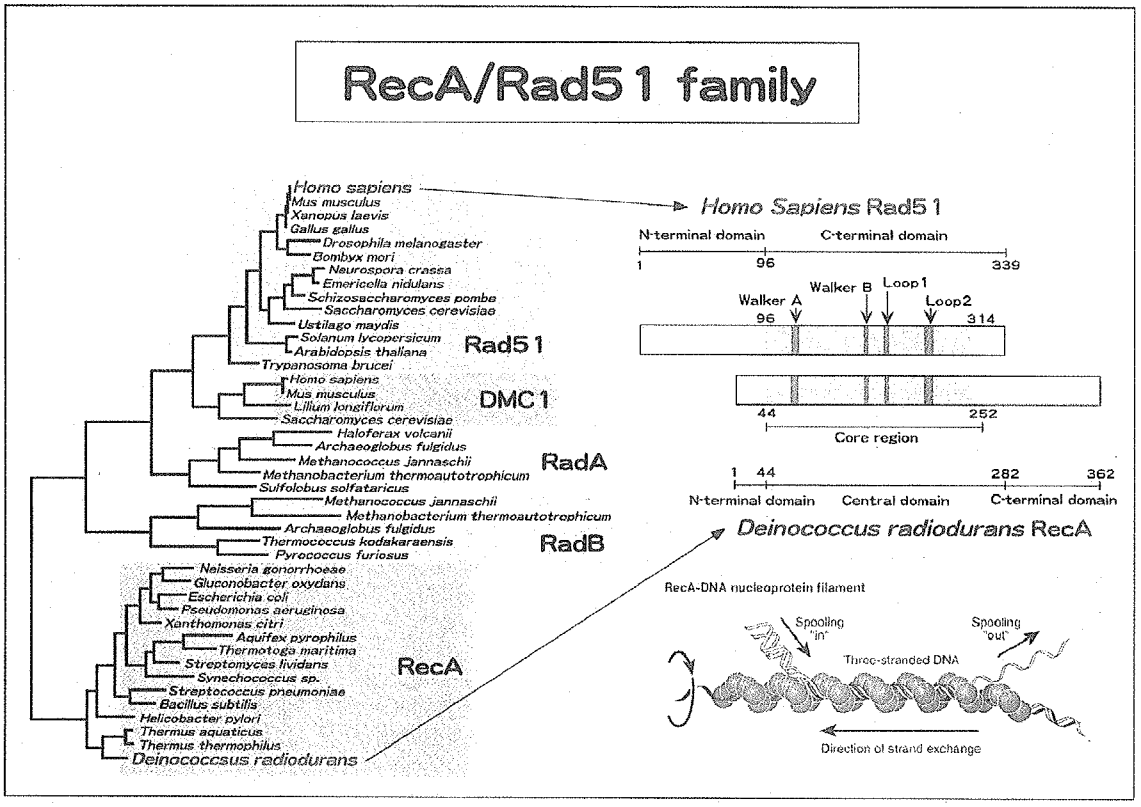
RecA/Rad51 family
Homo sapiens
Mus musculus
Xanopus laevis
Gallus gallus
Drosophila melanogaster
Bombyx mori
Neurospora crassa
Emericella nidulans
Schizosaccharomyces pombe
Saccharomyces cerevisiae
Ustilago maydis
Solanum lycopersicum
Arabidopsis thaliana
Rad51
Trypanosoma brucei
Homo sapiens
Mus musculus
Lilium longiflorum
DMC1
Saccharomyces cerevisiae
Haloferax volcanii
Archaeoglobus fulgidus
Methanococcus jannaschii
Methanobacterium thermoautotrophicum
RadA
Sulfolobus solfataricus
Methanococcus jannaschii
Methanobacterium thermoautotrophicum
Archaeoglobus fulgidus
Thermococcus kodakaraensis
Pyrococcus furiosus
RadB
Neisseria gonorrhoeae
Gluconobacter oxydans
Escherichia coli
Pseudomonas aeruginosa
Xanthomonas citri
Aquifex pyrophilus
Thermotoga maritima
Streptomyces lividans
Synechococcus sp.
Streptococcus pneumoniae
Bacillus subtilis
Helicobacter pylori
Thermus aquaticus
Thermus thermophilus
Deinococcus radiodurans
RecA
Homo Sapiens Rad51
N-terminal domain
C-terminal domain
1
96
339
Walker A
Walker B
Loop1
Loop2
96
314
44
252
Core region
1
44
282
362
N-terminal domain
Central domain
C-terminal domain
Deinococcus radiodurans RecA
RecA-DNA nucleoprotein filament
Spooling "in"
Spooling "out"
Three-stranded DNA
Direction of strand exchange

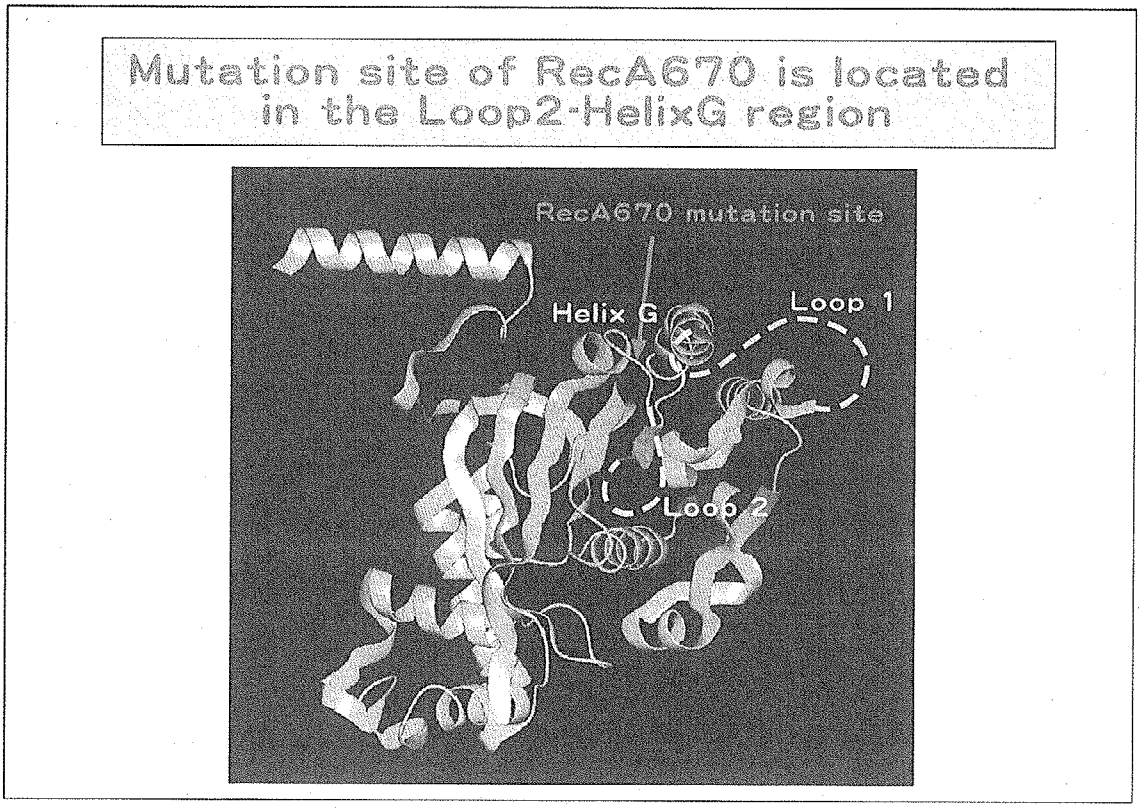
Mutation site of RecA670 is located in the Loop2-HelixG region
RecA670 mutation site
Helix G
Loop 1
Loop 2

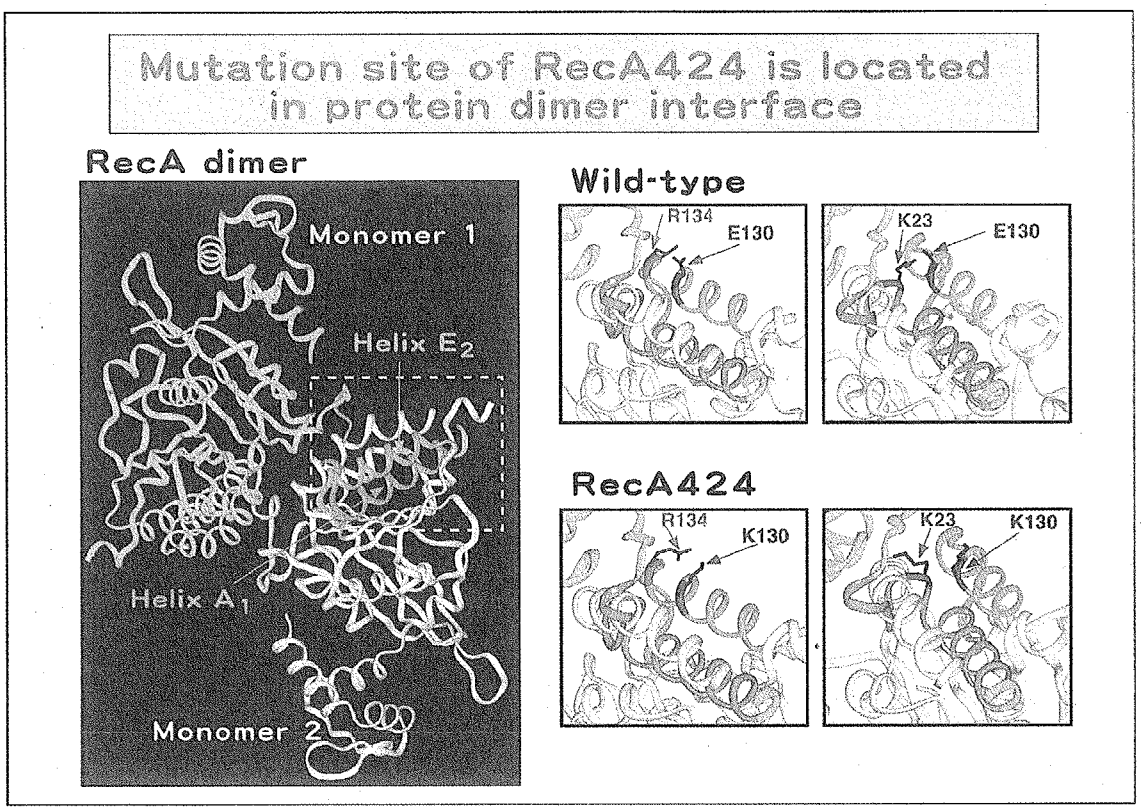
Mutation site of RecA424 is located in protein dimer interface
RecA dimer
Monomer 1
Helix E2
Helix A1
Monomer 2
Wild-type
R134
E130
K23
E130
RecA424
R134
K130
K23
K130

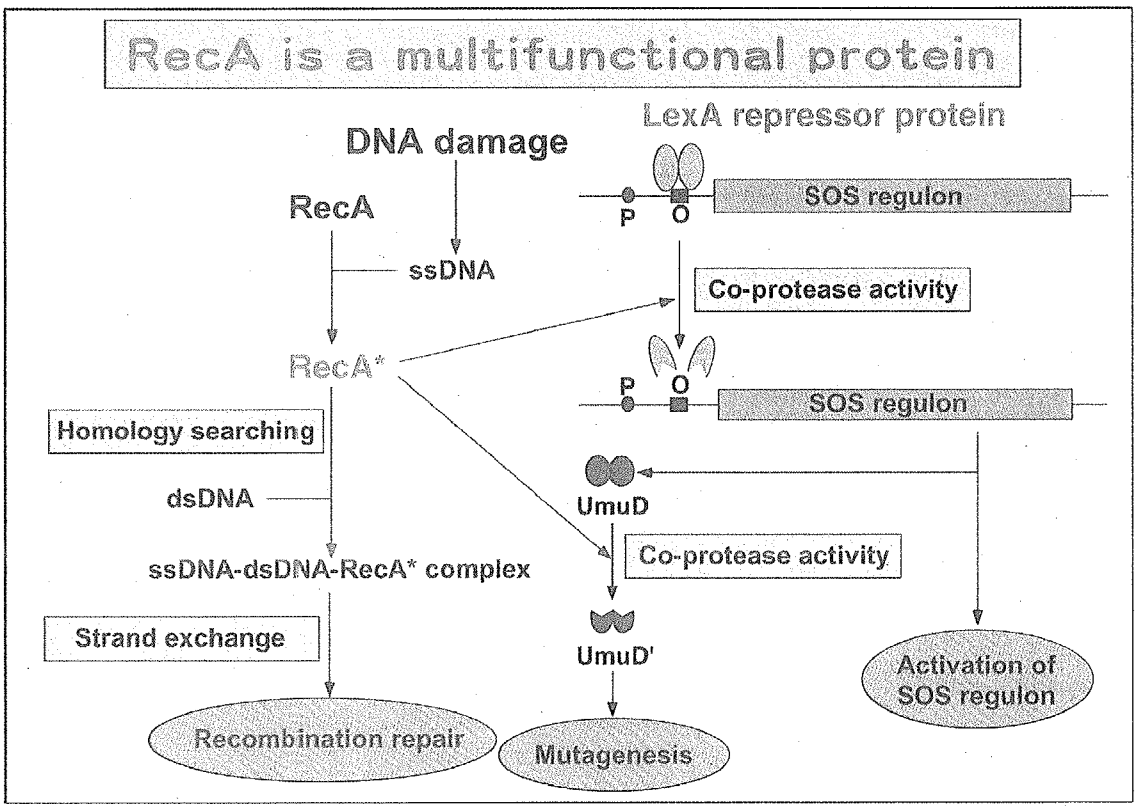
RecA is a multifunctional protein
LexA repressor protein
DNA damage
RecA
ssDNA
SOS regulon
P
O
Co-protease activity
RecA*
Homology searching
dsDNA
ssDNA-dsDNA-RecA* complex
Strand exchange
UmuD
UmuD'
Activation of SOS regulon
Recombination repair
Mutagenesis

Changes in *recA* promoter activity during growth phase and following irradiation

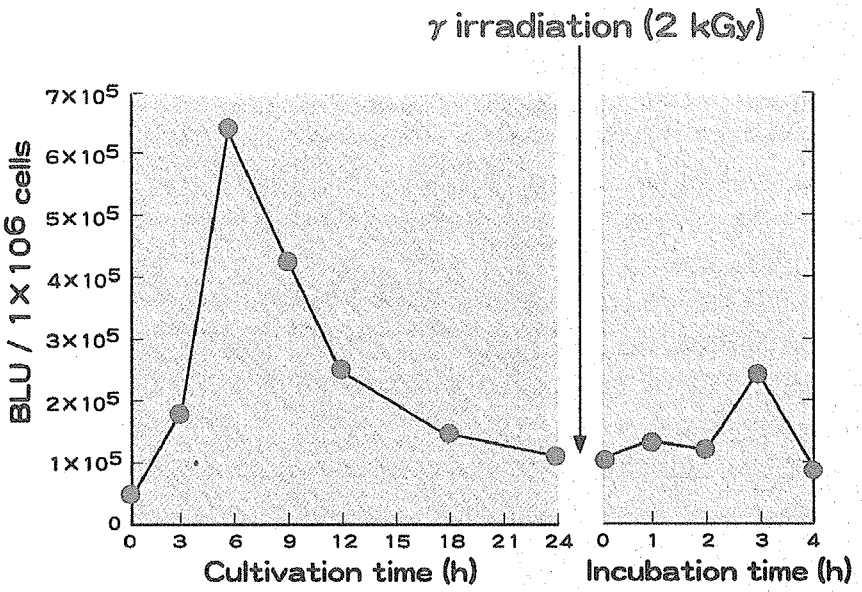

A Possible Mechanism of DSB Repair in *D. radiodurans*

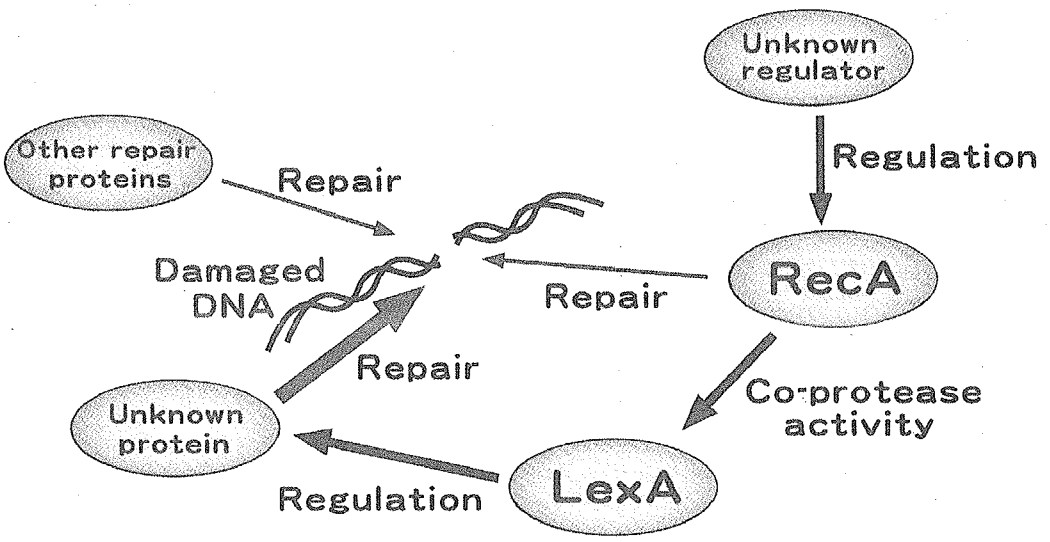

5. Poster Presentations

This is a blank page.

5.1

A Basic Approach for Radiation Chemical Dose-Response Estimation for Thymine Decomposition Products

Ken AKAMATSU[1], Kentaro FUJII[2] and Akinari YOKOYA[2]

[1]Risk Analysis Labs.,Tokai, JAERI, [2] SPring-8, Kansai, JAERI

Thymine decomposition products produced by monochromatic ultrasoft X(USX)- or ^{60}Co-γ-irradiation were studied to know their dependences on the absorbed energies from the photons and the secondary electrons. As the results of HPLC analyses, qualitatively, it was demonstrated that all chromatograms of the USX (395, 407, 538 eV)-irradiated samples were similar, and were almost the same as those of the γ-irradiated. Some products, uracil (Ura), hydroxymethyluracil (HMU), dihydrothymine (DHT) and formyluracil (foU) were found in most chromatograms (Fig. 1, 2). Quantitatively, on the other hand, the peaks after thymine were meaningfully smaller than those of USX, and the *G*-values of all thymine decomposition products produced by 538 eV photon-irradiation were smaller than the cases of the other USX energies, while those of the γ-irradiated were much larger than those of the all USX photon energies tested (Table 1). These findings suggest that the differences both of the irradiated photon energy and the absorbed energy from the photons or the secondary electrons are influential in quantities of the products and the *G*-values. The quantitative differences in the set of experiments imply that low-energy electrons such as the secondary electrons at the track end are susceptible to produce the products after thymine in our chromatograms, which were expected to be cross-linked products of thymine[1]. This finding can be supported by the product spectrum differences in connection with the sample thickness (or surface density: σ) (Fig. 3). The radiation chemical natures are important for DNA damage, particularly in connection with inter- and intra-strand DNA crosslink and DNA-protein crosslink, which may give rise to malignancy. Thus, our basic results are important for improvement of the radiation risk estimation and its difference in a variety of radiations.

[1] Gromova, M. et al., *Int. J. Radiat. Biol*, **74**, 81-97 (1998).

Fig. 1. HPLC Chromatograms of Thymine Irradiated by USX at the Energy of 395 eV (Nitrogen *K*-pre-edge)

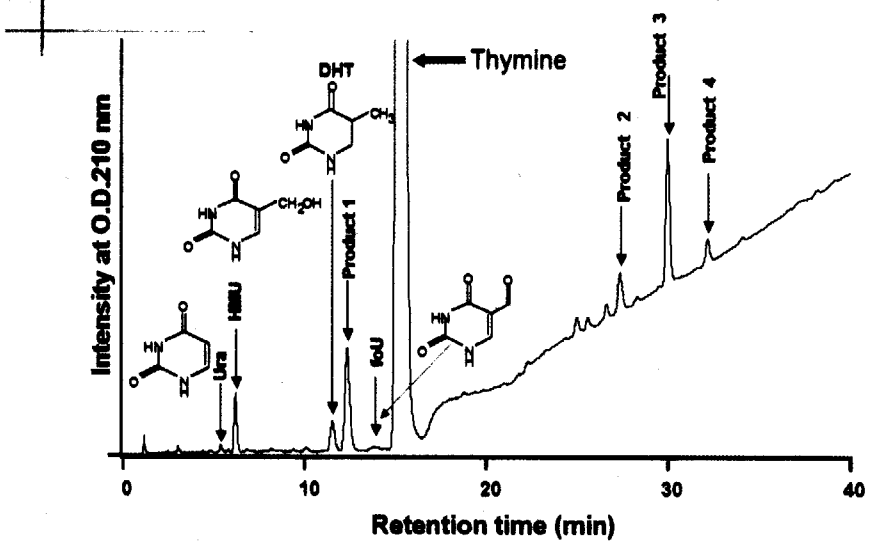

Fig. 2. HPLC Chromatograms of Thymine Irradiated with ^{60}Co γ-rays (1.25 MeV)

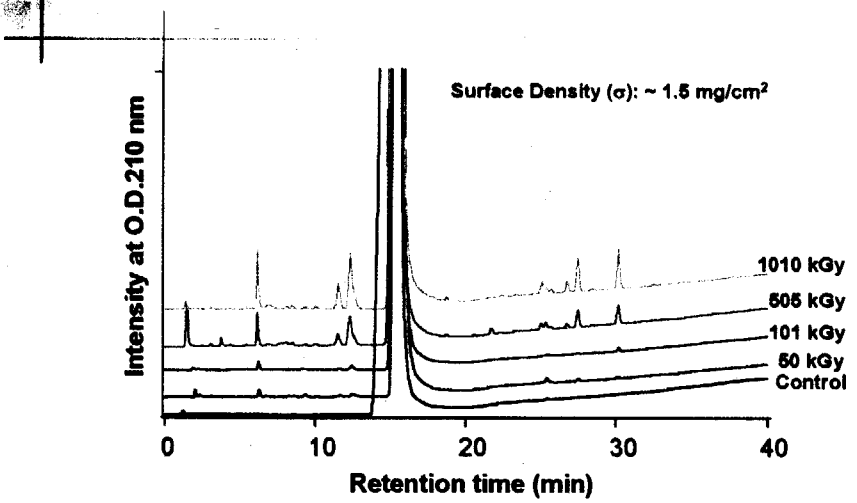

Table 1 *G* values of Thymine Decomposition Products by USX- and γ- Irradiation

Light source	Photon energy	*G* (× 10^{-3} μmole/J)			
		Ura	HMU	DHT	foU
USX	395 eV	0.34	4.1	2.2	2.9
	407 eV	0.35	3.6	2.2	3.1
	538 eV	0.21	2.9	1.2	1.7
^{60}Co γ-rays	1.25 MeV	N.D.	10	20	N.D.

(N.D.: not detected).

Fig. 3. Relative Strength of Thymine Decomposition Products to each DHT
Comparison between USX and ^{60}Co γ-rays

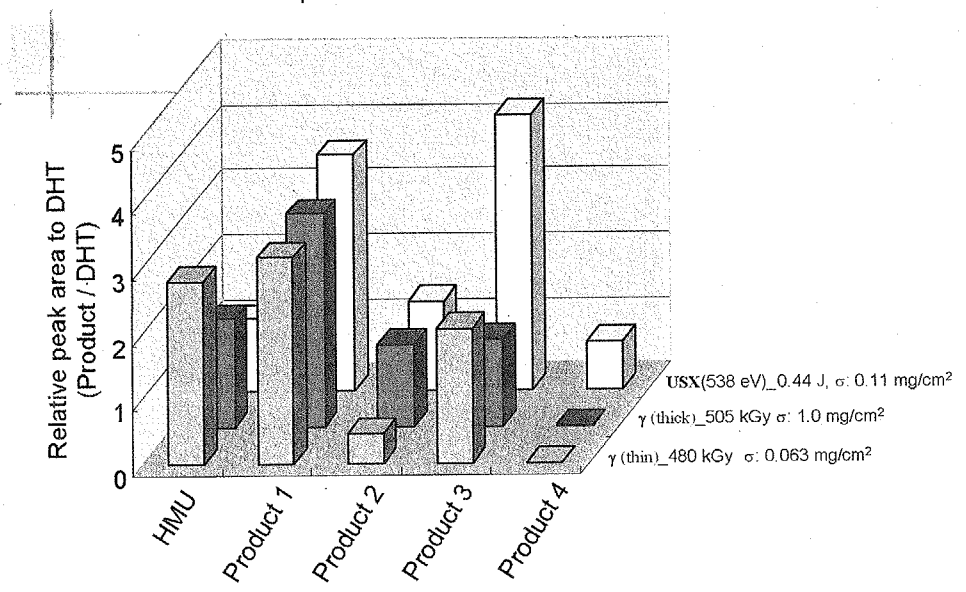

5.2

Photochemistry of the skin chromophore Urocanic acid - a quantum chemical study

Jonas Danielsson and Aatto Laaksonen

Div. of Physical Chemistry, Arrhenius Laboratory, Stockholm University, S-109 61 Stockholm, Sweden

Urocanic acid is a naturally abundant cromophore in human skin with both photoprotective and immunosuppressive properties. It has been shown that this cromophore has a rich photochemistry in the UV part of the spectrum, with absorption to different states leading to very different photoreactions, including *trans-cis* isomerization, excited state proton transfer, and singlet oxygen production, all of which might have biological significance. In this investigation we use DFT and *ab initio* methodologies together with the polarizable continuum model to investigate the primary steps in these reactions. A reassignment of the gas phase spectroscopy is proposed based on the different isomerization pathways found for different isomers. The influence of solvents on these pathways are discussed. We also show that it is likely that the ultrafast excited state proton transfer proceeds through the mechanism described by Sobelewski and Domcke.

JP0450230

5.3

Development of RISA (Radiation Induced Surface Activation) Detectors for Onsite Sensing and Microdosimetry

H. Date[1)], H. Tomozawa[2)], T. Takamasa[3)], K. Okamoto[4)], M. Shimozuma[1)]

1) College of Medical Technology, Hokkaido University, Sapporo 060-0812, JAPAN
2) Kyoto Semiconductor Corporation, Eniwa 061-1405, JAPAN
3) Tokyo University of Mercantile Marine, Tokyo 135-8533, JAPAN
4) Nuclear Engineering Research Laboratory, University of Tokyo, Tokai-mura 319-1188, JAPAN

Abstract

We investigate a new technique for radiation detection using radiation induced surface activation (RISA) phenomenon which is found in oxide materials (with high resistivity) causing current conduction through the irradiation of gamma or beta rays. The RISA current has been observed typically in Rutile-type TiO_2. We have performed a Monte Carlo simulation of gamma ray photons in TiO_2 and backing layers to make clear carrier generation processes leading to the conduction and to develop new type detectors for onsite sensing and microdosimetry. Results show that the dominant process to generate electron-hole pairs in thin TiO_2 layer is collisional interaction of electrons generated in backing layer, which suggest the RISA detector can be used for estimating the absorbed dose in bio-materials.

KEY WORDS: Radiation induced surface activation, TiO_2, Backing layer, Onsite sensing, Dosimetry

1. Introduction

Radiation induced surface activation (RISA) is a phenomenon observed in oxide materials of high resistivity, which causes current conduction through the irradiation of gamma or beta rays. One of the authors found the RISA current induced in Rutile-type TiO_2 film for the first time [1], and the conduction current has been detected also in some other oxide materials [2,3]. However, the mechanism leading to the conductivity has not been understood yet. Figure 1 shows a typical configuration of RISA detector. Radiation is normally incident on TiO_2 surface backed by Al_2O_3 layer. As is reported by Ref. [1], conductance of TiO_2 films reaches several pS (pico-siemens) with gamma ray irradiation of kGy/h intensity. This conduction may arise from electron-hole production and the carrier flow in TiO_2 layer. However, direct excitation of the layer by gamma ray irradiation is not feasible because the TiO_2 layer is so thin that gamma ray photons can penetrate without any interactions. Major possibility of producing electron-hole pairs may be attributable to the excitation by electrons generated in Al_2O_3 layer.

In this study, we simulate gamma ray interactions in the RISA detectors by a Monte Carlo method of photons to investigate the carrier generation processes. Then we seek appropriate conditions to design new type detectors using RISA for onsite sensing and dosimetry.

2. Methods

To examine the processes occurring in the RISA detector, we perform a Monte Carlo simulation of ^{60}Co gamma ray photons and estimate the production

rate of secondary electrons in the layers. In the Monte Carlo simulation, we consider three interaction processes: coherent scattering, incoherent scattering and photoelectric effect. The collision interaction cross sections for these processes are taken from Storm and Israel (1970) [4], and the scattering factor for incoherent scattering and the atomic form factor for coherent scattering by Hubbell et al. (1975) [5] are incorporated in the simulation code. A large number of photons (> 2000000) is followed in the Monte Carlo method until the photon energy comes down below a cutoff value (typically 1keV).

In addition to the simulation with TiO_2 and Al_2O_3 layers, we also take TiO_2 and $C_5H_8O_2$ (Lucite) substrate into account. $C_5H_8O_2$ is a typical tissue equivalent (TE) plastic, and if the conduction of TiO_2 is associated with the physical process in backing material, $C_5H_8O_2$ can be a bio-tissue substitute for sensing the absorbed dose. We evaluate the possibility for a dosimetric use of RISA detector by this model analysis.

3. Results & Discussion

Figure 2 shows energy distribution of electrons generated by photon processes in the 4×4cm TiO_2 and Al_2O_3 layers. The thickness of TiO_2 layer was set to be 0.25μm and three cases of the thickness for Al_2O_3 backing substrate, 0.05, 0.1 and 0.15cm, were adopted in the simulation. As was expected, the frequency of ^{60}Co gamma ray interaction with TiO_2 layer was extremely low compared to that with Al_2O_3 layer. It was also found that the electron generation is mainly caused by the Compton scattering (>99%). In regard to the distribution in Fig.2, it should be pointed out that

the maximum energy of electrons (i.e., the Compton edge) is given by

$$K_{max} = \frac{2\alpha}{1+2\alpha} E_0 \quad \left(\text{where } \alpha = \frac{h\nu}{0.511} \right) \qquad (1)$$

for the incident photon energy E_0(=hν) in MeV (1.33MeV and 1.17MeV for ^{60}Co gamma ray). The electron energy distribution for TiO_2 and $C_5H_8O_2$ layers is given in Fig.3 as well. We can see that the production rate of electrons in this combination of layers is almost one third of that in TiO_2 and Al_2O_3 layers. This ratio may be originated by the difference of mass density between $C_5H_8O_2$ and Al_2O_3, 1.18g/cm^3 and 3.80g/cm^3, since the interaction cross sections for both the materials are almost same in quantity.

Next, we investigated possible processes to induce a current conduction of TiO_2 through the reaction associated with electrons produced in the photon process. Rutile-type TiO_2 possesses the energy band structure for electrons with gap energy of 3.0eV, and there are supposedly two courses to generate electron-hole pairs in TiO_2 layer: collisional excitation by electrons and optical pumping by bremsstrahlung photons arising from the straggling motion of electrons. Figure 4 shows range of electrons taken from Ref.[6]. The range for several hundreds keV electrons is roughly from 0.01cm to 0.5cm, which is comparable to the thickness of backing layer. This means that a large number of electrons can reach TiO_2 layer to activate it. Especially the electron range in $C_5H_8O_2$ is several times larger than that in Al_2O_3, which may be advantageous for activating TiO_2. On the other hand, the energy transfer to bremsstrahlung emission can be estimated by bremsstrahlung yield. We determined the ratio of bremsstrahlung radiation energy to total energy of electrons using the following equation:

$$R = \frac{E_{rad.total}}{E_{elec.total}} = \frac{\int E \cdot Y(E) \cdot N_e(E) dE}{\int E \cdot N_e(E) dE} \qquad (2)$$

where E is the electron energy, $N_e(E)dE$ represents the number of electrons between E and E+dE, and Y(E) is the bremsstrahlung yield. In the present study, $N_e(E)dE$ was taken from the energy distribution in Figs.2 and 3, and Y(E) from Ref.[6]. The result is given in table 1 to show that the energy ratio transferring to bremsstrahlung is 10^{-3} order of magnitude. This number seems to be slight, but is sufficient to give a portion of energy for making photons contribute to optical pumping of TiO_2 layer (e.g., several hundreds eV of total energy is given by bremsstrahlung radiation per electron with 100keV kinetic energy).

4. Conclusions

As the provisional conclusion, we summarize the results that RISA phenomenon is primarily caused by the behavior of electrons generated by the Compton scattering in substrate layer. It is likely that the Compton electrons can activate TiO_2 layer though the collisonal excitation and the bremsstrahlung emission. Accordingly, it should be emphasized that substrate (backing) layer is essential in the RISA detector and if the layer is made of tissue equivalent (TE) plastic we can use this for dosimetric monitors in radiology. Natural modification of the detector geometry would be favorably made into a spherical shape for measuring the fluence and the absorbed dose of radiation.

References

[1] H. Tomozawa, J. Nakata, K. Okamoto, and T. Takamasa, Proc. 2001 Annual Meeting of the Atomic Energy Society of Japan, **C43**, 96 (2001)

[2] H. Tomozawa J. Nakata, T. Takamasa, and K. Okamoto, Proc. 38th Annual Meeting on Radioisotopes and Radiation in the Physical Science and Industries, **1a-II-3**, 16 & **1a-II-4**, 17 (2001)

[3] H. Tomozawa, T. Takamasa, K. Okamoto, and J. Nakata, Proc. 39th Annual Meeting on Radioisotopes and Radiation in the Physical Science and Industries, **2a-III-7**, 93 (2002)

[4] E. Storm and H. I. Israel, Nuclear Data Tables, **A7**, 565-681 (1970)

[5] J. H. Hubbell, Wm. J. Veigele, E. A. Briggs, R. T. Brown, D. T. Cromer, and R. J. Howerton, J. Phys. Chem. Ref. Data, **4**, 471-538 (1975)

[6] L. Pages, E. Bertel, H. Joffre, and L. Sklavenitis, Atomic Data **4**, 1-127 (1972)

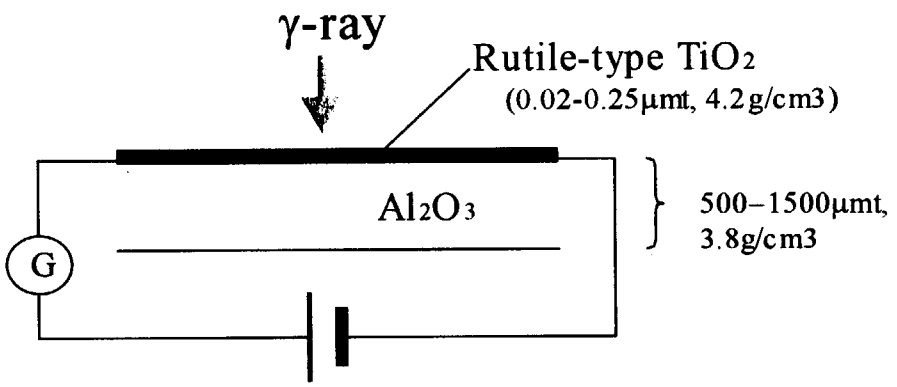

Fig.1 Schematic description of typical RISA detector

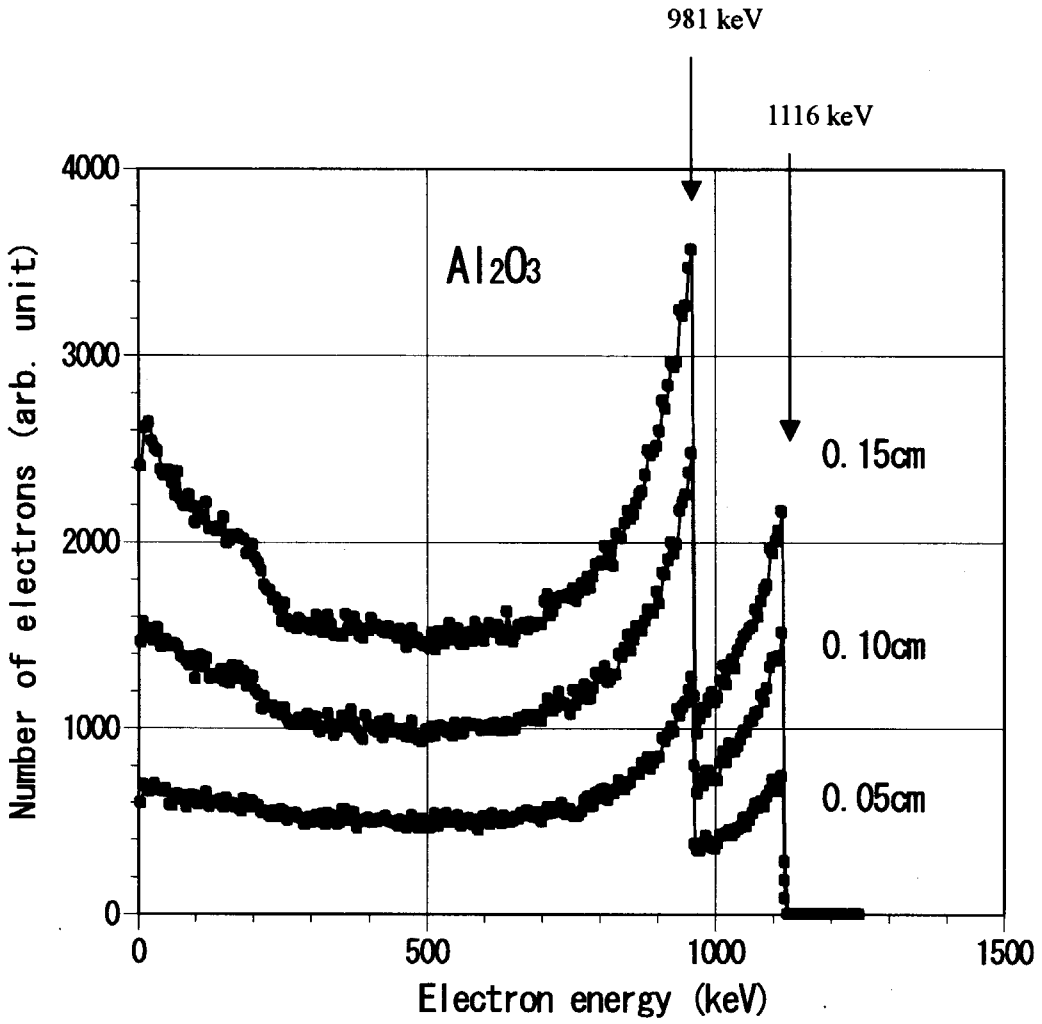

Fig.2 Energy distribution of electrons generated by photon processes in TiO_2 and Al_2O_3 layers

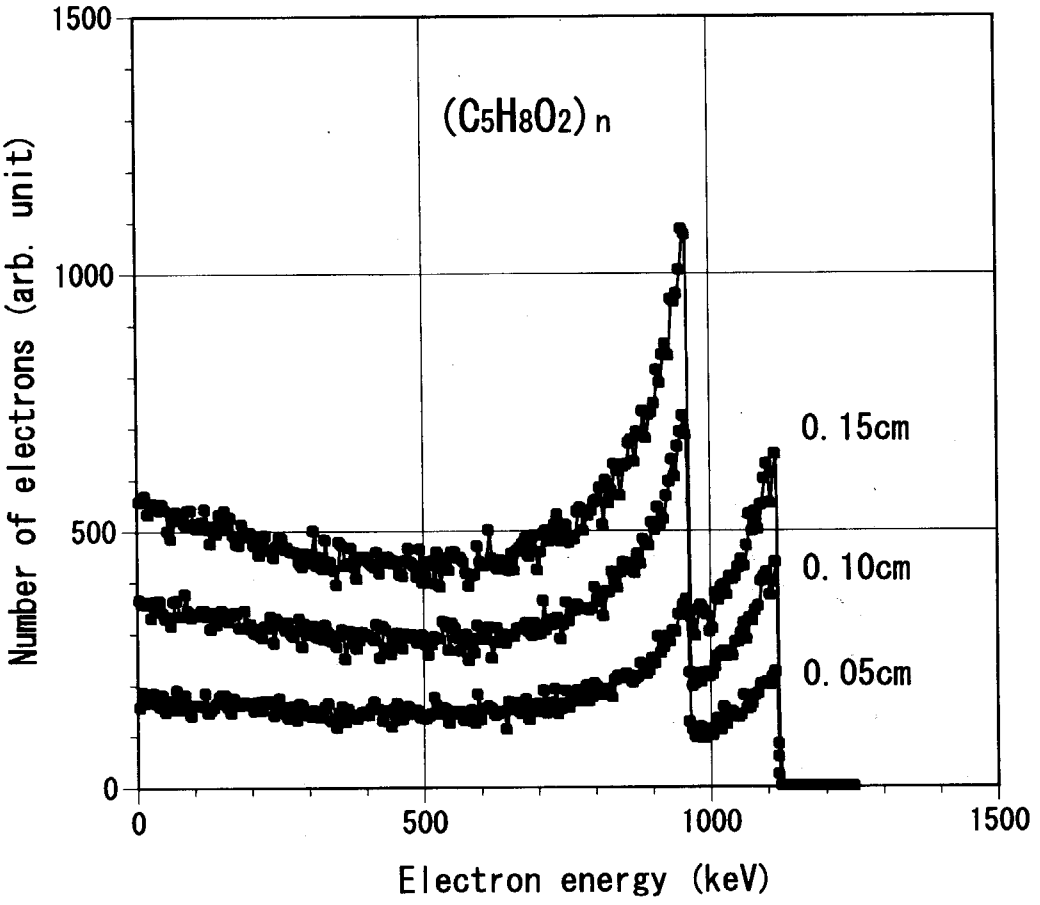

Fig.3 Energy distribution of electrons generated by photon processes in TiO_2 and $C_5H_8O_2$ layers

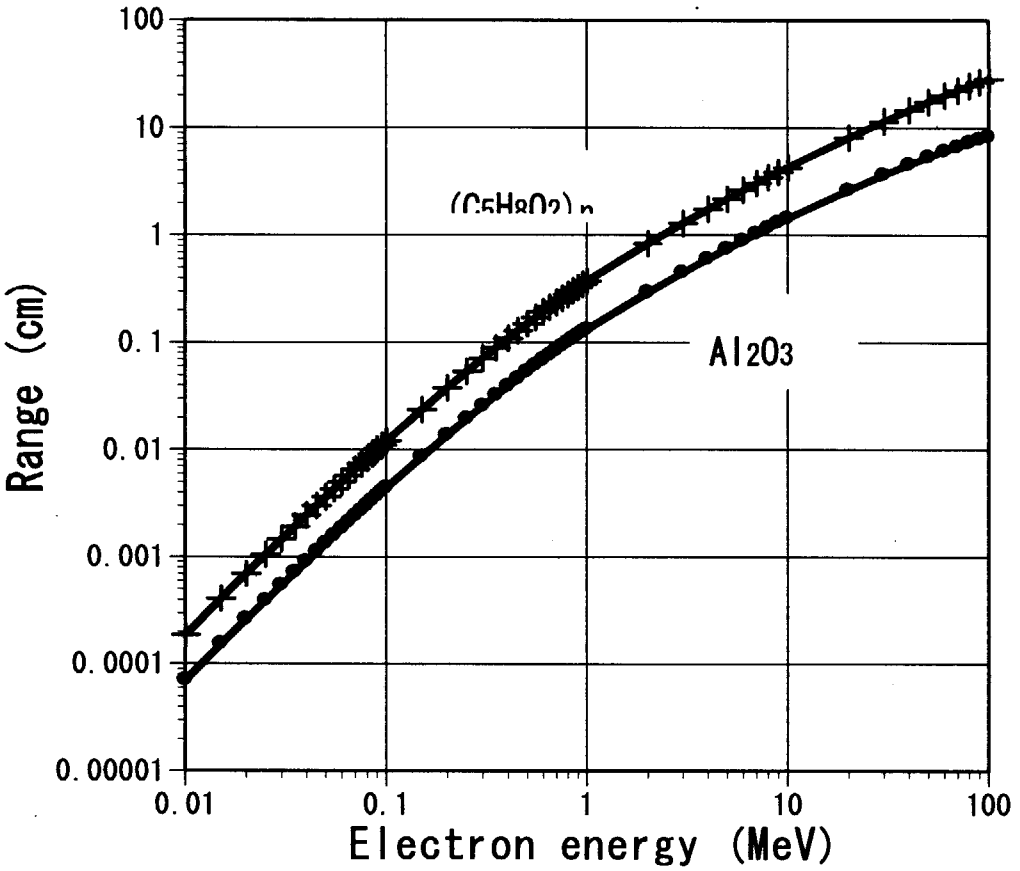

Fig.4 Range of electrons in $(C_5H_8O_2)_n$ and Al_2O_3 (Ref.[6])

Table 1. Ratio of bremsstrahlung radiation energy to total kinetic energy of electrons

	Al_2O_3		
Thickness (cm)	0.05	0.10	0.15
R	6.82E-03	6.78E-03	6.77E-03

	$(C_5H_8O_2)_n$		
Thickness (cm)	0.05	0.10	0.15
R	3.54E-03	3.53E-03	3.53E-03

5.4

Photon Stimulated Desorption of Ions from DNA Components induced by Core Excitation

Kentaro FujiiAkinari Yokoya, JAERI SPring-8
Ken Akamatsu, JAERI Tokai

1. Introduction

Photon stimulated desorption from DNA components, 2-deoxy-*D*-ribose, thymine, thymidine and TMP, were observed by using a residual gas analyzer installed in a synchrotron soft X-ray beamline to reveal the mechanism of DNA damage through direct ionization/excitation of DNA. Radiation damage to DNA, which induces serious biogenetic effects such as mutation, can be classified as (1) structural damage leading to a single- or double-strand break, (2) a release of nucleobases from DNA, and (3) chemical modification of the nucleobases. Some of the damages of (2) and (3) are known to be processed by base excision repair enzymes. However, there are very scarce of the reports for the direct measurement of the released nucleobases or molecular fragment from the damaged DNA. Core level excitation induced by monochromatized synchrotron soft X-rays is one of important probes to investigate the photon stimulated desorption of the nucleobases or smaller fragments as the consequence of photochemical reaction at the specific site in DNA. Recently, we measured XANES spectra of DNA nucleobases around oxygen and nitrogen K-edges[1]. In order to obtain the evidence of the base lesions as well as strand breaks by the site selective photoreaction, we have developed an apparatus for direct observation of molecular fragments from DNA or released nucleobases in the photon energy range (400 ~ 560 eV)[2].

2. Experimental

Desorbed ions by ultrasoft X-rays irradiation were detected by a quadrupole mass spectrometer (RC501PIC; Hiden Analytical Ltd.) analyzer was positioned at ~ 30 mm from the sample. By attract the positive ions to analyzer, the sample was floated at + 40 V during the measurement. The photon stimulated desorption measurement was carried out at the JAERI soft X-ray beamline (BL23SU) at the SPring-8. All the measurements were performed at room temperature.

3. Results and discussion

Figure 1 shows the mass spectra for (a) 2-deoxy-*D*-ribose, (b) thymine, (c) thymidine and (d) TMP thin films obtained by 538 eV photo-excitation. Since all the samples had large absorption intensity in σ* resonance near 538 eV, we choose excitation photon energy for observation of desorbed ions. As a desorbed ion od 2-deoxy-D-ribose, H^+, CH_2^+, CH_3^+, $C_2H_2^+$, $C_2H_3^+$, CO^+, CHO^+, CH_3O^+, $C_3H_3^+$, C_2HO^+, $C_2H_2O^+$ and $C_2H_3O^+$, were observed. In spite of exciting the oxygen core level, we could not observe O^+ or OH^+ ion signal which is the expected ion of the hydroxyl groups of 2-deoxy-*D*-ribose molecule. In thymine thin films, H^+, CH_2^+or N^+, CH_3^+or NH^+, CO^+, C_2NH^+ and $CNOH^+$ were observed as desorbed ions. The intense ion counts around 15 m/z were compared with that of higher higher mass number. As an assignment for this ion, CH_3^+ and NH^+ are candidates for product ions. It seems that the CH_3^+ is significant because there are less ion counts of $CHNO^+$ or CO^+, which are predicted conterions of NH^+. The mass pattern of dT and TMP can be expressed by linear combination of that of 2-deoxy-*D*-ribose and thymine. It means that the fragment ion which produced by the decomposition of both dT and TMP, is generated at the both site of the sugar and base.

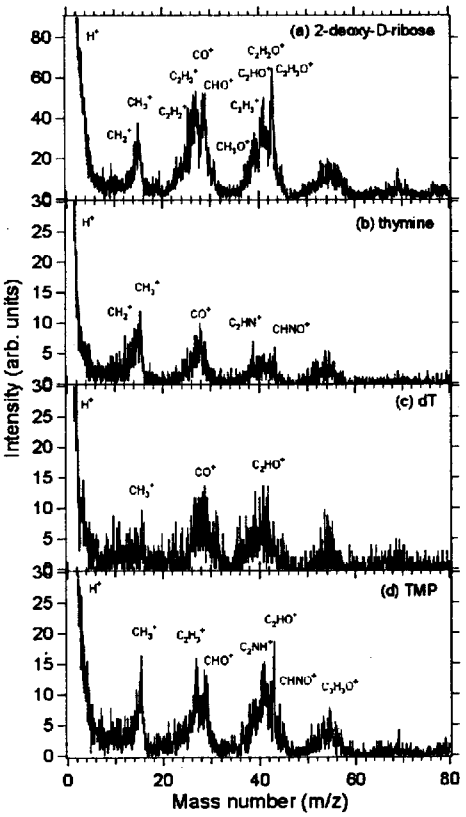

Fig. 1. Photon stimulated desorption mass spectra of positive ions from (a) 2-deoxy-D-ribose, (b) thymine, (c) thymidine and (d) TMP thin films following oxygen core excitation (538 eV). Ion counts were normalized with photon fkluence and absorption intensity.

References

1) K. Fujii, K. Akamatsu, Y. Muramatsu and A. Yokoya, *Nucl. Instr. Meth. B., in press*

2) K. Fujii, K. Akamatsu and A. Yokoya, *Surf. Sci., in press*

5.5

Irradiation of single mammalian cells with a precise number of energetic heavy ions

- Applications of microbeams for studying cellular radiation response -

Yasuhiko KOBAYASHI[1], Tomoo FUNAYAMA[1], Seiichi WADA[1,2], Mitsumasa TAGUCHI[1]
[1]JAERI-Takasaki; [2]Veterinary Medicine, Kitasato University

A single cell irradiation system has been developed for targeting cells individually with a precise number of high-LET heavy ions to elucidate radiobiological effects of single heavy ions and to investigate the interaction of damages produced by separate events. The system has been installed at a high-energy collimated heavy-ion microbeam apparatus under a vertical beam line of the JAERI-Takasaki AVF-cyclotron. Using the heavy ion microbeam apparatus, mammalian cells are irradiated in the atmosphere with a single or precise number of heavy ions, 13.0 MeV/u ^{20}Ne or 11.5 MeV/u ^{40}Ar. Positional data of the individual cells are obtained at an off-line microscope before irradiation, then the cells are targeted and irradiated semi-automatically using the on-line microscope of the microbeam apparatus according to the obtained data. The number of ions penetrating the cells attached on the ion track detector CR-39 were counted with a plastic scintillator-photomultiplier tube assembly and a constant fraction discriminator. Immediately after the irradiation, the position and the number of ion tracks traversed the cell was detected with etching of CR-39 from the opposite side of the cell with alkaline-ethanol solution at 37°C. The growths of the cells were observed individually up to 60 hours after irradiation by revisiting the cells according to the object database. The continuous observation of the individual cell growth indicated on a first rough estimate that a single ion traversal of a cell nucleus resulted in complete growth inhibition of the irradiated cells. The effect of cytoplasmic irradiation with more than two particles was as lethal as a single hit of the cell nucleus.

Heavy ions transfer their energy to biological organisms through high-density ionization along the particle trajectories. The population of cells exposed to a very low dose of high-LET heavy ions contains a few cells hit by a particle, while the majority of the cells receive no radiation damage. At somewhat higher doses, some of the cells receive two or more events according to the *Poisson* distribution of ion injections. This fluctuation of particle trajectories through individual cells makes interpretation of radiological effects of heavy ions difficult. Using microbeams, we will be able to overcome this limitation by delivering a counted number of ions to each cell to study a number of important radiobiological processes in ways that cannot be achieved using conventional "broad-field" irradiation. A microbeam can be used for selective irradiation of individual cells, which can be subsequently observed to ascertain what changes occur to that cell and to neighboring un-irradiated cells. Prompt detection of ion tracks provides us with accurate information about the spatial distribution of delivered ions just after irradiation time. The use of this single-cell irradiation system allows direct investigation of cell-to-cell communications such as "bystander effects", that is, radiation effects of heavy ions transmitted from irradiated cells to neighboring un-irradiated cells. Furthermore, a microbeam with sufficient spatial resolution will be useful for analyzing the interaction of damages produced by separate events in an irradiated cell, the dynamics of cellular repair, and the intra-cellular process such as apoptosis by means of highly localized irradiation of a part of a nucleus or cytoplasm.

1. Motivation

broad-field "random" irradiation

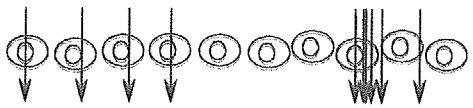

- inhomogeneous distribution of dose
- hit and non-hit cells not distinguished

single cell "targeted" irradiation

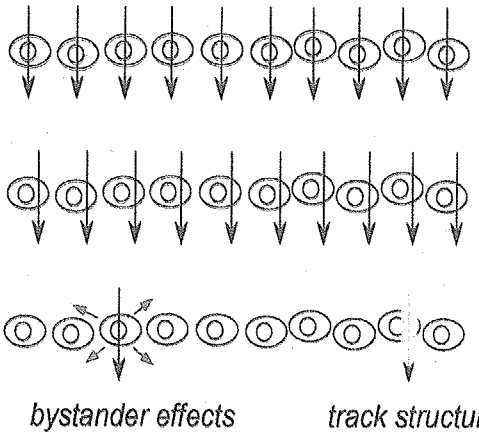

- selective irradiation of individual cells
- defined particle trajectories

> evaluate hit cells, nuclear / cytoplasm targeting

> evaluate non-hit cells (bystander effects)

> effect of track structure

> intra-cellular process

2. Requisites for single cell "targeted" irradiation

> microbeam irradiation with counted particles

> cell observation, targeting, precise particle delivery

> detection of ion-hit position on the target cells

> cell culture for targeting and irradiation

> cell culture for post-irradiation incubation

3. Procedure of the irradiation of cultured cells with collimated heavy ion microbeam apparatus developed at JAERI-Takasaki

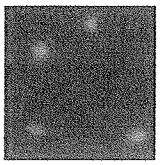

CHO-K1 cells stained with 5 μM "Cell Tracker Orange" were detected under fluorescent microscopy

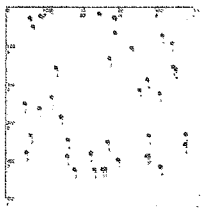

Automated cell finding: target mapping

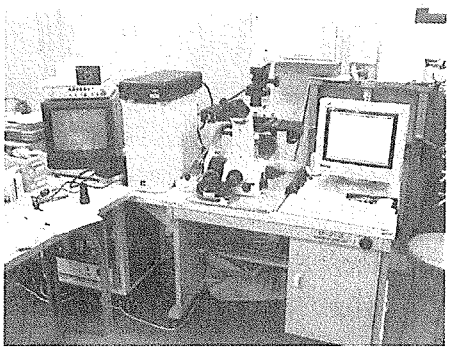

Off-line microscope in Preparation Room

Cell targeting, microbeam irradiation

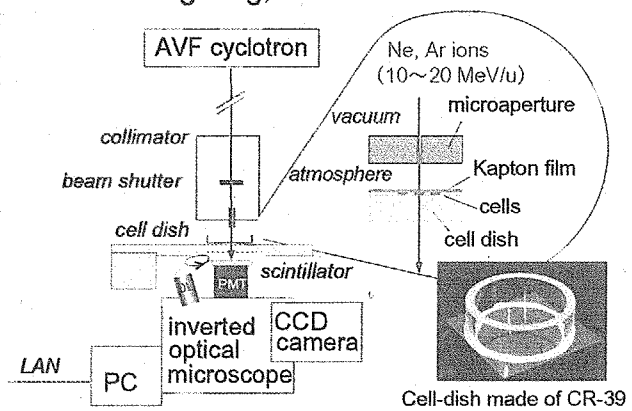

On-line microscope: Beam Room

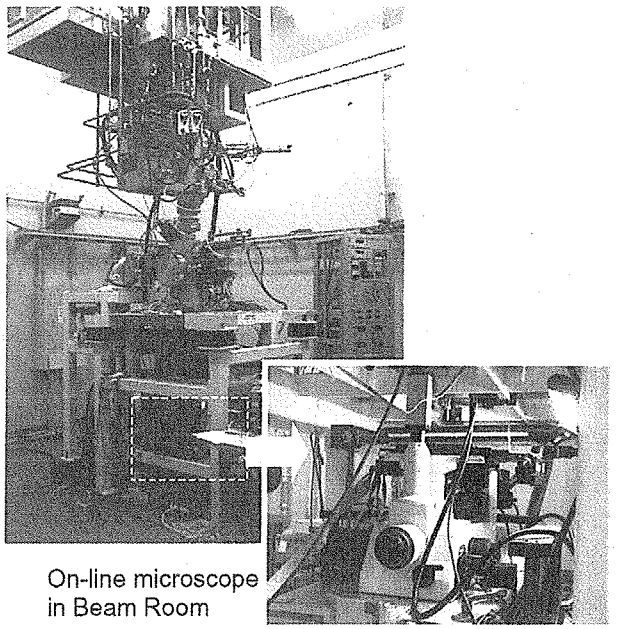

On-line microscope in Beam Room

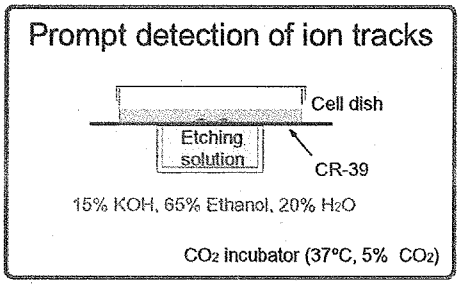

Off-line microscope: Preparation Room

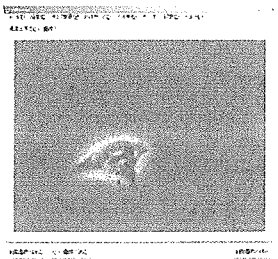

Revist irradiated cells during post-irradiation incubation

Cell / etched-ion-pit overlaid image

Before irradiation, positional data of the individual cells are obtained at the Off-line microscope in the preparation room by microscopically searching the sample dish. Using the object database, targeting and irradiation at the On-line microscope are carried out quickly. Immediately after irradiation, the cell dish is refilled with medium, and then the bottom is etched from the opposite side of the cells to detect the accurate position of ion tracks on the cells.

4. Schematic diagram of the microscope control system for cell finding, cell targeting, ion counting and cell revisiting

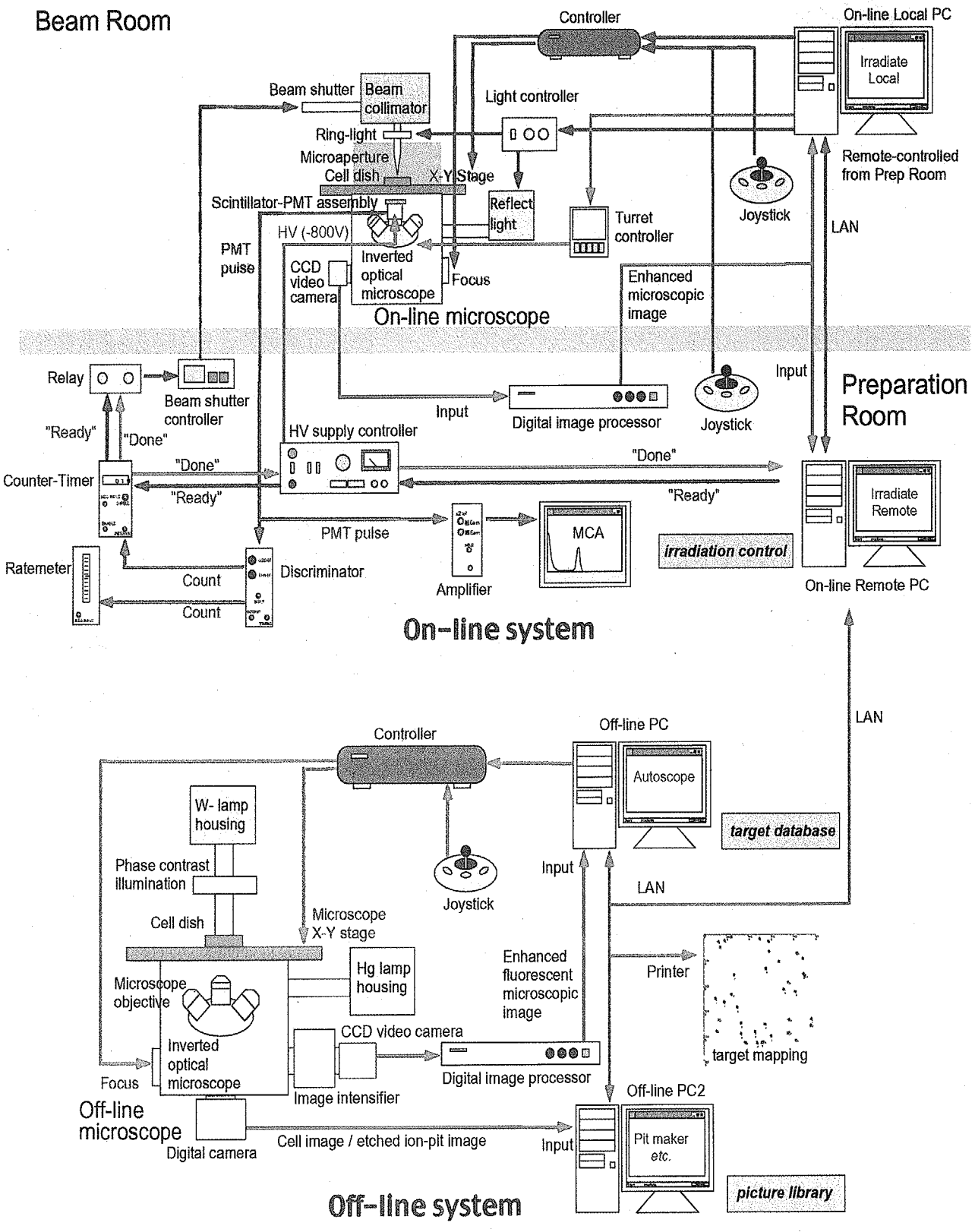

5. Effects of Ar ion hits on nucleus

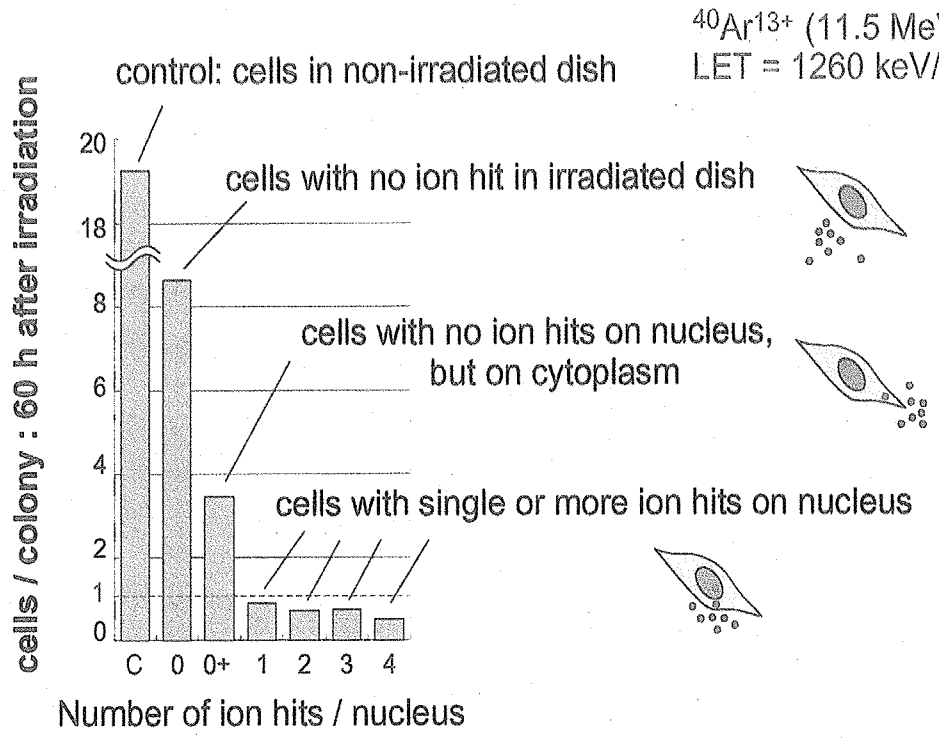

6. Conclusion

We have established the method for irradiating mammalian cultured cell with heavy ion microbeams.

Single Ar-ion hit on cell nucleus resulted to complete growth inhibition of the the cell.

Bystander-like effect in cell growth was also observed.

7. Current status & Further plan

Accuracy:	~100% counting efficiency (ϕ5μm Ne, Ar)	→ Focused beam, ϕ1μm He, C, Ne, Ar
Speed:	50~100 cells / 20 min	→ ~1000 cells / 1 sec
Cell culture:	attached on CR-39, >30 min at RT	→ Floating cells, tissue, organ

5.6

Molecular Dynamics of Damaged DNA and Oxoguanine DNA Glycosylase Complex

Hisashi Ishida[1] and Nobuhiro Go[1,2]

1. Center for Promotion of Computational Science and Engineering, Japan Atomic Energy Research Institute, 8-1 Umemidai Kizuchou, Souraku-gun, Kyoto, 619-0215, Japan, ishida@apr.jaeri.go.jp
2. Graduate School of Information Science, Nara Institute of Science and Technology, 8916-5 Takayamachou, Ikoma-shi, Nara, 630-0101, Japan, ngo@is.aist-nara.jp, go@apr.jaeri.go.jp

Oxidative DNA damage plays a critical role in several biological processes such as mutagenesis. Among oxidative base damages in DNA, 7,8-dihydro-8-oxoguanine (8oxoG) is one of the major base lesions which leads to G:C → T:A transversion mutations during DNA replication. OGG1 is an enzyme which repairs the oxidative DNA damage by excising the 8oxoG. In order to understand how OGG1 recognizes the damaged DNA, molecular dynamics (MD) simulations of single OGG1 molecule and OGG1 – 8oxoG DNA complex were performed for 1nanosecond at a constant pressure and temperature of one bar and 300K, respectively.

Principal Component Analysis (PCA) was performed to assess the dynamic properties of the single OGG1 and OGG1 — 8oxoG DNA complex. The lowest five effective frequencies were 1.00, 1.62, 2.05, 2.45, 2.53 cm^{-1} for the single OGG1; and 0.845, 1.24, 1.46, 1.55, 2.06 cm^{-1} for the complex. Moreover, the internal motions of the complex were divided into two parts, the internal motions changing the shape of each molecule, and the external rigid-body motions changing their mutual dispositions. The lowest five effective internal frequencies were 0.99, 1.87, 1.90, 2.33 and 2.75 cm^{-1} for the OGG1 in the complex. The six effective external frequencies were 1.63, 2.00, 3.10, 3.81, 4.40 and 5.18 cm^{-1}. It was found that the rotational external motions between OGG1 and 8oxoG DNA were taking place not to influence the amplitudes of their internal atomic fluctuations. An investigation of the relationship between the principal mode and the motions of 8oxoG DNA were strongly correlated with their motions.

A calcium ion which helped to bend 8oxoG DNA remained around the 8oxoG residue stably during the whole simulation time. In order to understand the role of the calcium ion, MD simulation of the complex without the calcium ion was also performed. The bended conformation of 8oxoG DNA was relaxed and the six effective external frequencies made a shift toward low frequency, 0.60, 1.82, 2.36, 3.80, 4.36 and 6.68 cm^{-1}. It is considered that the calcium ion stabilizes the conformation of the complex too.

JP0450231

5.7

AN ION-TRACK STRUCTURE MODEL APPLIED TO ESTIMATE CROSS SECTIONS FOR SV40 DNA STRAND BREAKS IN SOLUTION

Shin-ichi Ohno[1], Mitsumasa Taguchi[2], Yasuhiko Kobayashi[2], and Hiroshi Watanabe[2]
[1]Theoretical Radiation Research Laboratory, 12-5 Shiratori-dai, Aoba-ku, Yokohama 227-0054
[2]JAERI, Takasaki, 233 Watanuki-machi, Takasaki 370-1292

ABSTRACT

A track structure model, previously reported based on experimental measurements of the spatial dose distribution in low-pressure gases, was applied to calculate cross sections for DNA strand breaks in solution. The results give a good description of the compiled data of Taucher-Scholz and Kraft for DNA single- and double-strand breaks (SSB and DSB) with a wide range of ion species in SV40 DNA irradiated in solution *in vitro*. For each particle the track radius $t(D_{37})$ was defined and calculated from the present track structure model so as that the dose at $t(D_{37})$ is equal to the characteristic dose D_{37} experimentally obtained using X-ray irradiation and thus within this radius the reaction occurs. Using a target radius R_0 for a SV40 viral DNA (5243 bp) molecule in solution as a parameter, the cross section is simply given: $\sigma = \pi[t(D_{37}) + R_0]^2$. The agreement with experiments is quite satisfactory. The present model may help us to understand the reason why "hooks" or "maximum RBE" appear when cross sections are plotted *vs* LET-values of bombarding particles.

KEY WORDS: Track structure model, DNA strand breaks, Cross sections, Spatial dose distribution, SV40 viral DNA

1. Introduction

It is generally agreed that the number of primary products in a substance induced by any type of radiations is related linearly with the absorbed dose, but the experimentally observed effects, biological and chemical, caused by the same dose differ from each other for different radiations. These differences are related to different local energy concentrations and have been studied for several decades in terms of radiation quality. Katz and coworkers (1-3) among others have developed most successfully a track structure model to explain different yields caused by different radiations based on a number of simplifying assumptions: (1) Radiation effects are the same for δ-rays at same dose whether they are generated from δ- or X-rays or from energetic ions, (2) All the δ-rays emit perpendicularly to the ion-path and deposit energy linearly during their traversals (afterward modified by a power-law energy-range relationship), and (3) The cross section for δ-ray production follows the Rutherford scattering of incident ion with free electrons in matter. The results of Katz and coworkers are mostly presented by plotting cross section data as a function of LET-values as usually presented for this kind of data. On the other hand, we reported a ion-track structure model (4,7) different from that of Katz et al, which was

uniquely based on experimental measurements of the spatial dose distribution in low-pressure gases using a collimated ion-beam and a small, movable ionization chamber. We applied this model to calculate the yields of radiation-induced oxidation reaction of ferrous ions in aqueous solutions bombarded by various energetic ions(6,7).

We extend our calculation to derive cross sections for DNA single- and double-strand breaks (SSB and DSB). Our results will be compared with the compiled data of Taucher-Scholz and Kraft(10) with a wide range of ion species in SV40 DNA irradiated in solution *in vitro*. In this report, the cross section data will be displayed against $(Z^*/\beta)^2$ instead of LET-value, where Z^* is effective charge and β velocity of an incident ion. The definite reason for employing the cross section *vs* $(Z^*/\beta)^2$ plot instead of using LET is given in this report.

2. An ion-track structure model based on experimental measurements

To specify an energetic particle, we need generally three parameters, namely atomic number Z, mass number M, and the energy E of the particle, which can be reduced to two parameters, the effective charge Z^* and the velocity β relative to the velocity of light **c** ($\beta = v/\mathbf{c}$) travelling in matter, by using, for example, Barkas equation(8):

$$Z^* = Z[1 - \exp(-125\beta Z^{-2/3})] \qquad (1)$$

The track structure of an energetic particle of the effective charge Z^* and the velocity β may be expressed as the dose distribution as a function of the radial distance t around the ion path:

$$D(Z^*, \beta, t) \qquad (2)$$

The energy deposited comes as the result of (i) direct interaction between incident ion and molecules and (ii) indirect interaction in which energetic electrons generated in (i) ionize or excite molecules situated around the ion path. In the present paper, the ratio of the energy deposited through (i) and (ii) was calculated using binary encounter approximation cross-sections for the collision of incident charged particle and electrons in the water molecule (7). The results indicate that 22.7% of the energy is deposited through (i) within the range of 1 nm and the remaining (77.3%) is deposited through (ii), namely through the ejected electrons, and will be widely distributed. The spatial distribution of the dose delivered through (ii) is obtained on the basis of the experimental data obtained using low pressure gases and a narrow beam of energetic ions from 1 MeV proton to 5.9 MeV/nucleon uranium ion. These data can be found in the literature and have been documented to obtain a scaled radial dose distribution as is shown in **Fig. 1** (4,7);

$$(\beta/Z^*)^2 D(Z^*, \beta, t) = 200 \qquad \text{for } t = 0\sim1$$

$$= 200/t^2 \quad \text{for} \quad t = 1 \sim t_c \qquad (3)$$
$$= 200t_c/t^3 \quad \text{for} \quad t = t_c \sim \infty$$

where $D(Z^*, \beta, t)$ is the dose in unit of Gy, t the normalized radial distance in the liquid water in unit of nm, t_c the critical distance determined empirically for the given incident particle as:

$$t_c \fallingdotseq (10/87)6 \times 10^{-6}[2mc^2\beta^2/(1-\beta^2)]^{\alpha} \qquad (4)$$
$$\alpha = 1.667 \text{ when } \beta > 0.03$$
$$\alpha = 1.079 \text{ when } \beta < 0.03$$

Here, $6 \times 10^{-6}[2mc^2\beta^2/(1-\beta^2)]^{\alpha}$ $(= T_{max})$ is the expected maximum range in the liquid water of the δ-electron of kinematically limited (for free electron only) maximum energy W(in keV) $= 2mc^2\beta^2/(1-\beta^2)$. For derivation of these relations refer Waligorski, et al(3).

Figure 1 shows that an unified radial dose distribution is obtained for the high-energy particles from H to U hitherto examined if we use normalized dose by multiplying $(\beta/Z^*)^2$.

Here, it should be noted that LET-values of any particle can be calculated (6) from the present track structure model as

$$\text{LET} = (Z^*/\beta)^2 \pi(200)[3 + 2\ln(t_c)]/\ 0.772 \qquad (5)$$

3. Cross section calculation

The track structure model above mentioned can be applied to calculate cross sections for chemical and biological reactions induced by energetic ion bombardment of various types (6,7). We assume that radiation effects are the same for δ-rays at same dose whether they are generated from δ-rays or from energetic ions. Moreover, we utilize the reported dose D_{37} at which 37% of reactants goes to particular reaction and which can be obtained with δ-ray experiments. The pattern of energy deposition by energetic ions in matter consists of a central region of high-energy density and larger laterally extended region of lower density. For each energetic ion, we define here $t(D_{37})$, the radial distance at which the radial dose is equal to the characteristic dose D_{37}, and thus we can assume that the reaction occurs within the track of this radius and outside this radius no reaction occurs:

For high-velocity ions, using Eq. 3 one gets $(\beta/Z^*)^2 D_{37} = 200/t(D_{37})^2$ which gives

$$t(D_{37}) = (200/D_{37})^{1/2}(Z^*/\beta) \qquad (6)$$

For low-energy ions in the extremity case when we can take $t_c = 1$, Eq.3 gives $(\beta/Z^*)^2 D_{37} = 200/t(D_{37})^3$ or

$$t(D_{37}) = (200/D_{37})^{1/6}(Z^*/\beta)^{1/3} \quad (7)$$

Taking a target radius R_0 for a molecule to be considered, the cross section is simply given:

$$\sigma = \pi[t(D_{37}) + R_0]^2 \quad (8)$$

4. Results and Discussion

Equation 8 was used to calculate cross sections for SV40 viral DNA single- and double-strand breaks (SSB and DSB) in solution for which reliable experimental data of Taucher-Scholz and Kraft are available(10). The results are shown by solid curves in **Fig. 2** where cross sections were calculated with R_0 = 10 nm and using D_{37} = 13 Gy for SSB and D_{37} = 320 Gy for DBS as measured by Roots et al(9). The dotted curves show the results with R_0 = 0 and 20 nm for comparison's sake. The data with the bombarding particles from helium to uranium ions of varying energy obtained by Taucher-Scholtz and Kraft are included in Fig. 2.

From the data included in Fig. 2 we can pick up the high-velocity particle cases using the criterion of $t(D_{37}) < t_c$ and re-plot them as are shown in **Fig. 3,** together with the low-velocity ion data such that $t(D_{37})$< 100 nm and intermediate-velocity ion data such that 100 nm < $t(D_{37})$< 1000 nm. It is clearly seen that there appears no "hooks" in the cross section vs $(Z^*/\beta)^2$ curves that are usually seen in cross section *vs* LET curves. We recognize that the "hooks" appear only when we watch the cross-section change with respect to any particular ion-species. When we keep our attention on the velocity of the bombarding particles irrespective of the ion-species, no "hook" appears as is seen in Fig. 3.

As already mentioned the characteristics of a bombarding particle is determined by three parameters, *i.e.*, mass number M, atomic number Z, and energy E. Many researchers working on the radiation biological or chemical effects report useful experimental results as a function of one parameter such as LET-value. A parameter which we use in the present paper, $(Z^*/\beta)^2$, is one such examples and we believe we give a definite ground for using this parameter in calculating cross sections.

5. Conclusion

An ion-track structure model previously presented on the basis of experimental measurements was applied to calculate cross sections for DNA strand breaks assuming that the reaction occurs within the track of the radius of $t(D_{37})$, $t(D_{37})$ being obtained by γ-ray experiments combined with the present track structure model. The results were compared successfully with the compiled data of Taucher-Scholz and Kraft for SV40 DNA (5243 bp) single- and double-strand breaks (SSB and DSB) in solution *in vitro*. The model also help us to understand the reason why "hooks" appear in usual presentations of cross sections-LET relation.

References

(1) Butts, J.J. and Katz, R., *Radiat. Res.*, **30** (1967) 855.
(2) Zhang, C., Dunn, D.E., and Katz, R., *Radiat. Protec. Dosim.*, **13**(1985) 215.
(3) Waligorski, M.P.R., Hamm, R.N., and Katz, R., *Nucl. Tracks Radiat. Meas.*, **11** (1986) 309.
(4) Ohno, S., Furukawa, K., Taguchi, M., Namba, H., Watanabe, R., in *Microdosimetry, Roy. Chem. Soc.*, Goodhead, D.T. *Ed.* (1997), Oxford, pp.30.
(5) Furukawa, K., Ohno, S., Taguchi, M., Namba, H., Watanabe, R., *Radiat. Phys. Chem.*, **49** (1997) 641; Taguchi, M., Namba, H., Aoki, Y., Furukawa, K., Ohno, S., *Radit. Phys. Chem.*, **55** (1999) 511.
(6) Ohno, S., Furukawa, K., Taguchi, M., Namba, H., Watanabe, R., *Radiat. Phys. Chem.*, **55** (1999) 503.
(7) Ohno, S., Furukawa, K., Taguchi, M., Kojima, T., Watanabe, H., *Radiat. Phys. Chem.*, **60** (2001) 259.
(8) Barkas, W.H., and Berger, M.J., *NAS NRC*, Washington DC (1964) 103.
(9) Roots, R., Holley, W., Chatterjee, A.E., Kraft, G., *Adv. Space Res.*, **9** (1989) 45.
(10) Taucher-Scholz, G., and Kraft, G., *Radiat. Res.*, **151** (1999) 595.

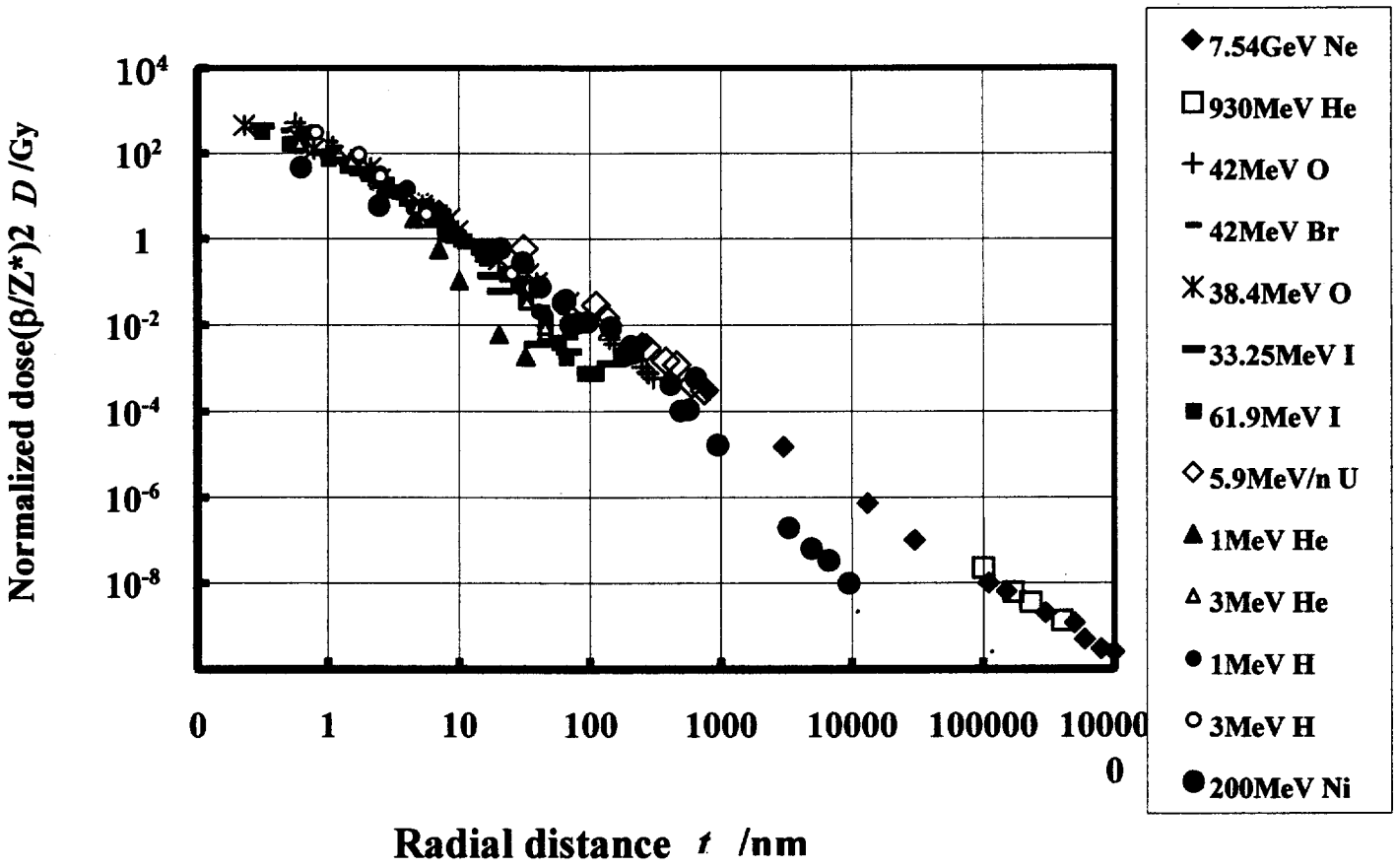

Fig. 1 Radial dose distribution around energetic ions having effective charge Z^*, mass number M, and energy E MeV/nucleon.

Normalized dose $(\beta/Z^*)^2 D(Z^*,\beta,t)$/Gy of available data in the literature are plotted as a function of simulated radial distance/nm in liquid water

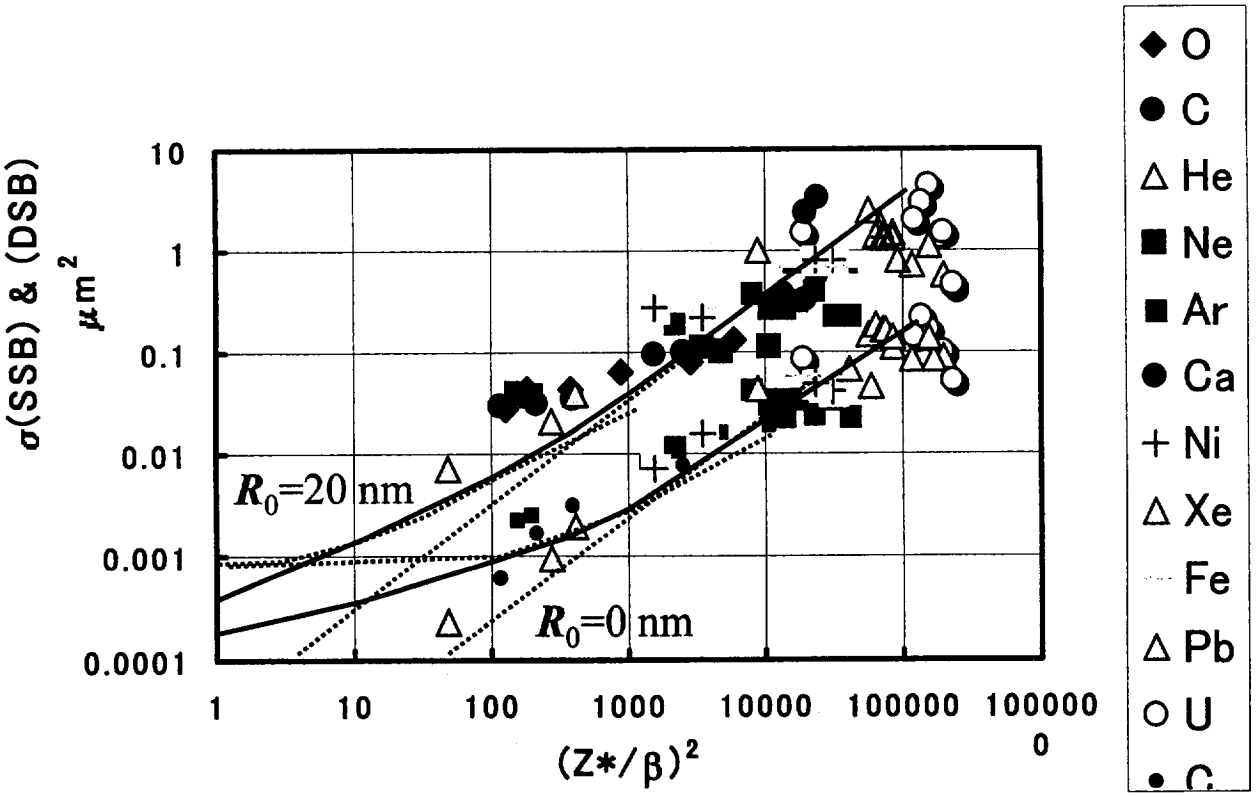

Fig. 2 Calculated cross sections for SV40 DNA single- and double-strand breaks in solution compared with Taucher-Scholtz and Kraft experiments.

Theoretical curves (solid lines: upper σ(SSB) and lower σ(DSB) were calculated with R_0 = 10 nm, and D_{37} = 13 Gy for SSB and 320 Gy for DSB. See the text. Calculated curves with R_0 = 0 and 20 nm are also shown by dotted lines for comparison. Data points were all from Ref. (10).

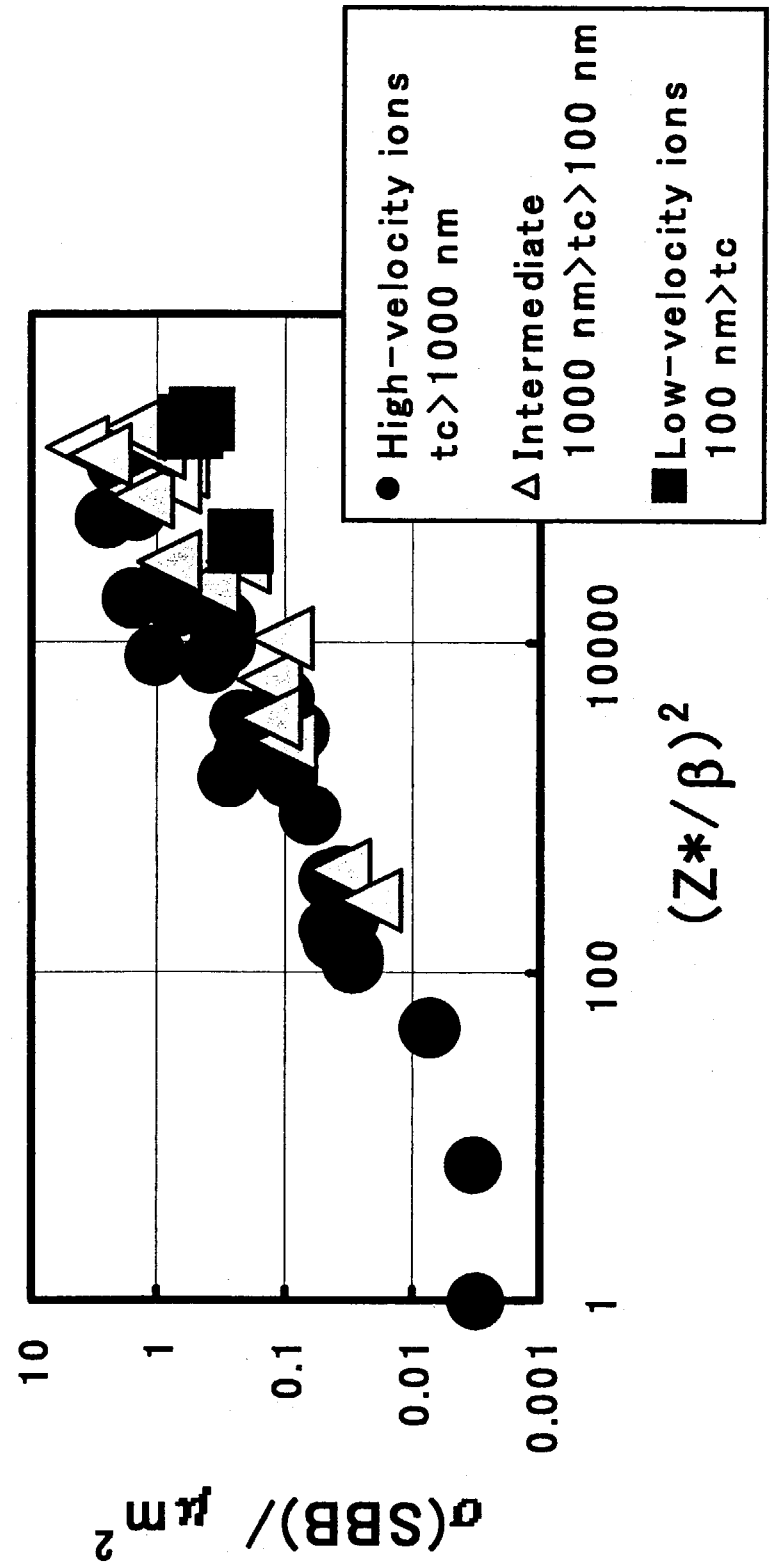

Fig. 3 Taucher-Scholtz and Kraft data on SSB-cross sections against $(Z^*/\beta)^2$-values (the same as in Fig. 2) marked according to the ion's velocity.

Data are marked (classified) as high-velocity particles for which t_c>1000 nm, intermediate-velocity particles for which 1000 nm>t_c>100 nm, and low-velocity particles for which 100 nm t_c. t_c is the transition point at which radial dose relation changes from t^{-2}- to t^{-3}-distribution and will be defined for each ion-species and energies as described in the text.

5.8

On the Biologically based Modelling and Simulation of Carcinogenesis

Noriyuki B. Ouchi

Radiation Risk Analysis Laboratory, Dept. of Health Phys.,
Japan Atomic Energy Research Institute, Tokai, Ibaraki 319-1195, Japan

Here we show the biologically based modeling and simulation of carcinogenesis at low doses. In general, we need a large number of experimental samples to detect mutations at low doses, but in practice it is difficult to get such a large number of data. To satisfy the requirements of the situation at low doses, it is good to study the process of carcinogenesis using biologically based mathematical model. We have mainly studied it by using as known as "multi-stage model", the model seems to get complicated, as we adopt the recent new findings of molecular biological experiments. Moreover, the basic idea of the multi-stage model is based on the epidemiologic data of log-log variation of cancer incidence with age, it seems to be difficult to compare with experimental data of irradiated cell culture system, which has been increasing in recent years. Taking above into consideration, we concluded that we had better make new model with following features: 1) a unit of the target system is a cell, 2) the new information of the molecular biology can be easily introduced, 3) having spatial coordinates for checking a colony formation or tumorigenesis. In this presentation, we will show the detail of the model and some simulation results about the carcinogenesis.

Concepts of the model

The dynamics of the carcinogenesis is studied by the simulation of the cell group in the cell level.

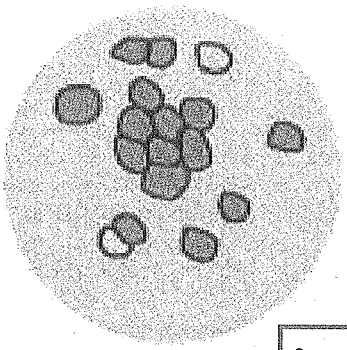

- mathematical model which has actually spatially arranged cells.
- Each cells has own biological dynamics
- The nature that a cell is physical changes due to a cellular change in (a molecule creature 生物-like) condition.
- The intracellular biological dynamics changes the physical properties of the cell.

- **Correspondence with the experiment.**
- **Decrease of the number of the parameters**
- **Molecular biology based model**

Dynamics of "cell transformation"

~ cell carcinogenesis

$$1 \xrightarrow[\downarrow k_d]{P_I} 2 \xrightarrow[\downarrow k_d]{P_{pm}} 3 \xrightarrow[\downarrow k_d]{P_C} 4 \quad \downarrow k_d$$

1→2 initiation
2→3 promotion
3→4 conversion

k_d Prob. of cell death

P_I, P_{pm}, P_c : prob. of cell state change (genetic)

cell type τ : normal, initiation, promotion, cancer

Cell division

If $a(\sigma) > a_c$ then cell division occur

Dynamics of the cell group

- Intracellular dynamics
  - State change in the broad sense (differentiation, carcinogenesis)
  - Cell-death
  - Proliferation (via cell division)
- Physical Dynamics
  - Cell movements
  - Cell deformation
  - Cell adhesion

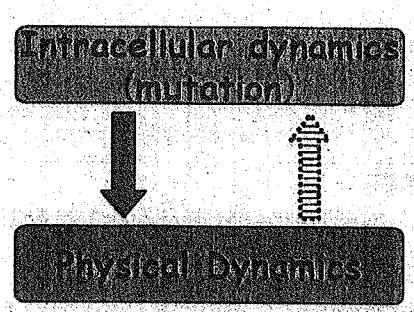

Results

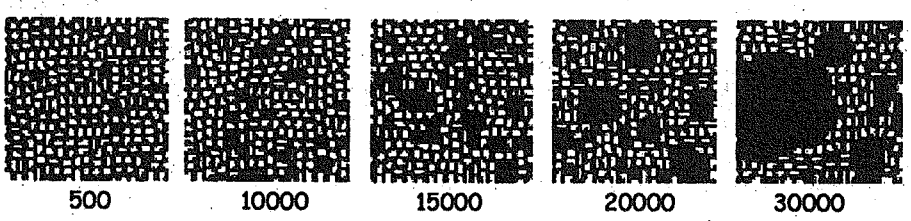

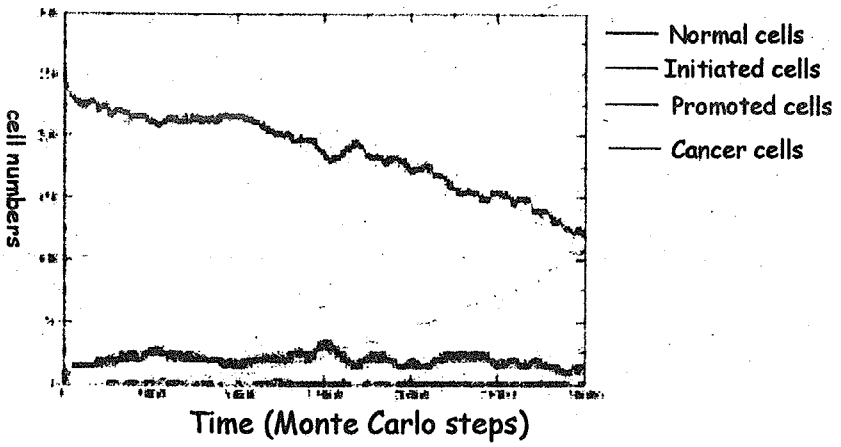

p1=0.0001
p2=0.0001
p3=0.001

kd1=0.0001
kd2=0.001
kd3=0.001
kd4=0.0001

JP0450232

5.9

Detection of DNA strand breaks in mammalian cells using the radioresistant bacterium PprA protein

Katsuya Satoh[1], Seiichi Wada[1,2], Issay Narumi[1], Masahiro Kikuchi[1], Tomoo Funayama[1], Yasuhiko Kobayashi[1]

[1]Biotechnology Laboratory, Department of Ion-beam-applied Biology, Takasaki Radiation Chemistry Research Establishment, Japan Atomic Energy Research Institute, 1233 Watanuki, Takasaki 370-1292, Japan

[2]Graduate School of Veterinary Medicine, Kitasato University, 23-35-1 Higashi, Towada 034-8628, Japan

Abstract

We have previously found that the PprA protein from *Deinococcus radiodurans* possesses ability to recognize DNA carrying strand breaks. In the present study, we attempted to visualize radiation-induced DNA strand breaks with PprA protein using immunofluorescence technique to elucidate the DNA damage response mechanism in mammalian cultured cells. As a result, colocalization of Cy2 and DAPI fluorescent signals was observed. This observation suggests that DNA strand breaks in the nucleus of CHO-K1 cells were effectively detected using the PprA protein. The amount of DNA strand breaks (integrated density of Cy2 fluorescent signals) was increased with the increase in the radiation dose.

Keywords; *Deinococcus radiodurans*, PprA protein, DNA strand breaks, mammalian cell, radiation risk

1. Introduction

For living organisms, it is essential to stably maintain and inherit DNA that carries genetic information. However, they are always facing risk of DNA damage during life in various environments. The damage is caused by both intrinsic and extrinsic factors; respiration-generating active oxygen, DNA replication error, desiccation, ionizing radiation and genotoxic chemicals etc. Failure in DNA damage repair can lead to the loss of genetic information by mutation, chromosome loss, or rearrangement, and thereby in some instances, the failure results in the death of cell. DNA damage is classified into two types; base damage (pyrimidine dimer, oxidative damage, base loss, and cross-link etc) and DNA strand break (single and double strand break). Among them, DNA double strand break is the most lethal damage. Organisms had acquired DNA repair mechanism to cope such genetic lesions. However, radiosensitivities of organisms vary

extensively with species. In mammalian cultured cells that are comparatively sensitive to ionizing radiation, it is important to assess intracellular distribution and generative frequency of lethal DNA strand breaks induced by irradiation in order to get insight into cell's damage response and repair potential. Therefore, the development of effective technique is required to analyze DNA damage response mechanism in mammalian cells. However, such development had been hampered by the lack of appropriate method to evaluate the number of DNA strand breaks in cells immediately after irradiation.

The radioresistant bacterium *Deinococcus radiodurans* is characterized by its extraordinary resistance to the lethal and mutagenic effects of ionizing and UV radiation and to many other DNA damaging agents (1-3). This resistance is considered to be due to a highly proficient DNA repair capacity. The most noteworthy characteristic is a remarkable capacity for repairing DNA double-strand breaks (4, 5). Through the analysis of a DNA repair-deficient mutant strain that exhibits considerably extreme sensitivities to gamma ray, UV, and mitomycin-C. We have previously demonstrated that the *D. radiodurans* genome encodes a novel DNA repair protein (designated PprA for promoting prominent repair) responsible for its DNA repair proficiency. We have found that the PprA protein could bind to double-stranded DNA (dsDNA) with open circular form and linear dsDNA, but not bind to either dsDNA with closed circular form or single-stranded DNA. This result suggested that PprA protein possesses ability to recognize DNA carrying strand breaks (6).

In the present study, we attempted to visualize radiation-induced DNA strand breaks with PprA protein using immunofluorescence technique to elucidate the DNA damage response mechanism in mammalian cultured cells.

2. Methods

2.1 Antibody

The *D. radiodurans* PprA rabbit antiserum was raised against purified *D. radiodurans* PprA protein. Preparation of the antiserum was carried out by Immuno-Biological Laboratories (Gunma, Japan). The antiserum was precipitated with ammonium sulfate (50% saturation). After dialysis, anti-PprA IgG was purified by several chromatographic separations using HiTrap rProtein A and Mono S columns (Amersham Biosciences) (Fig. 1). The fluorescent dye Cy2 was directly conjugated to the purified anti-PprA IgG using an Ab Cy2 labeling kit (Amersham Biosciences).

2.2 Cell preparation

Chinese hamster ovary (CHO-K1) cells were cultivated in Ham's F-12 medium supplemented with 10% fetal bovine serum (FCS) at 37°C in an atmosphere of 5% CO_2 and 95% air. Exponentially growing cells were washed twice with phosphate-buffered saline (PBS). The cells were trypsinized, collected, and resuspended in the same medium. The resulting cell suspension was applied onto a cover glass in a culture dish, and incubated for 2 h at 37°C in an atmosphere of 5% CO_2 and 95% air. The dish was filled with the same medium and incubated for 18 h to homogeneously adhere cells onto a cover glass.

2.3 Irradiation

CHO-K1 cells adhered onto a cover glass was irradiated at 4°C by ^{60}Co gamma rays (0, 0.5, 1, 5, 30, 50, 75, and 100 Gy). These doses were regulated by changing the distance of sample from the gamma ray source.

2.4 Immunofluorescent assay

After irradiation, the cells were immediately fixed with a fixation buffer (10 mM Tris-HCl [pH 7.6], 50 mM EDTA, and 4% paraformaldehyde) for 30 min at 4°C. Following fixation, the cells were washed in buffer 1 (10 mM Tris-HCl [pH 7.6], 10 mM $MgCl_2$, and 1 mM DTT) for 5 min (twice). The cells were then permeabilized with buffer 1 containing 1 μg/ml protenase K and 1% SDS for 30 s and washed in buffer 1 for 5 min (three times). The cells were incubated with buffer 1 containing 1% Nonidet P40 (Roche) for 90 min at 37°C and then incubated with buffer 1 containing 1% bovine serum albumin (BSA) for 60 min at 37°C. The cells were incubated with buffer 2 (10 mM Tris-HCl [pH 7.6], 10 mM $MgCl_2$, 1 mM DTT, and 0.1% BSA) containing 250 ng/ml PprA protein for 60 min at 37°C, followed by the incubation with Cy2-conjugated anti-PprA IgG (2 μg/ml in buffer 2) for 60 min at 37°C. The cells were counterstained with 0.1 μg/ml DAPI (4',6-diamino-2-phenylindole) for 1 min, mounted on a slide glass with an antifade solution (0.5% *p*-phenylendiamine in glycerol) and subjected to fluorescence microscopy observation (Fig. 2). Images were captured by using a cooled charged-coupled device (CCD) camera (Penguin 600CL, Pixera). The integrated density of Cy2 fluorescent signals in nuclei was measured by using Komet 4.0 (Kinetic Imaging).

3. Results & Discussion

3.1 Colocalization of Cy2 and DAPI fluorescent signals

Immunofluorescence analysis of irradiated CHO-K1 cells was performed with *D. radiodurans* PprA protein that possesses ability to recognize DNA carrying strand breaks. Incubation with Cy2-conjugated anti-PprA IgG enables to detect PprA protein bound with DNA strand break. Images of nuclei were captured with a DAPI (nucleus) filter (Fig. 3A), and images of the same field of view were then captured with a Cy2 filter (DNA strand breaks) (Fig. 3B). Colocalization of DAPI and Cy2 fluorescent signals was observed in the merged image (Fig. 3C). This observation suggests that DNA strand breaks in the nucleus of CHO-K1 cells are effectively detected with PprA protein.

3.2 Dose dependency of DNA strand breaks in CHO-K1 cells

To investigate whether the amount of DNA strand breaks is dependent on radiation dose, we examined the cells irradiated by ^{60}Co gamma rays with different doses (0, 0.5, 1, 5, 30, 50, and 100 Gy). The integrated density of Cy2 fluorescent signals of nuclei was scored for each dose. The integrated density corresponding to the amount of DNA strand breaks was increased with the increase in the radiation dose (Fig. 4, 5). The Cy2 fluorescent signals even were observed in non-irradiated cells (Fig. 4A), suggesting DNA strand breaks induced by respiration-generating active oxygen or during DNA replication. In previous study, some DNA strand breaks detection methods using DNA binding protein and its specific antibody were developed (7-9). However, it is difficult to detect an initial damage immediately after irradiation by these methods, because of necessity of post-irradiation incubation. In contrast, our method can apply for the effective detection of initial damage immediately after irradiation.

4. Conclusions

We have been successful in development of an effective detection method to evaluate DNA strand breaks in mammalian cells using PprA protein. Thus, this method can be useful in establishing the radiation risk assessment in molecular and cellular levels. By improving the sensitivity for the detection of DNA strand breaks, this method can be available as a biological dosimeter on the evaluation of low-dose radiation risk. This method is technically possible to apply to the genetic toxicity test that is used for the detection of genotoxic chemicals.

Acknowledgements

This work was performed as part of as Atomic Energy Crossover Project

of the Ministry of Education, Culture, Sports, Science, and Technology (MEXT), Japan.

References

1. Moseley, B. E. B., Photochem. Photobiol. Rev. 7 (1983) 223.
2. Smith, M. D., Masters, C. I. and Moseley, B. E. B., in Molecular Biology and Biotechnology of Extremophiles (eds. Herbert, R. A., and Sharps, R. J.), Chapman & Hall, New York, (1992) 258.
3. Battista, J. R., in DNA Damage and Repair. Vol. I. DNA repair in prokaryotes and Lower Eukaryotes (eds. Nickoloff, J. A., and Hoekstra, M. F.), Humana Press, Totowa, (1998) 287.
4. Dean, C.J., Feldschreiber, P., and Lett, J.T., Nature 209 (1966) 49.
5. Kitayama, S., and Matsuyama, A., Biochem. Biophys. Res. Commun. 33, (1968) 418.
6. Narumi, I., Satoh, K., and Kikuchi, M., JAERI-Conf 2002-005 (2002) 158.
7. Maser, R. S., Monsen, K. J., Nelms, B. E., and Petrini, J. H., Mol. Cell. Biol. 17 (1997) 6087.
8. Peterson, S., Casellas, R., Martin, B., Chen, H., Difilippantonio, M., Wilson, P., Hanitsch, L., Celeste, A., Muramatsu, M., Pilch, D., Redon, C., Ried, T., Bonner, W., Honjo, T., Nussenzweig, M., and Nussenzweig, A., Nature 414 (2001) 660.
9. Limoli, C. L., Giedzinski, E., Bonner W. M., and Cleaver, J. E., Proc. Natl. Acad. Sci. USA 99 (2002) 233.

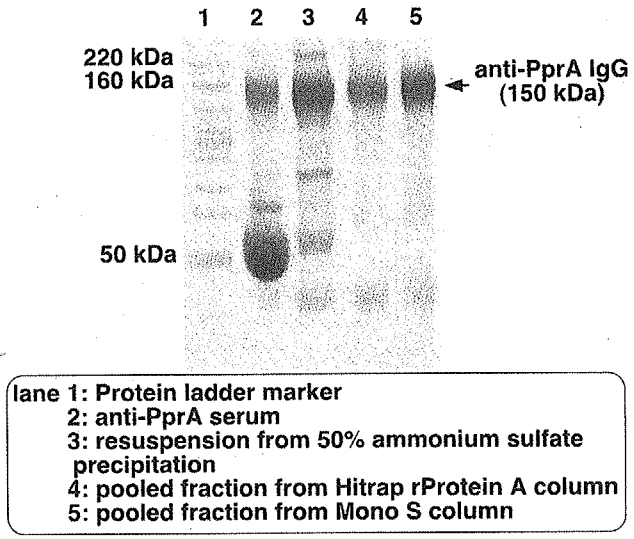

Fig. 1. Purification of anti-PprA IgG. The purified anti-PprA IgG migrated on a polyacrylamide gel with an apparent molecular mass of 150 kDa. The fluorescent dye Cy2 was directly conjugated to purified anti-PprA IgG.

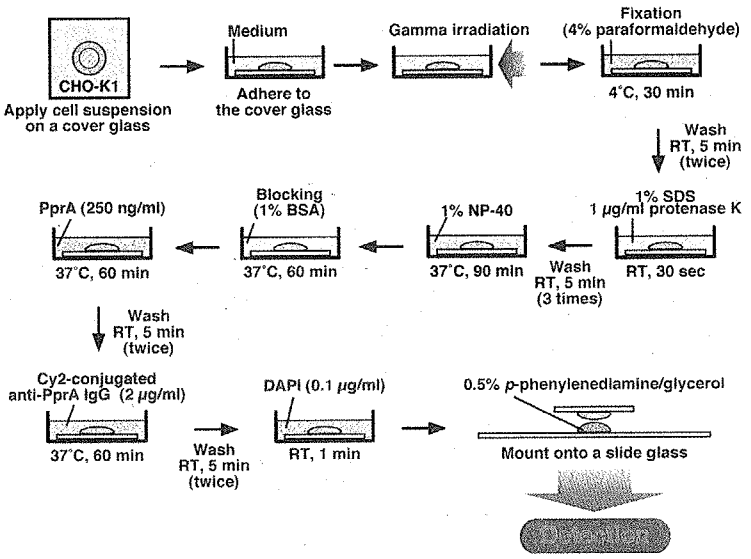

Fig. 2. Procedure for detection method of radiation-induced DNA strand breaks.

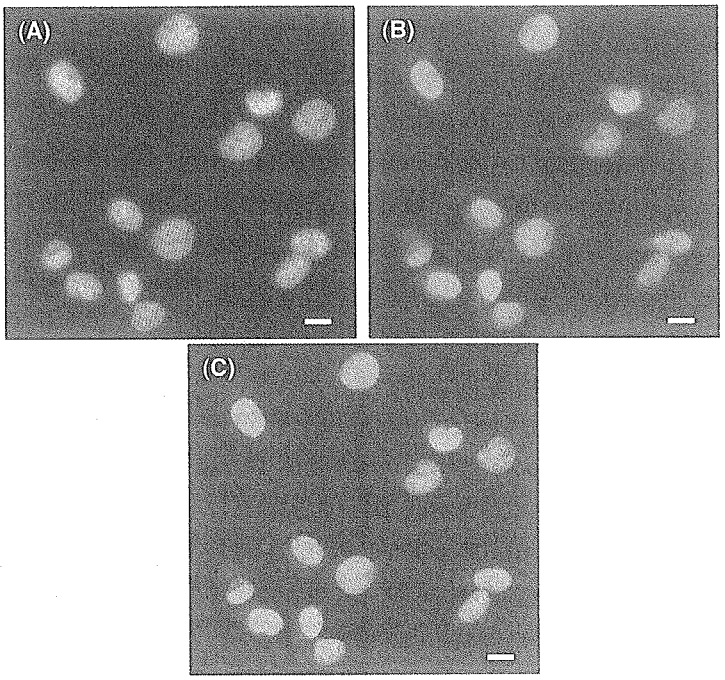

Fig. 3. Colocalization of Cy2 and DAPI fluorescent signals. Cells were stained with Cy2-conjugated anti-PprA IgG and DAPI. Images of the same field of view were captured under DAPI (nucleus) (A), Cy2 (DNA strand breaks) (B) filters, and merged (C). Bars indicate 10 μm.

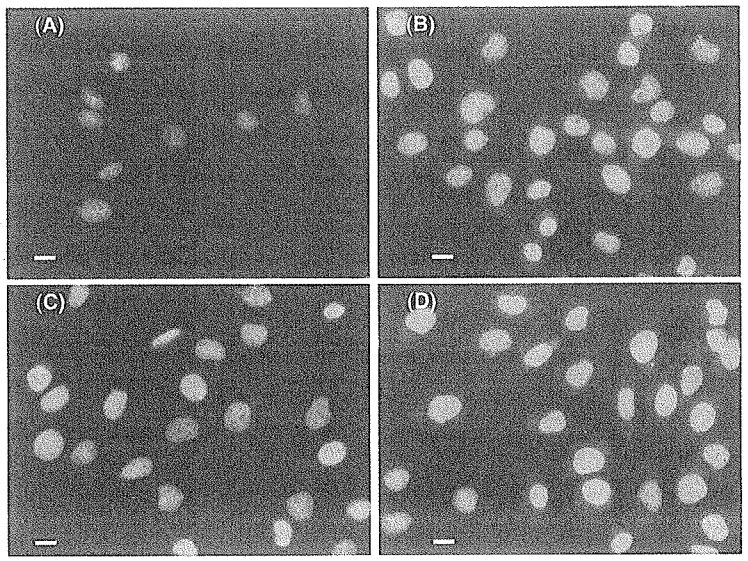

Fig. 4. Increase of DNA strand breaks in CHO-K1 cells following gamma irradiation. The cells were irradiated by ^{60}Co gamma rays; non-irradiation (A), 30 Gy (B), 50 Gy (C), and 100 Gy (D), and stained Cy2-conjugated anti-PprA IgG. Bars indicate 10 μm.

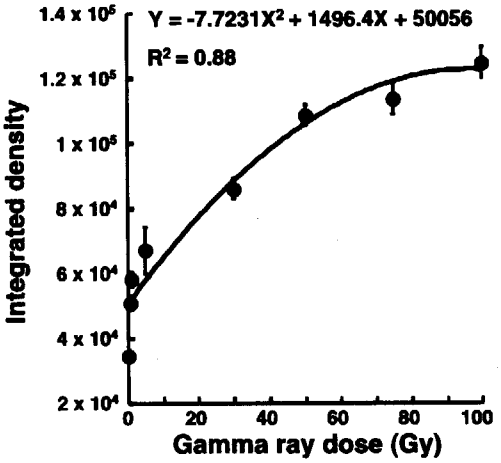

Fig. 5. Dose response curve of DNA strand breaks in CHO-K1 cells. The cells were irradiated by ^{60}Co gamma rays (0, 0.5, 1, 5, 30, 50, and 100 Gy) and treated with Cy2-conjugated anti-PprA IgG. Dots indicate the integrated density of Cy2 fluorescent signals in nuclei at each dose. The integrated density is corresponding to the amount of DNA strand breaks.

5.10

Characterization of carbon ion-induced mutations in *Arabidopsis thaliana*

Naoya Shikazono, Satoshi Kitamura, Chihiro Suzuki, Hiroshi Watanabe, Shigemitsu Tano, and Atsushi Tanaka
Department of Ion Beam Applied Biology, Japan Atomic Energy Research Institute

Irradiation of *Arabidopsis thaliana* by carbon ions was carried out to investigate the mutational effect of ion particles in higher plants. The averaged mutation rate of carbon ions was 2.0 X 10^{-6}/ Gy, which was 17-fold higher than that of electrons (1). PCR analysis of the mutants showed that, out of 28 mutant alleles, 14 had point-like mutations within the gene, while 14 contained large structural alterations (Table 1). Further sequence analysis revealed that most of the point-like mutations were short deletions (Table 2). In the case of rearrangements, DNA strand breaks were found to be rejoined using, if present, short homologous sequences for both types of radiation. After carbon ion-irradiation, small deletions were frequently observed around the breakpoints, whereas duplications of terminal sequence were found after electron-irradiation (Table 3) (2). These results suggest that non-homologous end joining (NHEJ) pathway operates after plant cells are exposed to both ion particles and electrons but that different mode of rejoining deals with the broken ends produced by each radiation.

From the present results, it seems reasonable to assume that carbon ions could predominantly induce null mutations. The fact that the molecular nature of carbon ion-induced mutation was different from that of electrons and that the molecular mechanisms of cells to induce mutation appeared to be also different implicates that ion particle is not only valuable as a new mutagen but also useful as a new tool to study repair mechanisms of certain types of DNA damage.

Table. 1 PCR analysis of carbon ion- and electron-induced mutants

	Point-like mutation	Rearrangement		Point-like mutation	Rearrangement
No. of alleles	14	14	No. of alleles	9	3

Table 2. Sequence analysis of carbon ion-induced point-like mutations

allele	sequence change
tt3-3	TC→AA
tt4(C2)	G→deletion
tt4(C3)	22bp→deletion
tt4(C4)	C→deletion
tt4(C5)	CCAACAGTG→A
tt5-2	G→T
tt6-2	A→insertion
tt6-3	100bp→deletion
tt18-1	TT→deletion
tt18-2	GTTGA→deletion
ttg1-23	A→deletion
ttg1-24	ACTCT→deletion
gl1-5	38bp→deletion
gl2-7	13bp→deletion

Table 3. Sequence analysis of breakpoints and junctions of rearrangements

Carbon ions	
homology/rejoined sites	13/17
deletion/breakpoints	11/18
duplication/breakpoints	4/18

electrons	
homology/rejoined sites	6/7
deletion/breakpoints	1/8
duplication/breakpoints	6/8

References

(1) N.Shikazono, S. Kitamura, C. Suzuki, H.Watanabe, S.Tano, A.Tanaka, Genetics, in press (2003)
(2) N.Shikazono, A. Tanaka, H.Watanabe, S.Tano, Genetics, 157, 379-387 (2001)

5.11

Essential Dynamics of T4 Endonuclease V

J.-G. Siebers[1], H. Yamaguchi[2] and R. Osman[3]
[1]Presently: RIKEN Tsukuba Institute, Japan, [2]NIRS, Chiba, Japan, [3]MSSM, New York, USA

The program suite AMBER 4.1 has been used to carry out a molecular dynamics study of wild type T4 Endonuclease V and the mutants R3Q and E23Q. The corresponding PDB codes are 2END, 1ENI and 1ENJ, respectively. Explicit water has been taken into account including crystalline water, ions and about 8000 water molecules in a rectangular box. The all-atom parm94 forcefield, TIP3P for water and PME for long range interactions have been used. After a simulated annealing protocol for 37.5 ps and an equilibration phase of 92 ps including NTP and NVT ensembe simulations a 0.5 ns NVT ensemble production run has been generated at a temperature of 300K. The root mean square deviations from the average structures indicate equilibrated trajectories with the smallest deviations for the wild type protein.

The program WHATIF has been used to perform an essential dynamics analysis on the trajectory data. As we are interested in contributions to the entropic energy of the system low frequency, large amplitude motions could be of key importance. To simplify the task we restricted the analysis to all C-alpha atoms of the peptide backbone. The connected subspace should still be capable of describing key motions of the overall protein. The trajectories are sampled at regular intervals so that the sampling theorem is fulfilled. This approach allows for considerable data reduction of the original trajectories. A covariance matrix is calculated from the reduced data set allowing for a principal component analysis which has been termed essential dynamics. The results indicate the largest overall flexibility for E23Q followed closely by the wild type enzyme. The overall stiffness of R3Q is considerable higher indicating coupling of the introduced arginine to many other residues in the center of the molecule. Inspection of the eigenvectors mapped to 3D-space allows for the recognition of motions that may facilitate biological function.

The selection of C-alpha atoms allows for a direct comparison of T4 Endonuclease V and its two mutants by virtue of their respective large amplitude motions. Simple partial transformation matrices can be used to study changes and relationships in these motions. In both mutants the first eigenvector is not conserved. Among the seven largest amplitude eigenvectors only the second appears to be conserved in R3Q. Four out of seven eigenvectors are conserved in E23Q. It is interesting to note that R3Q is not capable to bind to thymine dimer (TD) damaged DNA while E23Q has been used to produce a crystalline TD damaged DNA protein complex.

5.12

X-ray induced DNA synthesis and its regulation by SMT3A gene in Nevoid basal cell carcinoma syndrome (NBCCS) cells.

Shigeru Sugaya, Katsuo Sugita, Kazuko Kita and Nobuo Suzuki

Department of Environmental Biochemistry, Graduate schoool of Medicine, Chiba University

ABSTRACT

Nevoid basal cell carcinoma syndrome (NBCCS) is an autosomal dominant disorder that predisposes to both cancer and developmental defects such as multiple basal cell carcinomas (BCCs), odontogenic keratocysts, plantar and palmar pitting, and skeletal anomalies [1]. In addition to BCCs, GS patients are also at increased risk for lesions such as medulloblastoma, meningioma and fibrosarcoma [2-4]. However, details of the molecular mechanisms underlying these features of NBCCS remain unclear [5].

Interestingly, DNA synthesis activity was found to be increased after X-ray irradiation in NBCCS patients-derived cells, in contrast to the decrease observed in healthy donor-derived cells [6]. Genes for which expression is modulated in association with DNA synthesis induction, were investigated by PCR-based mRNA differential display analysis in an NBCCS cell line, NBCCS1. Decreased levels of SMT3A gene expression was found in X-ray-irradiated NBCCS1 cells. The decrease was moreover shown by RT-PCR analysis in not only NBCCS1 cells but also another cell line, NBCCS3. In addition to NBCCS cells, normal fibroblast cells showed DNA synthesis induction after X-ray irradiation when they were treated with antisense oligonucleotides for *SMT3A*. However, treatment of normal fibroblasts with the random oligonucleotides resulted in decreased synthesis. Thus, down-regulation of SMT3A gene expression may be responsible for the DNA synthesis induction after X-ray irradiation in the NBCCS cells at least tested.

REFERENCES

1. Gorlin, R. J. (1987) *Medicine* 66, 98-113.
2. Gorlin, R. J. (1995) *Dermatol. Clin.* 13, 113-125.
3. Springate, J. E. (1986) *J. Pediatr. Surg.* 21, 908-910.
4. Evans, D. G. R., Ladusans, E. J., Rimmer, S., Burnell, L. D., Thakker, N., and Farndon, P. A. (1993) *J. Med. Genet.* 30, 460-464.
5. Dezawa M., Fujii K., Kita K, Nomura J., Sugita K., Adachi-Usami E., Suzuki N.(1999) J Lab Clin Med Dec;134(6):585-91
6. Fujii, K., Suzuki, N., Ishijima, S., Kita, K., Sonoda, T., Dezawa, M., Sugita, K., and Niimi, H. (1997) *Biochem. Biophys. Res. Com.*. 240, 269-272.

5.13

Ab Initio Approach to Nanoscale Dynamics of DNA

Shigenori Tanaka (tanaka2@arl.rdc.toshiba.co.jp)
Advanced Materials & Devices Laboratory, Toshiba Research & Development Center,
1 Komukai Toshiba-cho, Saiwai-ku, Kawasaki 212-8582, Japan

An overview is given of our JST (Japan Science & Technology Corporation) project entitled "Ab Initio Approach to Nanoscale Dynamics of DNA", which is a collaboration by NIHS, AIST, Toyohashi University of Technology, Tsukuba University and Toshiba Corporation. One of the primary purposes of this project focuses on the ab initio calculations for the electronic states and stable structures of DNA systems from first principles. Such calculations are essential for the analysis on the electron transfer or transport properties of DNA which have recently attracted considerable attention in the context of radiation biology and nanotechnology. In addition, the detailed information on the electronic states of DNA is useful for the elucidation of the mechanism of transcriptional regulation in which the molecular recognition between DNA and proteins plays a vital role. The structural changes and stabilities of DNA also have a number of biological implications concerning the molecular processes in replication, transcription and translation.

We are developing basic computational tools such as the fragment molecular orbital (FMO) method and the charge equilibration (QEq) method. The FMO method has enabled us to perform the ab initio MO calculations for macromolecules such as protein and nucleic acids with good accuracy and much reduced time. Further, we are attempting to take account of the electron correlation effects on the basis of the density functional theory (DFT) since the electron correlation plays an important role for the description of the hydrogen bonding and stacking between the DNA bases. We are currently analyzing the DNA duplexes with ten or more base pairs at the Hartree-Fock or DFT level using parallel supercomputers or PC clusters. Concerning the QEq method for constructing semiclassical force fields taking into account the polarization and charge transfer effects, we are improving the original method with respect to the accuracy, simplicity and inclusion of the solvent effects.

Regarding the issue of electron transfer in DNA, major requisites for theoretical analyses are highlighted in the context of radiation-induced damage and "DNA molecular electronics". We then present our approaches based on the MO and molecular dynamics (MD) calculations in order to obtain theoretical results for kinetics comparing well with experimental data. Computational results toward a first-principles understanding of DNA electron transfer will then be given, thus providing guidelines for the in silico designs of DNA molecular wire and electrochemical DNA chip.

5.14

Monte Carlo simulation of clustered DNA damage by low-energy photons

Ritsuko Watanabe[1], Kimiaki Saito[1] and Akinari Yokoya[2];
1 Radiation Risk Analysis Lab. Japan Atomic Energy Research Institute
2 SPring-8, Japan Atomic Energy Research Institute

It has been suggested that clustering of several lesions within a small region on DNA should be specifically formed by significant energy depositions after exposure with ionizing radiation. Such clustered DNA damage is considered to be difficult to be repaired and important for biological consequences. To evaluate the effect of low -LET (linear energy transfer) radiation as γ-rays or X-rays, the contribution of inner-shell absorptions by DNA constituent atoms should be carefully investigated. Since Auger process of the DNA constituent atoms is considered to provide a situation apt to produce more clustered damage because of localized energy deposition on or around the DNA by low-energy Auger electrons. Actually, for example, several studies have reported enhancement effects due to phosphorus K-shell photoabsorption in cell lethality, double-strand break (DSB) yield and reduction of reparability.

Track structure simulation could provide the energy deposition pattern on and around DNA and useful tool with which to get knowledge on structure of DNA damage. We developed the model of damage induction process due to inner-shell photoabsorption and verified it by comparing the simulation results with available experimental results. We used a Monte Carlo code which allows the simulation of electron track structure, production of water radicals and reaction of radicals in nanometer scale. Simulation was carried out for both of direct energy deposition on DNA and indirect reaction of diffusible water radicals with DNA. DNA strand break induction was modelled and the yields of single- and double-strand breaks, and spatial distribution of breaks were calculated. Using the model calculation, spatial distribution of DNA damage was analyzed in detail. As a result, nearly all of cluste red DNA damage was shown to be induced by direct action. Formation of clustered damage, such as two DSBs and DSB with extra single-strand break (SSB) in the small region (within 30 bp), was shown to be enhanced at the resonance peak of phosphorus K-edge. The enhancement ratio for the damage is more significant than those for single SSB or DSB. Clustered damage produced by inner-shell absorption may have important role for reduction of reparability or cell lethality.

5.15

EPR study for DNA Base Damages Induced by Core Level Resonance Excitation of Oxygen

Akinari YOKOYA [a], Ken AKAMATSU [b] and Kentaro FUJII [a],
[a] JAERI/SPring-8, [b] JAERI/Tokai

1. Introduction

Studies employing soft X-rays under a few keV as probes to investigate genetic changes have highlighted the high efficiency of the biological effects, such as mutations, related with the molecular process on DNA damages. To understand the physicochemical mechanism of the DNA damages induced by K-photoabsorption in the energy region, we have developed an X-band EPR system combined with a synchrotron soft X-ray beamline[1]. Short-lived radical process following the *K*-absorption of oxygen in DNA bases has revealed by *in-situ* EPR signal detection[2]. In this study, we further examined the radical yield of guanine around the oxygen *K*-edge.

2. Experimental

EPR signal of DNA bases, guanine and thymine, was measured using a newly developed X-band electron paramagnetic resonance device (SLEEPRS: Synchrotron Light Excited Electron Paramagnetic Resonance Spectrometer) [1] installed in a JAERI soft X-ray beamline (BL23SU) in SPring-8. The sample pellet was irradiated with soft X-ray photons at a microwave cavity in a vacuum chamber ($<10^{-6}$ Pa). A closed-cycle cryogenic system was used to control the sample temperature from 77 K to room temperature. Relatively low microwave power ranging 0.1 to 7 mW was used to avoid power saturation of EPR signals. Based on a XANES spectrum of guanine film reported in our previous paper[3], several photon energies were chosen for irradiation. Resolution power, $E/\Delta E$ ~ 1,000 at the O K-edge (0.5 keV) region, and a photon flux of the order of 10^{11} (photons/sec/100 mA ring current/0.02 % band width) were realized at the sample position.

3. Results and discussion

Fig. 1 shows the EPR spectra of the short-lived guanine radicals obtained around *K*-exciation energy (540 eV) of oxygen (O6 of guanine). Two components were observed in the spectra as described by ***a*** and ***b*** in the Fig.1. The component ***b*** was insignificant by irradiation below and above the *K*-edge (524 and 548 eV). These are thought to be respective radicals because of different power saturation response. The signal intensity of both components immediately disappeared by beam-off. Fig. 2 shows a photon energy dependency of the signal intensity of the component ***a***. A characteristic large peak was found in the spectrum. At the peak (536 eV), the signal intensity was about 5 and 2 times larger than those obtained at 524 eV and 548 eV. It is inferred that the short-lived species is radical cations as the result of the core level excitation of a 1*s* electron of O6 to an anti-bonding orbital (σ^*) of O-C and following resonant Auger decay process in the molecule. These radicals would be instantly transformed to be a stable radical previously reported. These results clearly demonstrate that the *in situ* measurement of EPR combined with a brilliant soft X-ray source will provide a possibility for pursuing physicochemical process for induction of DNA base damage such as 8-oxo-guanine, which efficiently induce a point mutation on DNA in a living cell.

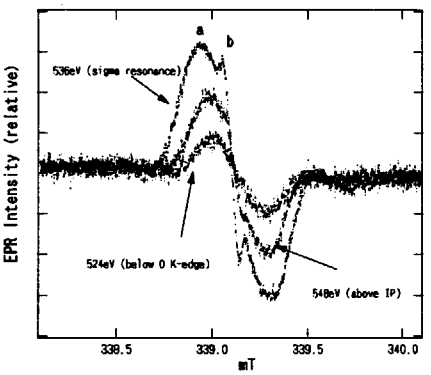

Fig.1. EPR spectra of guanine pellet irradiated at oxygen K-resonance (536 eV), below (524 eV) and above (548 eV) at 77 K.

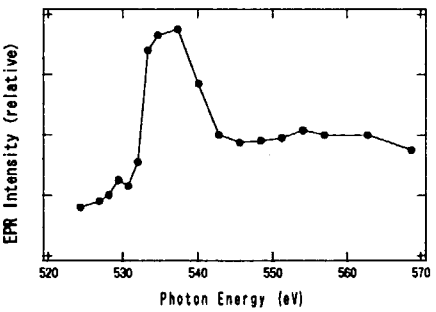

Fig.2. Photon energy dependence of EPR signal intensity around oxygen *K*-dege. The intensity of the component ***a*** is normalized with photon flux and the EPR gain

References

1) A. Yokoya and K. Akamatsu, *Nucl. Instr. Meth A*.**467-468**, 1333-1337, 2001
2) A. Yokoya, K. Akamatsu and K. Fujii, *Nucl. Instr. Meth B*, in press.
3) K. Fujii, K. Akamatsu and A. Yokoya, *Nucl. Instr. Meth B*, in press.

6. List of Participants

This is a blank page.

Name	Affiliation	Tel./Fax	E-mail
Ken AKAMATSU	Radiation Risk Analysis Laboratory, JAERI	029-282-6267/ 029-282-6768	kakamatu@riskest.tokai.jaeri.go.jp
Jonas DANIELSSON	Division of Physical Chemistry, Arrhenius Laboratory, Stockholm University	(46) 8-163656/ (46) 8-152187	jonas@physc.su.se
Hiroyuki DATE	College of Medical Technology, Hokkaido University	011-706-3423/ 011-706-4916	date@cme.hokudai.ac.jp
Marc DOBLER	Dept. of Materials Science, JAERI		marc@mummy.tokai.jaeri.go.jp
Akira ENDO	Dept. of Health Physics, JAERI	029-282-3754/ 029-282-6063	a.endo@popsvr.tokai.jaeri.go.jp
Kentaro FUJII	Spring-8, JAERI	0791-58-0802/ 0791-58-2740	fujiken@spring8.or.jp
Katsuyoshi FUJIKAWA	Institute for Environmental Sciences	0175-71-1282 /0175-71-1270	fujic@mac.com
Hirofumi FUJIMOTO	National Institute of Infectious Diseases	03-5285-1111/ 03-5285-1194	fuj@ss.ab.a.u-tokyo.ac.jp
Akira FURUKAWA	Natonal Institute of Radiological Sciences	043-206-3076/ 043-251-9231	furukawa@nirs.go.jp
Yoshiko HARIMA	CRC Solutions Corp.	03-5634-5801/ 03-5634-7338	harima@viola.ocn.ne.jp
Shinji HATO	Visible Information Center, Inc.	029-282-1914 / 029-282-8788	hato@vic.co.jp
Toshihiko HOSHINA	Atomic Industrial Journal	03-5777-0755/ 03-5777-0758	hoshina@jai8.or.jp
Hisashi ISHIDA	Quantum Bioinformatics Group (ITBL Bldg.)	0774-71-3464/ 0774-71-3460	ishida@apr.jaeri.go.jp
Akira ITO	The Cancer Institute	03-5394-3817/ 03-3918-0167	aito@jfcr.or.jp
Ikuo KANNO	Graduate School of Engineering, Kyoto University	075-753-5844/ 075-753-3571	kanno@nucleng.kyoto-u.ac.jp
Yosuke KATSUMURA	Nuclear Engineering Research Laboratory, School of Engineering, The University of Tokyo	029-287-8430/ 029-287-8488	katsu@q.t.u-tokyo.ac.jp
Yasushi KAWAKAMI	Institute of Research and Innovation, Department of Biotechnology	04-7144-9133/ 04-7143-6550	ykawa@iri.or.jp
Sakae KINASE	JAERI, Internal Dosimetry Laboratory, JAERI	029-282-5195/029-282-	skinase@popsvr.tokai.jaeri.go.jp
Katsumi KOBAYASHI	Photon Factory, KEK	029-864-5655/029-864-	katsumi.kobayashi@kek.jp
Naohiro KUROSAWA	Visible Information Center, Inc.	029-282-1654 / 029-282-8788	kurosawa@vic.co.jp
Junji MAGAE	Institute of Research and Innovation	04-7144-9142/ 04-7143-6550	jmagae@sannet.ne.jp
Junko MATSUBARA	Nuclear safety Commission	03-3581-3470/ 03-3581-3475	
Takeshi MATSUBARA	Visible Information Center, Inc.	029-282-1914 / 029-282-8788	matsubara@vic.co.jp
Hidehiko MATSUBAYASHI	Radiation Protection Center, Nuclear power Systems Division, Hitachi, Ltd.	0294-55-4288	hidehiko_matsubayashi@pis.hitachi.co.jp
Seiichi MIZUSHITA	Nuclear Technology and Education Center, JAERI	2380 / 03-3942-4290	mizusita@hems.jaeri.go.jp
Kosuke MORIKAWA	Biomolecular Engineering Research Institute	06-6872-8211/ 06-6872-8219	katsu@q.t.u-tokyo.ac.jp
Shigemitsu MORIZONO	Mito Atomic Energy Office, MEXT	029-224-3830/ 029-231-3789	morizono@mext.go.jp
Nobuteru NARIYAMA	Japan Synchrotron Radiation Research Institute	0791-58-2723/ 0791-58-0830	nariyama@spring8.or.jp
Issay NARUMI	Takasaki Radiation Chemistry Research Establishment, JAERI	027-346-9542/ 027-346-9688	narumi@taka.jaeri.go.jp
Nobuo NIIMURA	Neutron Structural Biology, JAERI	029-282-5906/ 029-282-5927	niimura@kotai3.tokai.jaeri.go.jp
Ohtsura NIWA	Kyoto University Radiation Biology Center	075-753-7563/ 075-753-7564	oniwa@house.rbc.kyoto-u.ac.jp

Hiroshi NOGUCHI	JAERI, Internal Dosimetry Laboratory	029-282-5242/029-282-	noguh@popsvr..tokai.jaeri.go.jp
Takehiko NOHMI	National Institute of Health Sciences	03-3700-9873/ 03-3707-6950	nohmi@nihs.go.jp
Hiromitsu OGATA	National Institute of Public Health	048-458-6111/ 048-469-0326	ogata@niph.go.jp
Shin-ichi OHNO	Theoretical Radiation Research Laboratory	047-981-8752/ 045-981-7950	ohno-trl@01.246.ne.jp
Toshihiko OHNUKI	JAERI, Advanced Science Research Center	029-282-5361/029-282-	ohnuki@sparcle.tokai.jaeri.go.jp
Akira OIKAWA	JAERI-NAKA, Tokamak Research Program Division	029-270-7316/ 029-270-7419	oikawaa@fusion.naka.jaeri.go.jp
Roman OSMAN	Mount Sinai School of Medicine	1-212-241-6530/ 1-212-860-3369	roman.osman@mssm.edu
Noriyuky OUCHI	JAERI, Radiation Risk Analysis Laboratory	029-282-5840/ 029-282-6728	bob@riskest.tokai.jaeri.go.jp
Donald A. PIERCE	RERF Hiroshima	082-261-3131/ 082-262-9768	pierce@rerf.jp
Miroslav PINAK	JAERI, Radiation Risk Analysis Laboratory	029/282-5583/ 029-282-6768	pinak@ismws001.tokai.jaeri.go.jp
Susumu RYUFUKU	Visible Information Center, Inc.	029-282-1914 / 029-282-8788	ryufuku@vic.co.jp
Shin SAIGUSA	Research Center for Radiation Safety, NIRS	043-206-3163/ 043-206-4138	saigusa@nirs.go.jp
Kimiaki SAITO	JAERI, Radiation Risk Analysis Laboratory	029-282-6168/ 029-282-2728	komei@popsvr.tokai.jaeri.go.jp
Kazuo SAKAI	Low Dose Radiation Research Center, CRIEPI	03 3480 2111/ 03 3480 3113	kazsakai@criepi.denken.or.jp
Yukio SAKAMOTO	JAERI, External Dosimetry Lab.		sakayuki@popsvr.tokai.jaeri.go.jp
Hisako SAKIYAMA	Takagi School	043-287-2443	shisako@gb3.so-net.ne.jp
Kiyoshi SAKURAI	JAERI, Nuclear Safety Research	029-282-5492	sakurai@melody.tokai.jaeri.go.jp
Tatsuhiko SATOH	JAERI, External Dosimetry Lab.	029-282-5629/ 029-282-5609	t.sato@popsvr.tokai.jaeri.go.jp
Kaoru SATOH	JAERI, Internal Dosimetry Laboratory	029-282-5195/029-282-	ksato@popsvr..tokai.jaeri.go.jp
Katsuya SATOH	Takasaki Radiation Chemistry Research Establishment, JAERI	027-346-9542/ 027-346-9688	katsuya@taka.jaeri.go.jp
Naoya SHIKAZONO	Plant Resources Lab., JAERI Takasaki	027-346-9537/ 027-346-9688	naoya@taka.jaeri.go.jp
Yuichi SHIMIZU	JAERI, Advanced Photon Research Center		
Joerg-Gerald SIEBERS	RIKEN Tsukuba Institute	029-836-9164/ 029-836-9080	siebers@rtc.riken.go.jp
Shigeru SUGAYA	Department of Environmental Biochemistry, Graduate School of Medicine, Chiba University	043-226-2041	s-sugaya@med.m.chiba-u.ac.jp
Fumiyaki TAKAHASHI	JAERI, External Dosimetry Lab.		taka23@popsvr.tokai.jaeri.go.jp
Shigenori TANAKA	Toshiba R & D Center, AML	044-549-2113/ 044-520-1801	tanaka2@arl.rdc.toshiba.co.jp
Sergei TOLMACHYOV	JAERI, Internal Dosimetry Laboratory	029-282-5195/029-282-	tolmachv@popsvr.tokai.jaeri.go.jp
Syuichi TSUDA	JAERI, External Dosimetry Lab.	029-282-5629	tsuda@popsvr.tokai.jaeri.go.jp
Shuzo UEHARA	School of Health Sciences, Kyushu University	092-642-6696/ 092-642-6674	shuzohsg@mbox.nc.kyushu-u.ac.jp
Diane VANNAIS	RERF Hiroshima	082-261-3131/ 082-263-7279	
Charles A. WALDREN	RERF Hiroshima	082-261-3131/ 082-263-7279	cwaldren@rerf.or.jp
Hiroshi WATANABE	JAERI, Takasaki	027-346-9311/ 027-347-2561	watanabe@taka.jaeri.go.jp
Ritsuko WATANABE	JAERI, Radiation Risk Analysis Laboratory	029-282-5840/ 029-282-2728	ritsuko@riskest.tokai.jaeri.go.jp

Takashi WATANABE	Radiation Safety Control & Radiological Emergency management Group, Tokyo Electric Power	03-4216-4873/ 03-3596-8547	wata.tak@tepco.co.jp
Yoshinobu YAMAGISHI	Ishikawa Prefectural Institute of Public Health and Environmental	076-229-2011/ 076-229-3118	yamay@pref.ishikawa.jp
Hiroshi YAMAGUCHI	NIRS		yamag@nirs.go.jp
Yasuhiro	JAERI, External Dosimetry Lab.	029-282-6067	yachan@popsvr.tokai.jaeri.go.jp
Akira YASUI	Institute of Development, Aging and Cancer, Tohoku University	022-717-8465/ 022-717-8470	ayasui@idac.tohoku.ac.jp
Akinari YOKOYAMA	SPring-8, JAERI	0791-58-0802/ 0791-58-2740	yokoya@spring8.or.jp
Sumi YOKOYAMA	JAERI, Internal Dosimetry Laboratory	029-282-5195/029-282-	simi@popsvr..tokai.jaeri.go.jp
Yoshizawa MICHIO	JAERI, Calibration Standards and Measurement Division	029-282-5205	m-yoshi@popsvr..tokai.jaeri.go.jp
Kei YURA	Quantum Bioinformatics Group (ITBL Bldg.)	0774-71-3462/ 0774-71-3460	yura@apr.jaeri.go.jp
Tomoji TAKAMASA	Tokyo University of Mercantile Marine	03-5245-7410/03-5245-	takamasa@ipc.tosho-u.ac.jp
Morio TSUJIMURA	Japan Nuclear Cycle Development Institute	029-282-1111(ex2743)/0 29-283-0457	tujimura@tokai.jnc.go.jp
Yoshiharu NAGAOKA	Dept. of Health Physics, JAERI		
Isamu SHIMIZU	Dept. of Health Physics, JAERI		
Ryuichi SAKAMOTO	Dept. of Health Physics, JAERI		
Yoshiaki OKUI	JAERI		
Takenori YAMAGUCHI	Dept. of Health Physics, JAERI		
Milan MAREK	NRI		
Hajimu YABUTA	Dept. of Health Physics, JAERI		
Toshio KUMAI	Dept. of Research Reactor, JAERI		
Nobuo SUZUKI	Dept. of Health Physics, JAERI		
Yoshiyuki HOSHI	RIST		
Norihiro MATSUDA	Facility Safety Group, JAERI		
Masahiro SUTSUMI	Dept. of Health Physics, JAERI		
Hisashi SEKINO	Dept. of Health Physics, JAERI		
Toshimitsu HONMA	Dept. of Reactor Safety Research		
Akira MIHARA	Dept. of Health Physics, JAERI		
Takenori SUZAKI	Dept. of Nuclear Energy System		
Katsunori YAMADA	Dept. of Health Physics, JAERI		
Toshio KIMURA	Dept. of Health Physics, JAERI		
Kenji YOTSUJI	Visible Information Center, Inc.		
Mitsuru MAEDA	Advanced Science Research Center, JAERI		
Yoshinori SUZUKI	JAERI		
Takuya TSURUOKA	RIST		
Kotaro YAMASOTO	Dept. of Health Physics, JAERI		
Hidenori YAMAMOTO	Secretariat for Nuclear safety Commission		
Kazuo FUJIKI	Dept. of JMTR, JAERI Oarai		
Shinya TAKAHASHI	Plant Resources Lab., JAERI		
Katsuo KAWAI	Dept. of Health Physics, JAERI		
Takahiro YOSHIDA	Advanced Science Research Center, JAERI		
Takemasa SHIBATA	Advanced Science Research Center, JAERI		
Ichiro TANAKA	Advanced Science Research Center, JAERI		
Hideo MATSUZURU	Dept. of Health Physics, JAERI		
Hideaki YAMAMOTO	Dept. of Health Physics, JAERI		
Fuminori SAKAMOTO	Dept. of Research Reactor, JAERI		

This is a blank page.

国際単位系 (SI) と換算表

表 1　SI 基本単位および補助単位

量	名称	記号
長さ	メートル	m
質量	キログラム	kg
時間	秒	s
電流	アンペア	A
熱力学温度	ケルビン	K
物質量	モル	mol
光度	カンデラ	cd
平面角	ラジアン	rad
立体角	ステラジアン	sr

表 2　SI と併用される単位

名称	記号
分，時，日	min，h，d
度，分，秒	°，′，″
リットル	l，L
トン	t
電子ボルト	eV
原子質量単位	u

1 eV = 1.60218 × 10^{-19} J

1 u = 1.66054 × 10^{-27} kg

表 5　SI 接頭語

倍数	接頭語	記号
10^{18}	エクサ	E
10^{15}	ペタ	P
10^{12}	テラ	T
10^{9}	ギガ	G
10^{6}	メガ	M
10^{3}	キロ	k
10^{2}	ヘクト	h
10^{1}	デカ	da
10^{-1}	デシ	d
10^{-2}	センチ	c
10^{-3}	ミリ	m
10^{-6}	マイクロ	μ
10^{-9}	ナノ	n
10^{-12}	ピコ	p
10^{-15}	フェムト	f
10^{-18}	アト	a

表 3　固有の名称をもつ SI 組立単位

量	名称	記号	他の SI 単位による表現
周波数	ヘルツ	Hz	s^{-1}
力	ニュートン	N	$m \cdot kg/s^2$
圧力，応力	パスカル	Pa	N/m^2
エネルギー，仕事，熱量	ジュール	J	N·m
工率，放射束	ワット	W	J/s
電気量，電荷	クーロン	C	A·s
電位，電圧，起電力	ボルト	V	W/A
静電容量	ファラド	F	C/V
電気抵抗	オーム	Ω	V/A
コンダクタンス	ジーメンス	S	A/V
磁束	ウェーバ	Wb	V·s
磁束密度	テスラ	T	Wb/m^2
インダクタンス	ヘンリー	H	Wb/A
セルシウス温度	セルシウス度	℃	
光束	ルーメン	lm	cd·sr
照度	ルクス	lx	lm/m^2
放射能	ベクレル	Bq	s^{-1}
吸収線量	グレイ	Gy	J/kg
線量当量	シーベルト	Sv	J/kg

表 4　SI と共に暫定的に維持される単位

名称	記号
オングストローム	Å
バーン	b
バール	bar
ガル	Gal
キュリー	Ci
レントゲン	R
ラド	rad
レム	rem

1 Å = 0.1 nm = 10^{-10} m

1 b = 100 fm^2 = 10^{-28} m^2

1 bar = 0.1 MPa = 10^5 Pa

1 Gal = 1 cm/s^2 = 10^{-2} m/s^2

1 Ci = 3.7 × 10^{10} Bq

1 R = 2.58 × 10^{-4} C/kg

1 rad = 1 cGy = 10^{-2} Gy

1 rem = 1 cSv = 10^{-2} Sv

（注）

1. 表 1 − 5 は「国際単位系」第 5 版，国際度量衡局 1985 年刊行による。ただし，1 eV および 1 u の値は CODATA の 1986 年推奨値によった。
2. 表 4 には海里，ノット，アール，ヘクタールも含まれているが日常の単位なのでここでは省略した。
3. bar は，JIS では流体の圧力を表わす場合に限り表 2 のカテゴリーに分類されている。
4. EC 閣僚理事会指令では bar，barn および「血圧の単位」mmHg を表 2 のカテゴリーに入れている。

換算表

力	N(=10^5 dyn)	kgf	lbf
	1	0.101972	0.224809
	9.80665	1	2.20462
	4.44822	0.453592	1

粘度　1 Pa·s(N·s/m^2) = 10 P(ポアズ)(g/(cm·s))

動粘度　1 m^2/s = 10^4 St(ストークス)(cm^2/s)

圧力	MPa(=10 bar)	kgf/cm^2	atm	mmHg(Torr)	lbf/in^2(psi)
	1	10.1972	9.86923	7.50062 × 10^3	145.038
	0.0980665	1	0.967841	735.559	14.2233
	0.101325	1.03323	1	760	14.6959
	1.33322 × 10^{-4}	1.35951 × 10^{-3}	1.31579 × 10^{-3}	1	1.93368 × 10^{-2}
	6.89476 × 10^{-3}	7.03070 × 10^{-2}	6.80460 × 10^{-2}	51.7149	1

エネルギー・仕事・熱量	J(=10^7 erg)	kgf·m	kW·h	cal(計量法)	Btu	ft·lbf	eV
	1	0.101972	2.77778 × 10^{-7}	0.238889	9.47813 × 10^{-4}	0.737562	6.24150 × 10^{18}
	9.80665	1	2.72407 × 10^{-6}	2.34270	9.29487 × 10^{-3}	7.23301	6.12082 × 10^{19}
	3.6 × 10^6	3.67098 × 10^5	1	8.59999 × 10^5	3412.13	2.65522 × 10^6	2.24694 × 10^{25}
	4.18605	0.426858	1.16279 × 10^{-6}	1	3.96759 × 10^{-3}	3.08747	2.61272 × 10^{19}
	1055.06	107.586	2.93072 × 10^{-4}	252.042	1	778.172	6.58515 × 10^{21}
	1.35582	0.138255	3.76616 × 10^{-7}	0.323890	1.28506 × 10^{-3}	1	8.46233 × 10^{18}
	1.60218 × 10^{-19}	1.63377 × 10^{-20}	4.45050 × 10^{-26}	3.82743 × 10^{-20}	1.51857 × 10^{-22}	1.18171 × 10^{-19}	1

1 cal = 4.18605 J (計量法)

= 4.184 J (熱化学)

= 4.1855 J (15 °C)

= 4.1868 J (国際蒸気表)

仕事率　1 PS (仏馬力)

= 75 kgf·m/s

= 735.499 W

放射能	Bq	Ci
	1	2.70270 × 10^{-11}
	3.7 × 10^{10}	1

吸収線量	Gy	rad
	1	100
	0.01	1

照射線量	C/kg	R
	1	3876
	2.58 × 10^{-4}	1

線量当量	Sv	rem
	1	100
	0.01	1

（86 年 12 月 26 日現在）

Selected Materials of the International Workshop on Radiation Risk and its Origin at Molecular and Cellular Level February 6-7, 2003